2019

Portable water filled barrier with internal honeycomb cells

Zhe Wang
Iowa State University

Portable water filled barrier with internal honeycomb cells

by

Zhe Wang

A thesis submitted to the graduate faculty

in partial fulfillment of the requirements for the degree of

MASTER OF SCIENCE

Major: Civil Engineering (Structural Engineering)

Program of Study Committee:
An Chen, Major Professor
Simon Laflamme
Michael Perez

The student author, whose presentation of the scholarship herein was approved by the program of study committee, is solely responsible for the content of this thesis. The Graduate College will ensure this thesis is globally accessible and will not permit alterations after a degree is conferred.

Iowa State University

Ames, Iowa

2019

TABLE OF CONTENTS

Page

LIST OF FIGURES

Page

LIST OF TABLES

Page

ACKNOWLEDGMENTS

I would like to express my gratitude to my major professor, Dr. An Chen, for accepting me as a member of the research team, and providing me required support and guidance during my master program. I would like to thank Dr. Simon Laflamme and Dr. Michael Perez for serving on my POS committee and valuable guidance throughout the course of this research.

I would like to thank Dr. Hao Wu for the guidance of finite element software since I was an undergraduate student. In addition, I would like to thank my friends and colleagues: Hanming Zhang, Elizabeth Miller, Zhao Cheng, Jin Yan and more.

I would like to express special thanks to my parents for selfless love and support during my years of study in the United States. I can not get where I am without my parents' encouragement and belief in me to be a better person.

ABSTRACT

Longitudinal traffic barriers are widely used as road safety features in the United States to keep vehicles within the roadway and prevent them from colliding with dangerous obstacles. Portable water-filled barriers (PWFBs) are one type of temporary longitudinal traffic barriers, commonly used in speed limit zones and, roadside working zones. Current market PWFBs are cost-effective and exhibiting high efficiency while resisting vehicle impact at low speed. However, high-level impact severity results in structural failure and extensive lateral deflection. Based on evaluation criteria from Manual of Assessing Safety Hardware (MASH), some PWFBs are inefficient to meet the requirements from newly published evaluation documents. Since newly developed PWFB with interior honeycomb cells aims to improve energy absorption behavior and structural resistance in terms of impact loading. The PWFB with internal cells is designed based on the prototype of the JB-32 barrier, where quadrangle-shaped honeycomb cells are bounded on the interior surface. In the early stage of this research, small-scale barrier specimens are obtained via 3D printing and pendulum impact testing is developed to investigate the energy absorption behavior of barrier structure filled with water. Additionally, numerical simulation is conducted via Finite Element Analysis (FEA) software (ABAQUS). Utilizing the obtained FE results, a parametric study is used to further validate the observation from testing. With both testing and numerical results, the energy absorption exhibited by water and structural strength of the system can be addressed.

A design recommendation and optimal condition combining each design parameter is given regarding the conducted parametric study.

CHAPTER 1. INTRODUCTION

1.1 Background

The Portable Water Filled Barrier (PWFB) is a temporary roadway safety feature commonly used to channel construction work zones and pedestrian zones or designated parking areas. PWFBs are made of high-density polyethylene and can be installed by workers manually, exhibiting high portability. The barriers are allowed to fill ballast weight at a field site to increase the crashworthiness of the barrier shell. According to the different classification of PWFBs, the blast weight can be filled with either water or sand. PWFB segments can be connected together forming a flexible longitudinal road barrier which effectively redirects and contains the collision vehicles. Recently, there has been an increasing need for protection of roadway workers and occupants due to the growing frequency of vehicle collision in the work zone. Current high-level impact resistant PWFBs are either reinforced with steel frames or tension cable to increase structural strength against failure. Failure of structural integrity may result in failing to redirect or contain the collision vehicle or potentially lead to a secondary crash.

To increase the strength of the barrier shell, the idea of using internal honeycomb cells has been proposed. A honeycomb-shaped structure enables the barrier to have a relatively high out-of-plane compressive strength and out-of-plane shear resistance. Recently, researchers have investigated the in-plane characteristics of honeycomb cells. Comparing to out-of-plane, in-plane cells have relatively smaller

compressive strength but have a significant effect regarding energy absorption (T. Thomas and G. Tiwari, 2018). The discovery in honeycomb cells can be applied to PWFB structures to increase the energy absorption of barrier shells and minimize the lateral deflection consequently.

1.2 Problem Statement

Excessive lateral displacement of roadside barriers is hazardous to vehicle occupants and workers in temporary work zones. The purpose of developing higher impact energy absorption PWFB with internal honeycomb cells is to improve the performance of temporary roadway safety barriers. Currently several market PWFBs present good quality for lateral displacement control. Many PWFBs may fail to meet the evaluation criteria from newly published Manual for Assessing Safety Hardware (MASH-20116). Higher impact energy absorption of longitudinal road safety barriers has a significant contribution in terms of minimizing lateral deflection. Moreover, higher energy absorption is preferred to meet the evaluation criteria of Structural Adequacy, Occupant Risks, and minimize the potential to result in a secondary vehicle collision. Higher impact energy absorption helps to redirect and contain an impact vehicle smoothly, which minimizes the risks of occupants and stops the collision vehicles in a controlled manner. Therefore, the energy absorption is a crucial parameter to evaluate the performance of PWFBs. In the early stage of this research, this paper presents research that investigates the energy absorption behavior of developed PWFB with internal honeycomb cells in terms of vehicular impact followed by newly published MASH.

1.3 Thesis Organization

This thesis is organized in six chapters each corresponding to various tasks accomplished in the research. The chapters are summarized below.

Chapter 1-Introduction: provides background information for the problems that the research is exploring and presents the objectives of the study.

Chapter 2-Literature Review: a review of relevant documentation and testing guidelines from the newly published document for longitudinal safety barriers.

Chapter 3-Experimental Study: description of small-scale 3D printed barrier specimens, developed small-scale test plan, and conducted small-scale pendulum impact testing.

Chapter 4-Finite Element Modeling and Parametric Study: analysis of FE models is used to validate testing results and further investigates the post-impact behavior of barrier specimens

Chapter 5-Design Recommendations: provides design recommendations and determines the optimal design case based on the parametric study.

Chapter 6-Conclusions and Future Work: generally summarizes the main findings from the research and gives several guidelines for future work.

CHAPTER 2. LITERATURE REVIEW

With the rapid development of the transportation system, the increased frequency of vehicle collisions has drawn the public's attention. Through the great progress of developing road safety hardware, road safety devices can effectively minimize the hazards of a traffic collision. Recently, safety issues have been raised in temporary work zones due to roadway maintenance and utility working. Temporary Portable Water Filled Barrier (PWFB) devices have been developed to protect occupants and field workers in these areas. This section will discuss relevant testing guidelines and evaluation criteria in terms of roadway safety features.

2.1 Road Safety Barriers

Recent researchers have demonstrated that collision with solid objects beside highways results in a considerable number of fatal injuries (Wang et al., 2011). Hence, road safety barriers are treated as a significant road safety feature for preventing vehicles from colliding with dangerous road obstacle, such as bridge abutments, public facilities, construction work zones and cliffs (Bruce et al., 2010). According to the Manual of Assessing Safety Hardware (MASH), categories of road safety barriers can be divided into three groups in terms of the deflection behavior exhibited when the barrier is impacted by vehicles as well as the mechanism formed to resist impact forces. These categories include flexible and semi-rigid barriers, rigid barriers, and barrier transitions (MASH). The rigid barrier systems are normally reinforced concrete structures which have very high stiffness and could require little to no maintenance, dependent on the concrete type. The rigid barriers experience small

impact effects and are more practical in small impact angles. They are commonly used in the highway for divided opposing lanes. Concrete barriers effectively prohibit vehicles from crossing to the opposite road and protect drivers from injury or death and prevent vehicle damage (Hasan Mohammed and M.F.M. Zain, 2015).

Figure 2- 1. Reinforced Concrete Safety Barrier (Rigid)

The semi-rigid safety barrier has stiffness between rigid and flexible road safety barriers, commonly made of rails or steel beams (W-Beam Steel Barrier). W-Beam guardrails are made of steel coiled into a W-shape and galvanized to get rid of corrosion that could occur from weather effects to increase the life cycle. Typically, 10-gauge or 12-gauge corrugated steel rail is adequate for containing the most vehicle collision accidents. The W-Beam can be installed on both steel strong posts and weak posts. The AASHTO standard W-Beam Steel Barrier is manufactured as 12’-6’’ or 25’, and typically applied in 6’-3’’ spacing.

Figure 2- 2. W-Beam Steel Safety Barrier (Semi-Rigid)

Concerning the flexible road safety barrier, cable barriers are normally made of steel wire ropes mounted on weak posts, also referred to as guard cable or wire rope safety barriers (WRSB). The systems are able to stretch and absorb energy. Flexible barriers are more forgiving comparing to rigid and semi-rigid safety barriers. The flexible barriers enable absorption of impact energy and dissipate a portion of it due to lateral displacement, which effectively minimizes the occupant risks of collision, and allows collision vehicles to be smoothly redirected (Road Design Guide-ASSHTO, 2006). The cable barriers are the most cost-effective road safety feature and are becoming increasingly prevalent. The practical use of cable occurs at the median for a divided highway. There are two types of cable barriers: low-tension and high-tension. In low-tension cable, the tension force in the cable is sufficient to eliminate sags between posts. Installed springs at the ends of the cables are compressed to provide low tensile stress along the cable. With respect to high-tension cable barriers, the cables generally use three or four high strength steel wires and are

pre-tensioned during the installation process. In comparing the two cable barriers, high-tension cables exhibit a smaller lateral deflection and more effectively redirect collision vehicles. The following picture shows the typical configuration of High-Tension Cable.

Figure 2- 3. High-Tension Cable Barrier at Posts End (Flexible)

2.2 Safety Issues in Temporary Work Zone

A work zone is a segment of the roadway network with construction, maintenance, or utility activities. A work zone network is marked by signs at both the head and end work zone, and channelizing devices are used to separate the work zone and roadway. Conducted road safety analyses reveal an increase in crash rates in the road work zone (Waleczek. H et al., 2016). The phenomenon addresses work zone as an unsafe section of the road network which is hazardous to both highway infrastructure workers and occupants. This is mainly because construction work zones affect the serviceability of roadway. According to statistics data from the Federal Highway Administration (FHWA), from 2008 to 2015, vehicle collision frequency of

both work zone and non-work present a rising trend. In 2015, crash frequencies reached a peak. For every 70 work zone crashes that happen, at least one leads to injury.

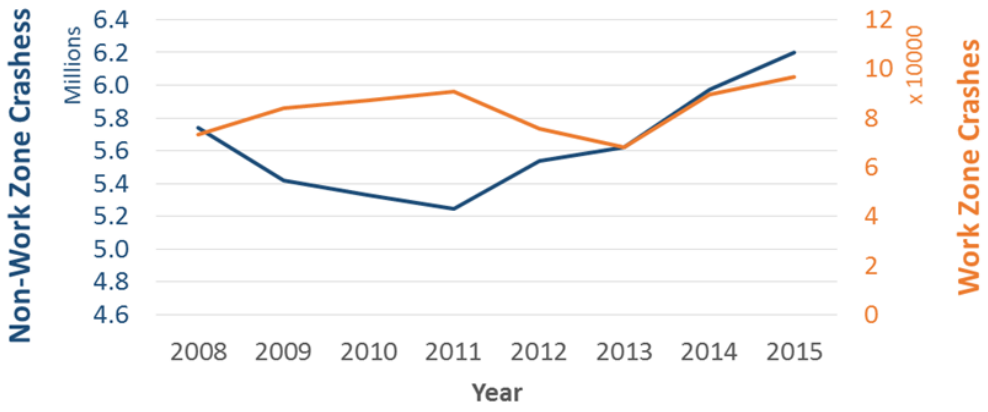

Figure 2- 4. 2008 to 2015 Crash Frequency of Work Zone and Non-Work Zone (FARS/GES Data)

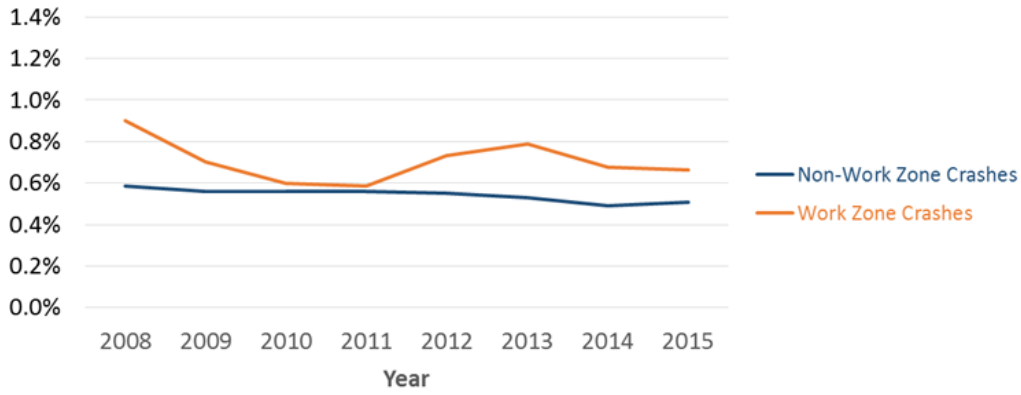

Figure 2- 5. 2008-2015 Percentage of Crashes Resulting in Fatality (FARS/GES Data)

In 2015 the work zone crashes by severity include: 73.0% (70,499) of work zone crashes were Property Damage Only (PDO), 26.4% (25,485) of work zone crashes involving at least one injured party, and 0.7% (642) of work zone accidents involved at least one fatality. The trend of deaths in work zone area crashes exhibits a higher frequency of fatalities versus non-work zone area crashes. Overall, while

crashes are increasing, there is a trend that the casualties associated with these crashes in both non-work zones and work zones are declining slowly. The field worker also is a vulnerable party in work zone crashes. However, combined data of Injury Hazards in Road and Bridge construction, Fatal Occupational Injuries at Road Construction Sites, and Census of Fatal Occupational Injuries indicate that the fatality trends briefly declined since 2005. In addition, roadway workplace fatalities are responsible for 1.5% to 3% of total workplace fatalities. Over the past few years, the leading causes of fatalities in the roadway have been removers/backovers, often by dump trucks (48%), collision between vehicles/mobile equipment (14%), and caught in between/struck by construction equipment and objects (14%). Roughly half of the fatalities are due to crush or backing up by vehicles or the use of mobile devices. Of these fatalities, more than half of the fatalities caused by construction vehicles. All these effects point out that current working zone safety features are weak to redirect and contain the collision vehicles. Overall, the crash frequency of work zone and non-work zone have an increasing trend in recent years. Although fatalities of non-work zone crash show a slightly decreasing trend, there is no significant sign of improvement of the fatalities in work zone. The safety issues of work zone draw highway infrastructure workers and researcher's considerable attention.

2.3 Portable Water Filled Barriers (PWFBs)

Because of the safety issue presented in the work zone, temporary safety barriers have been developed to minimize hazard in the work zone. A temporary road barrier as an essential road safety feature is designed to protect vehicle occupants and

workers. One type is Portable Water Filled Barrier (PWFB). There is a disadvantage for the application of PWFBs; the filled water freezes in a low-temperature circumstance. Solidified water results in expansion and damages the structures. Calcium Chloride is used to protect the structures at low-temperature conditions. Calcium Chloride is the chemical compound compromised by dissolving marble or limestone ships in hydrochloric acid. Calcium chloride remains in a solid state and dissolves into water and ethanol in cold weather conditions which significantly lowers the freezing and melting point of filled water. Continuous PWFBs are another type of flexible safety barrier that exhibits good performance in containing and redirecting collision vehicles. The barriers are made of lightweight plastic shell, commonly plastic polymer. Water is filled in the barriers at the site to increase crashworthiness. Non-dead weight supplied barriers have portability and can be installed without heavy machinery or equipment.

Figure 2- 6. Configuration of Installed PWFB at Roadside (MB 350 Barrier System)

Single barriers can be joined together with a simple shear connection which allows some horizontal flexibility, similar to acting as a string. These characteristics make PWFBs a highly cost-effective road safety feature. PWFBs are also known as temporary road safety barriers which are flexible barriers and commonly used in work zones and slow traffic zones.

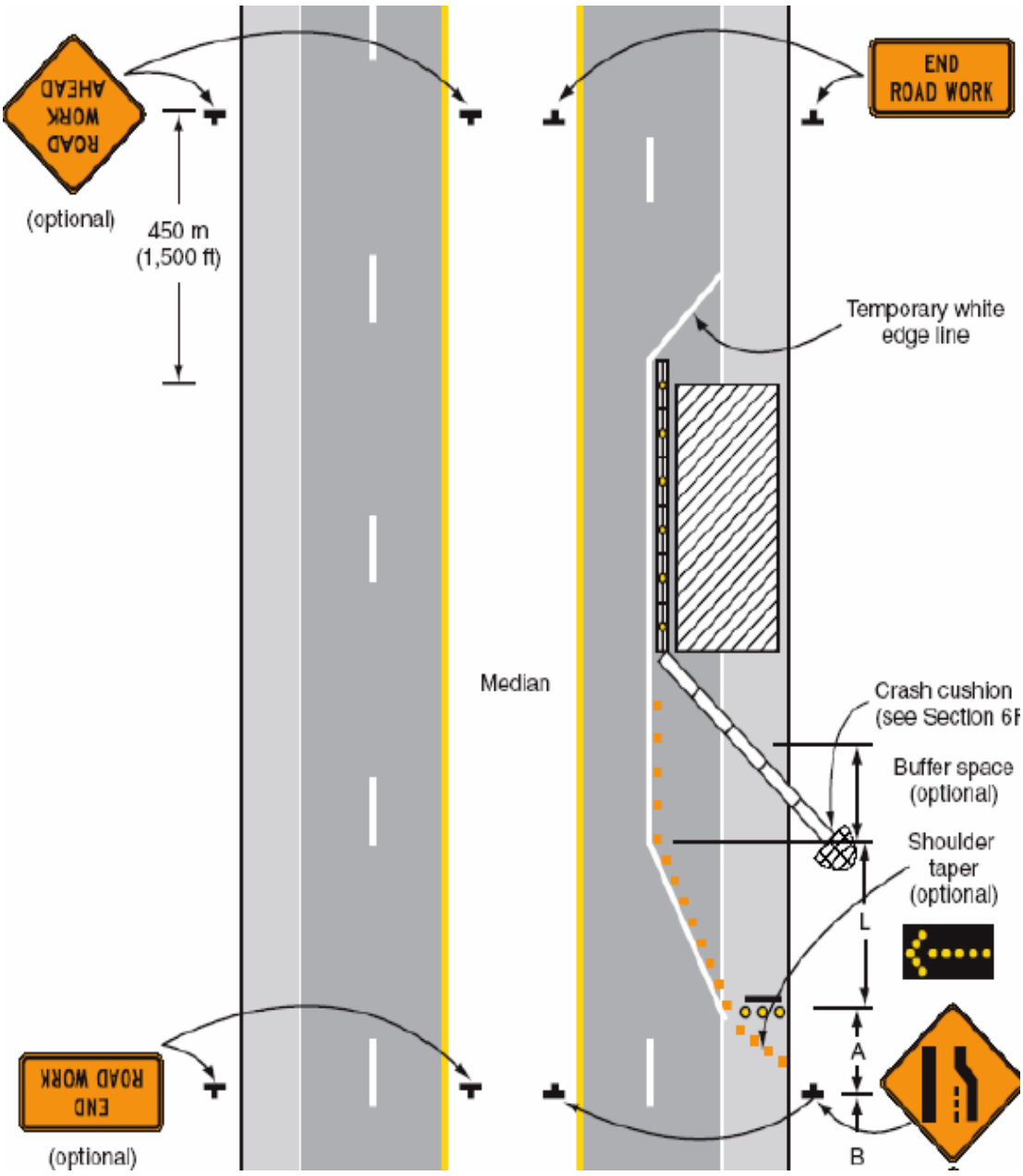

Figure 2- 7. Application of PWFBs at Work Zone (AHMCT Research Report)

The usage of PWFBs around work zone reduces the potential hazard due to errant vehicles in the area where the road conditions change frequently (R.B.Gover. et al. 2014). The additional colorful appearance of the barriers effectively alerts drivers to change their driving pattern when moving towards the work zone or reduced speed regions.

The kinematic response of PWFBs is significantly related to the impact severity and location of the impact point. A more than 10-degree impact angle substantially raises the probability of injuries associated with whiplash to the component (Salgo, 2004). PWFBs show excellent performance at low speeds, but the performance at higher speeds needs to be improved, to contain and redirect collision vehicles. When a high severity impact occurs, plastic shells of PWFBs tend to deform inelastically and fracture to absorb the impact energy. Both failures of the barrier shells and joint mechanisms fail to contain and redirect vehicles.

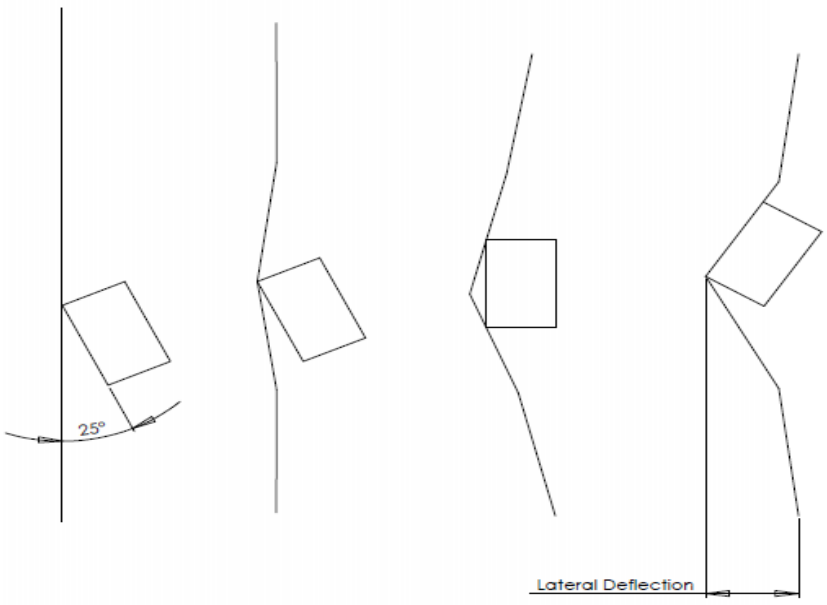

Figure 2- 8. Typical Vehicular Impact Sequence of PWFBs (AHMCT Research Report)

Unlike rigid barriers, the kinetic energy imparted to a plastic barrier result in lateral and longitudinal displacements of the barrier. A sizeable lateral displacement increases the probability of vehicle pocketing, snagging and over/under-riding the barrier (M.I. Thiyahuddin et al. 2013). Oversized lateral deflection is hazardous for the highway works and motorist safety. In most cases, the channelized work area is small, and the sizeable lateral displacement puts the workers in danger. In the collision, the failure of joint mechanisms results in PWFBs losing efficiency. Current PWFB joints used pin-joint mechanisms connected by male-female connections for convenient installation on site.

PWFBs first appeared in Europe playing a role as a channeling device. Later modules soon followed with increased physical size and a variety of interlocking joining mechanisms (Grzebieta et al., 2005). The PWFB was invented to match the size of the Jersey Concrete Barrier, which was developed in the 1950s at the Stevens Institute of Technology in New Jersey. With the application of PWFBs in the roadway, a phenomenon was observed that the polymetric barriers were vulnerable to plastic material cutting and fracture (Grzebieta et al., 2015). The failure of structural adequacy can lead to unpredictable occupant risk and potentially involve in a secondary collision. In order to improve the performance against structural failure, research has been done to improve the inherent structure of PWFB. Most of the current barriers contain irregular geometries on the barrier surface to prevent large deformation and fracture. Furthermore, steel reinforcements are also installed to increase the stiffness of the contact surface. These techniques are widely used in

current high impact level PWFBs and the crashworthiness of barriers has been significantly improved in recent years.

2.3.1 Triton PWFBs

Triton barriers are made of a lightweight polyethylene to contain water ballast weight. Segment shells are connected by sections interlocked together with pins. The lightweight polyethylene makes Triton a highly portable temporary barrier and convenient for on-site installation. The barrier shell is supported by a reinforced steel framework, and a cable connects barrier segments along the top of the barrier shell, providing the tensile capacity to adjacent barrier segments. Triton Barriers are designed to meet the requirement of test level 2 (TL) in NCHRP 350. Currently updated Triton Barriers are adequate for TL-3. The updating adjusts the height and raise its center of gravity through setting two 7 inches plastic pedestal. Both TL-2 and TL-3 Triton Barriers are accepted by the Federal Highway Administration and service to protect work zone roadway. The Triton Barrier can function on both foundation types of concrete and asphalt, and no anchored installation is needed.

Table 2- 1. Section Details of Triton PWFB (Triton Barrier Product Description Manual)

Test Level	TL-1	TL-2	TL-3
Height	2'-8"	2'-8"	3'-3"
Width	1'-9"	1'-9"	1'-9"
Length	6'-6"	6'-6"	6'-6"
Weight (Empty)	99 lbs	140 lbs	140 lbs
Weight (Full Filled)	1312 lbs	1350 lbs	1350 lbs
Color	White and Orange	White and Orange	White and Orange
Dynamic Deflection	8.9' (100')	12.8' (325')	22.6' (195')

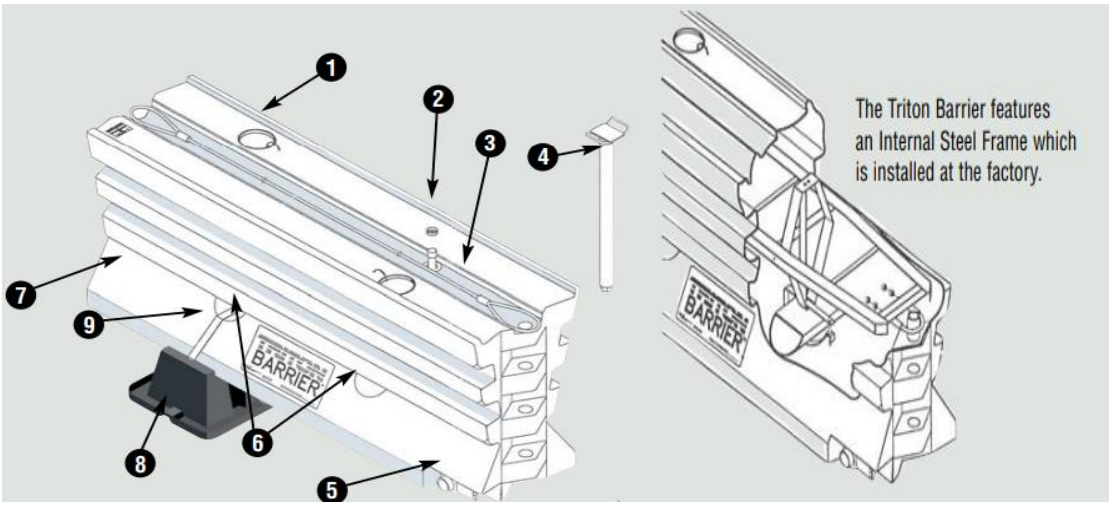

Figure 2- 9. Configuration of Triton PWFB Segment Shell and Internal Steel Frame (Triton Barrier Product Description Manual)

1. Fill hole cap
2. Fill level indicator
3. Factory installed tension cable
4. Connecting pin
5. Gate valve drain
6. Forklift ports
7. steel reinforced barrier section
8. TL-3 pedestal
9. TL-3 mounting straps

2.3.2 Yodock PWFBs

The Yodock barrier is another popular PWFB system based on the prototype of the Jersey concrete barrier. The barriers are divided into several different types of channelizing devices, each designed for a specific purpose. The 2001MB type is one of high performance and is a comprehensively used PWFB system. Similarly, the Yodock 2001 MB barrier is a longitudinal channelizing device designed based on evaluation criteria of NCHRP 350 and is approved for service in temporary work zones by Manual on Uniform Traffic Control Devices (FHWA). In addition, the Yodock PWFB system is the Americans with Disabilities Act of 1990 approved,

which enables the barrier to provide required pedestrian access in temporary work zones. The barrier shell is made of high-density polyethylene (HDPE) plastic and reinforced with steel rails, and the segment shells use the polyethylene couplers and rail kit connections. Unlike Triton PWFB, the application of Yodock 2001 MB is limited to concrete pavement. Additionally, the barrier can be filled with sand, rather than limited to water. In some states, especially in California, the drainage water is considered an environmental hazard and required to be transported and treated which raises total cost. In terms of crashworthiness, the behavior of the Yodock, 2001 MB is adequate from TL-1 to TL-3 of NCHRP 350 and presents reversative small post lateral deflection which is endurable in limited space of temporary work zone.

Table 2- 2. Section Details of Yodock 2001 MB PWFB Shell (Trinity Highway Rentals, Inc)

Test Level	TL-1	TL-2	TL-3
Height	2'-8"	2'-8"	3'-10"
Width	1'-6"(Base),8" (Top)	1'-6"(Base),8" (Top)	2'(Base),11" (Top)
Length	6'	6'	6'
Weight (Empty)	85 lbs.	85 lbs.	130 lbs.
Full Filled Weight	750 lbs.	750 lbs.	1530 lbs.
Color	Ivory and Orange	Ivory and Orange	Ivory and Orange
Dynamic Deflection	12' (150')	12' (150')	14' (148')

Figure 2- 10. Configuration of Yodock PWFB Shell (Trinity Highway Rentals, Inc)

2.3.3 Sentry Cable PWFB

The Sentry cable PWFB also has internally reinforced steel cable to protect the failure of structural adequacy. The steel cables provide additional strength in catching misguided vehicles and redirecting them when the fracture occurs in a barrier shell. The barrier shell is made of HDPE and has a total of 11 connecting lugs distributed at left-side and right-side end. The Sentry cable PWFB also is evaluated by NCHRP 350 criteria for TL-1 to TL-3, and is permitted to use as a longitudinal channelizing device by FHWA. The barrier is free standing and can be applied on concrete or a compacted dirt foundation type. Overall, the redirection capability and post-impact behavior of Sentry PWFB shows excellent behavior. However, the cost of the Sentry segment shell is higher than the average cost of market PWFB systems, so the application of Sentry may be limited by cost.

Table 2- 3. Section Details of Sentry PWFB (Sentry Water-Cable Barrier Installation, Maintenance, and Repair Manual)

Test Level	TL-1	TL-2	TL-3
Height	3'-10"	3'-10"	3'-10"
Width	1'-10.5"	1'-10.5"	1'-10.5"
Length	7'	7'	7'
Weight (Empty)	165 lbs.	165 lbs.	165 lbs.
Weight (Full Filled)	2150 lbs.	2150 lbs.	2150 lbs.
Color	White and Orange	White and Orange	White and Orange
Dynamic Deflection	5.9' (158')	5.9' (158')	9' (158')

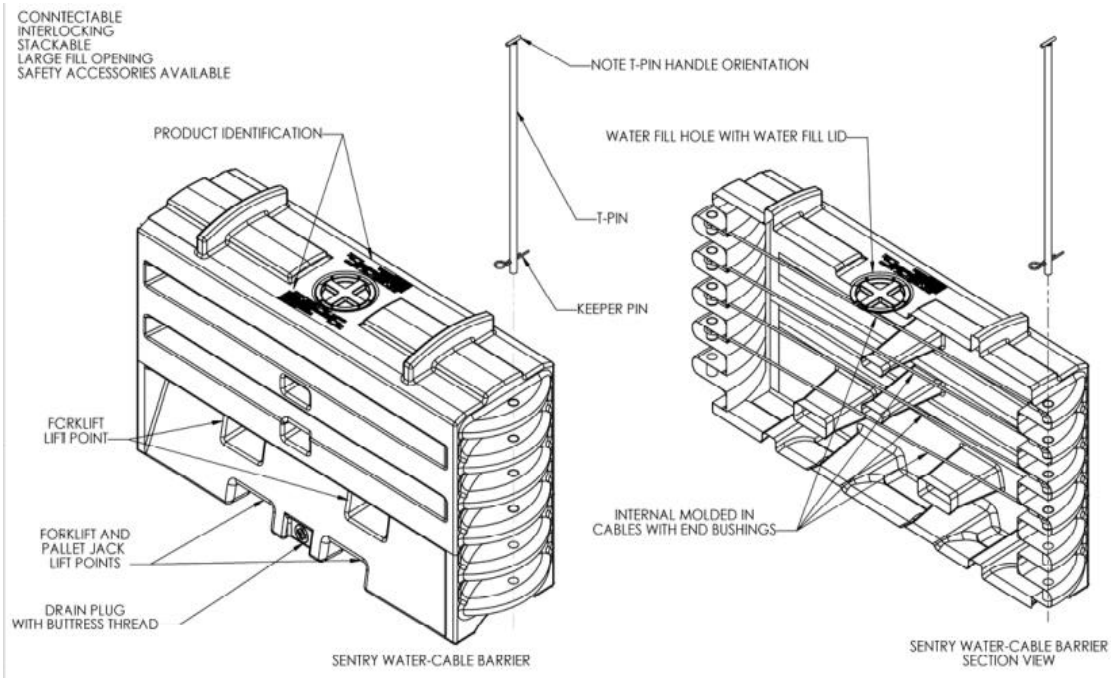

Figure 2- 11. Configuration of Sentry PWFB Components Details (Sentry Water-Cable Barrier Installation, Maintenance, and Repair Manual)

2.4 Experimental Investigation Guidelines

Currently, there are two valuable references for presenting uniform guidelines for crash testing of both permanent and temporary road safety features in the United States. Respectively, they are the Manual for Assessing Safety Hardware (MASH) and Recommended Procedures for the Safety Performance Evaluation of Highway

Features (NCHRP Report 350). Both MASH and NCHRP Report 350 recommends evaluation criteria to access experimental results. MASH is recommended for highway design engineers, bridge engineers, safety engineers, maintenance engineers, and others concerned with the safety features used in the highway environment. The recently updated new version of MASH (2016) gradually supersedes NCHPR Report 350. Guidelines for the design of roadside safety were contained within the Roadside Design Guide-AASHTO and adopted jointly by AASHTO. The new version of MASH was developed based on NCHRP Project 22-14(02), "Improvement of Procedures for the Safety-Performance Evaluation of Roadside Features." It has revised evaluation criteria of impact performance for all highway safety hardware. After the publication of a new version of MASH, Federal Highway Administration states all highway safety hardware accepted before the adoption of MASH – using criteria contained in NCHRP Report 350 admitted remaining in place and may continue to be manufactured and installed. In addition, highway safety hardware accepted by using NCHRP Report 350 criteria is not required to be retested using MASH criteria. However, newly developed highway safety hardware is mandatory to be evaluated followed by experimental guidelines and evaluation criteria of MASH.

2.4.1 Impact Conditions (MASH-2016)

Based on available run-off-the-road passenger vehicle crashes information, 85% of real-world impact conditions address the critical impact speed of 62mph (100 km/h) and approximately a 25-impact degree. This impact condition is considered suitable for high-speed, high-volume roadways. With respect to a lower volume and

lower impact speed condition, the impact speeds are respectively reduced to 44 mph (70 km/h) and 31mph (50 km/h). The impact angle of large trucks is reduced to 15 degrees due to cornering characteristics. However, the type, size, and weight of test vehicles have a significant bearing on the magnitude of the impact associated with the crash test. MASH developed and updated representative sizes and weights to adequately describe test conditions for impact. However, it is still difficult to obtain the exact weight of test vehicles. Excessive or inadequate vehicle mass leads to increasing or decreasing the impact loading. Hence, the tolerance intervals of test vehicle masses have been established. During testing, the ballast can be used for increasing the vehicle mass, and some removable components of vehicles can be used to decrease vehicle mass. The impact location also profoundly affects the performance of safety barriers. The impact location is determined based on the most critical condition that results in failure. For longitudinal barriers, critical impact points (CIPs) are selected to maximize loading at rail splices and maximize the potential for wheel snag and vehicle pocketing (MASH). The post-and-beam type barrier terminals are determined where the transition is predicted to present redirected behaviors. The testing agencies are recommended to conduct advanced analysis to locate the CIPs, such as computer numerical simulation.

Table 2- 4. Vehicle Test Inertial Mass Upper and Lower Limits (MASH-2016)

Test Vehicle Designation and Type	Target Vehicle Weight, lb (kg)	Acceptable Variation, lb (kg)
1100C (Passenger Car)	2,420 (1,100)	±55 (25)
1500A (Passenger Car)	3,300 (1,500)	±220 (100)
2270P (Pickup Truck)	5,000 (2,270)	±110 (50)
10000S (Single-Unit Truck)	22,000 (10,000)	±660 (300)
36000V (Tractor-Van Trailer)	79,300 (36,000)	±1,100 (500)
36000T (Tractor-Tank Trailer)	79,300 (36,000)	±1,100 (500)

2.4.2 Test Matrices

Longitudinal barriers are connected continuously along the side roadway which contains length-of-need and transition between barriers. The transition designs should depend on stiffness changes when adjacent barriers have an issue of stiffness changes. For example, if in a transition one barrier is more flexible than the other, the transition design should depend on the stiffness change in between the two barriers. This is mainly because stiffness changes potentially result in vehicle rollover, pocketing, or rail rupture. Although the road safety barriers are classified based on the structural stiffness, the test matrices of different types of barrier are almost the same where some special cases are introduced in the section of test installation of MASH. MASH developed six different test levels (TL) for helping users to find an appropriate application of design, operation, and maintenance of the roadway networks.

Table 2- 5. Recommended Test Matrices for Longitudinal Barriers (MASH-2016)

Test Level	Barrier Section[c]	Test No.	Vehic.	Impact Speed,[a] mph (km/h)	Impact Angle,[a] θ, deg.	Im-pact Point	Acceptable IS Range,[a] kip-ft (kJ)	Evaluation Criteria[b]
1	Length-of-Need	1-10 1-11	1100C 2270P	31 (50.0) 31 (50.0)	25 25	(c) (c)	≥13 (17.4) ≥27 (36.0)	A,D,F,H,I A,D,F,H,I
	Transition	1-20[d] 1-21	1100C 2270P	31 (50.0) 31 (50.0)	25 25	(c) (c)	≥13 (17.4) ≥27 (36.0)	A,D,F,H,I A,D,F,H,I
2	Length-of-Need	2-10 2-11	1100C 2270P	44 (70.0) 44 (70.0)	25 25	(c) (c)	≥25 (34.2) ≥52 (70.5)	A,D,F,H,I A,D,F,H,I
	Transition	2-20[d] 2-21	1100C 2270P	44 (70.0) 44 (70.0)	25 25	(c) (c)	≥25 (34.2) ≥52 (70.5)	A,D,F,H,I A,D,F,H,I
3	Length-of-Need	3-10 3-11	1100C 2270P	62 (100.0) 62 (100.0)	25 25	(c) (c)	≥51 (69.7) ≥106 (144)	A,D,F,H,I A,D,F,H,I
	Transition	3-20[d] 3-21	1100C 2270P	62 (100.0) 62 (100.0)	25 25	(c) (c)	≥51 (69.7) ≥106 (144)	A,D,F,H,I A,D,F,H,I
4	Length-of-Need	4-10 4-11 4-12	1100C 2270P 10000S	62 (100.0) 62 (100.0) 56 (90.0)	25 25 15	(c) (c) (c)	≥51 (69.7) ≥106 (144) ≥142 (193)	A,D,F,H,I A,D,F,H,I A,D,G
	Transition	4-20[d] 4-21 4-22	1100C 2270P 10000S	62 (100.0) 62 (100.0) 56 (90.0)	25 25 15	(c) (c) (c)	≥51 (69.7) ≥106 (144) ≥142 (193)	A,D,F,H,I A,D,F,H,I A,D,G
5	Length-of-Need	5-10 5-11 5-12	1100C 2270P 36000V	62 (100.0) 62 (100.0) 50 (80.0)	25 25 15	(c) (c) (c)	≥51 (69.7) ≥106 (144) ≥404 (548)	A,D,F,H,I A,D,F,H,I A,D,G
	Transition	5-20[d] 5-21 5-22	1100C 2270P 36000V	62 (100.0) 62 (100.0) 50 (80.0)	25 25 15	(c) (c) (c)	≥51 (69.7) ≥106 (144) ≥404 (548)	A,D,F,H,I A,D,F,H,I A,D,G
6	Length-of-Need	6-10 6-11 6-12	1100C 2270P 36000T	62 (100.0) 62 (100.0) 50 (80.0)	25 25 15	(c) (c) (c)	≥51 (69.7) ≥106 (144) ≥404 (548)	A,D,F,H,I A,D,F,H,I A,D,G
	Transition	6-20[d] 6-21 6-22	1100C 2270P 36000T	62 (100.0) 62 (100.0) 50 (80.0)	25 25 15	(c) (c) (c)	≥51 (69.7) ≥106 (144) ≥404 (548)	A,D,F,H,I A,D,F,H,I A,D,G

Table 2- 6. Detailed Description of Test Level (MASH-2016)

Test Level	Test Vehicle Designation* and Type	Test Conditions	
		Speed mph (km/h)	Angle (degrees)
1	1100C (Passenger Car) 2270P (Pickup Truck)	31 (50) 31 (50)	25 25
2	1100C (Passenger Car) 2270P (Pickup Truck)	44 (70) 44 (70)	25 25
3	1100C (Passenger Car) 2270P (Pickup Truck)	62 (100) 62 (100)	25 25
4	1100C (Passenger Car) 2270P (Pickup Truck) 10000S (Single-Unit Truck)	62 (100) 62 (100) 56 (90)	25 25 15
5	1100C (Passenger Car) 2270P (Pickup Truck) 36000V (Tractor-Van Trailer)	62 (100) 62 (100) 50 (80)	25 25 15
6	1100C (Passenger Car) 2270P (Pickup Truck) 36000T (Tractor-Tank Trailer)	62 (100) 62 (100) 50 (80)	25 25 15

MASH developed recommended test matrices for conducting full-scale testing of longitudinal barriers. The matrices combined mandatory test parameters in corresponding TLs to guide users to develop an appropriate testing setting.

2.4.3 Evaluation Criteria

The establishment of properly performance-based evaluation criteria has been a practical solution to improve the performance of safety features. Dependent on the technical and economic circumstances will depend on the performance and cost-effectiveness of the barrier. The recommended evaluation criteria should be considered as general guidelines rather than absolute criteria due to the complex nature of dynamic responses of a complex vehicular collision. Ultimately, test agencies have responsibilities to establish evaluation criteria for the implementation of evaluated safety features. The developed evaluation criteria are only related to the

impact performance of the safety feature, which means that the cost, aesthetics, maintainability, durability, and other service requirements need to be further evaluated.

Table 2- 7. Evaluation Criteria of Occupant Risk (MASH-2016)

<table>
<tr><th>Evaluation Factors</th><th>Evaluation Criteria</th><th>Applicable Tests</th></tr>
<tr><td rowspan="6">Occupant Risk (see Section 5.2.2)</td><td>D. Detached elements, fragments, or other debris from the test article should not penetrate or show potential for penetrating the occupant compartment, or present undue hazard to other traffic, pedestrians, or personnel in a work zone.

Deformations of, or intrusions into, the occupant compartment should not exceed limits set forth in Section 5.2.2 and Appendix E.</td><td>All</td></tr>
<tr><td>E. Detached elements, fragments, or other debris from the test article, or vehicular damage should not block the driver's vision or otherwise cause the driver to lose control of the vehicle.</td><td>70, 71, 72</td></tr>
<tr><td>F. The vehicle should remain upright during and after collision. The maximum roll and pitch angles are not to exceed 75 degrees.</td><td>All except those listed in Criterion G</td></tr>
<tr><td>G. It is preferable, although not essential, that the vehicle remain upright during and after collision.</td><td>12, 22</td></tr>
<tr><td>H. Occupant impact velocities (OIV) (see Appendix A, Section A5.2.2 for calculation procedure) should satisfy the following limits:
<table>
<tr><th colspan="3">Occupant Impact Velocity Limits, ft/s (m/s)</th></tr>
<tr><th>Component</th><th>Preferred</th><th>Maximum</th></tr>
<tr><td>Longitudinal and Lateral</td><td>30 ft/s (9.1 m/s)</td><td>40 ft/s (12.2 m/s)</td></tr>
<tr><td>Longitudinal</td><td>10 ft/s (3.0 m/s)</td><td>16 ft/s (4.9 m/s)</td></tr>
</table></td><td>10, 11, 20, 21, 30, 31, 32, 33, 34, 35, 36, 37, 38, 40, 41, 42, 43, 44, 50, 51, 52, 53, 80, 81, 82, 90, 91

60, 61, 62, 70, 71, 72</td></tr>
<tr><td>I. The occupant ridedown acceleration (see Appendix A, Section A5.2.2 for calculation procedure) should satisfy the following limits:
<table>
<tr><th colspan="3">Occupant Ridedown Acceleration Limits (G)</th></tr>
<tr><th>Component</th><th>Preferred</th><th>Maximum</th></tr>
<tr><td>Longitudinal and Lateral</td><td>15.0 G</td><td>20.49 G</td></tr>
</table></td><td>10, 11, 20, 21, 30, 31, 32, 33, 34, 35, 36, 37, 38, 40, 41, 42, 43, 45, 50, 51, 52, 53, 54, 60, 61, 62, 70, 71, 72, 80, 81, 90, 91</td></tr>
</table>

Table 2- 8. Evaluation Criteria of Structural Adequacy (MASH-2016)

Evaluation Factors	Evaluation Criteria	Applicable Tests
Structural Adequacy (see Section 5.2.1)	A. Test article should contain and redirect the vehicle or bring the vehicle to a controlled stop; the vehicle should not penetrate, underride, or override the installation although controlled lateral deflection of the test article is acceptable.	10, 11, 12, 20, 21, 22, 30[a],31[a],32[a],33[a], 34[a], 35, 36, 37[a], 38[a]
	B. The test article should readily activate in a predictable manner by breaking away, fracturing, or yielding.	60, 61, 62, 70, 71, 72, 80, 81, 82
	C. Acceptable test article performance may be by redirection, controlled penetration, or controlled stopping of the vehicle.	30[b], 31[b], 32[b], 33[b], 34[b], 37[b], 38[b], 40, 41, 42, 43, 44, 50, 51, 52, 53, 90, 91

Table 2- 9. Evaluation Criteria of Post-Impact Vehicular Response (MASH-2016)

Evaluation Factors	Evaluation Criteria	Applicable Tests
Post-Impact Vehicular Response (see Section 5.2.3)	J. through M. Reserved.	
	N. Vehicle trajectory behind the test article is acceptable.	30[b], 31[b], 32[b], 33[b], 34[b], 37[b], 38[b], 40, 41, 42, 43, 44, 45, 60, 61, 70, 71, 72, 80, 81, 82, 90, 91

According to MASH, three Evaluation Factors were introduced for longitudinal barriers. These include structural adequacy, occupant risk, and post-impact vehicular response. Structural adequacy is generally the first factor to be investigated. The structural adequacy should enable the redirection of vehicles, stopping the cars in a controlled manner, or permitting the cars to break through the devices. The structural requirement is only expected to associate with impact itself instead of other structural aspects of safety features. The occupant risk has a large extent depends on the crashworthiness of the impacting vehicle. The crashworthiness is associated with occupant compartments, such as structural integrity, padding, restraint system, etc. No penetration of any elements should be allowed, and the displacement of the full-size barrier should be limited.

Furthermore, it is not realistic to establish absolute criteria in terms of trajectory, debris scatters, or barrier displacement. However, related test data are supposed to be recorded for making an objective assessment and intended application by test agencies. The post-impact vehicular response is a measurement of the potential risk of impact vehicles being involved in a secondary collision which increases the potential risk to occupants of the crash vehicle and other vehicles. Excessive pocketing or snagging can result in a high vehicular exit angle or spin-out of the vehicle which is difficult to describe post-impact trajectory. However, a smoothly redirected vehicular post-response is desirable.

CHAPTER 3. EXPERIMENTAL STUDY

3.1 Introduction

A general test configuration was considered to evaluate the collision energy absorption ability of barriers with an inner diamond honeycomb shape cell. Compared to small-scale testing, full-scale vehicle-barrier tests are very costly. Hence, in the early stage of this research, a preliminary impact test was developed in small scale. The test evaluated the effectiveness of energy absorption concerning different ratios of total diamond cells length and the different volume of infilled water regarding fixed and friction boundary conditions. A small-scale designed PWFB was printed via the MakerBot 3D printer, and a simple pendulum impact test was developed. The impact energy was generated via a motion of a free-falling body of weight. In the process, a video camera was used to record the process of the kinetic responses of the barrier specimens and determine the post-impact location at the highest point to obtain the energy absorption due to barrier-collision object, based on the law of conservation of energy. A similar test has been done by two undergraduate students (Siyuan Chen and Hongchuan Li) in their independent study, but the testing does not address the energy absorption of varied water level, friction BC and varied impact angle. The tests presented in this thesis introduces several more test parameters to further the research. The energy absorption-based evaluation criterion is developed from longitudinal traffic barrier evaluation criteria in the American Association of State Highway and Transportation Officials-Manual for Accessing Safety Hardware (ASSHTO-MASH).

3.2 Barrier Design and Small-Scale Specimens

In terms of energy absorption of PWFB systems, the energy can neither be created nor destroyed; it can only be transformed or transferred from one form to another. The energy absorption is the total energy reduction of the collision object before impact and after impact. The absorbed energy transfers to kinetic energy and a small portion of the absorbed energy is dissipated by the system. Farren and Taylor indicate that the process of energy dissipation is irreversible in which the input of mechanical energy transferred to thermal energy (Farrer and Taylor, 1925). Uang and Bertero give an equation for energy balance as followed (Uang and Bertero, 1990).

$$E_i = E_k + E_\xi + E_a = E_k + E_\xi + E_s + E_h, \text{ where} \quad (1)$$

E_i: (absolute) input energy

E_a: absorbed energy

E_k: (absolute) kinetic energy

E_s: elastic strain energy

E_ξ: viscous damping energy

E_h: hysteric energy

In this formulation, the input energy is impact energy caused by collision vehicle, and the absorbed energy is the total energy reduction by PWFB systems. With respect to PWFBs, the system consists of barrier shell and filled water. In this case, a portion of the absorbed energy transfers to the kinetic energy of barrier shell and filled water. During the impact process, the deformation patterns of the barrier shell are elastic and inelastic corresponding to the elastic strain energy dissipation and hysteric

(plastic) strain energy dissipation, respectively. Additionally, frictional dissipation is also part of the total energy dissipation in terms of vehicular collision.

The honeycomb cell structures present a high specific stiffness and a superior energy absorption capacity compared to structures made of the same materials and mass (Zhang X et al., 2014 and Gaitanaros S et al., 2015). Based on the characteristics of honeycomb cells, honeycomb cells are popularly used to increase structural strength and reduce material cost simultaneously, similar to the idea of using steel frames to reinforce the barrier shells against extensive deformation due to impact loading. The research team developed a PWFB system with internal honeycomb cell structures to increase the crashworthiness of the PWFB system.

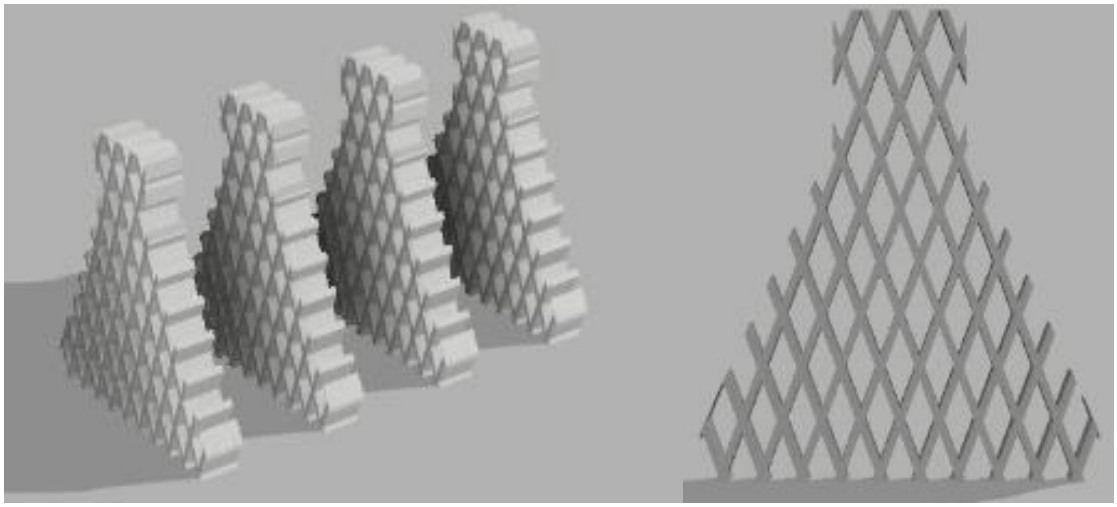

Figure 3- 1. Configuration of the Developed Quadrangle Shaped Interior Honeycomb Cells

Comparing with triangle, quadrangle, and hexagon shape of diamond, the quadrangle shape diamond presents the highest effective stiffness while the missing or fracture of cells occurs (Wang A and Mcdowell D.L., 2003). The Triangle diamond shape has the highest initial stiffness, but the effective elastic stiffness is reduced

much more than the quadrangle hexagon type of diamond when honeycomb cells fracture. Hence, the quadrangle shape of diamond was chosen to reinforce and increase the energy absorption of PWFB segments. The developed honeycomb PWFB is based on a prototype of a plastic jersey JB-32 barrier. The developed PWFB keeps the same full-scale dimension of the JB-32 barrier in which the appearance and barrier dimensions are most representative of currently marketed PWFB. The research team created JB-32 based barrier shell and added honeycomb cells in the SolidWorks platform. Two undergraduate students Siyuan Chen and Hongchuan Li printed small-scale barrier specimens via MakerBot 3D Printer. Due to space limitations on the printing platform, 9% scale ratio is selected. The configuration of the developed barrier prototype is shown below.

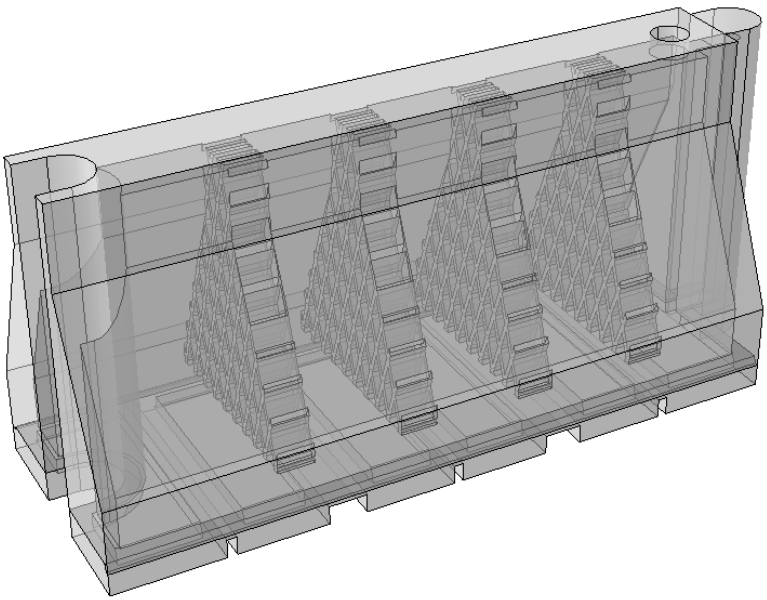

Figure 3- 2. Configuration of the developed PWFB with a Length Ratio of 0.25 Internal Cells

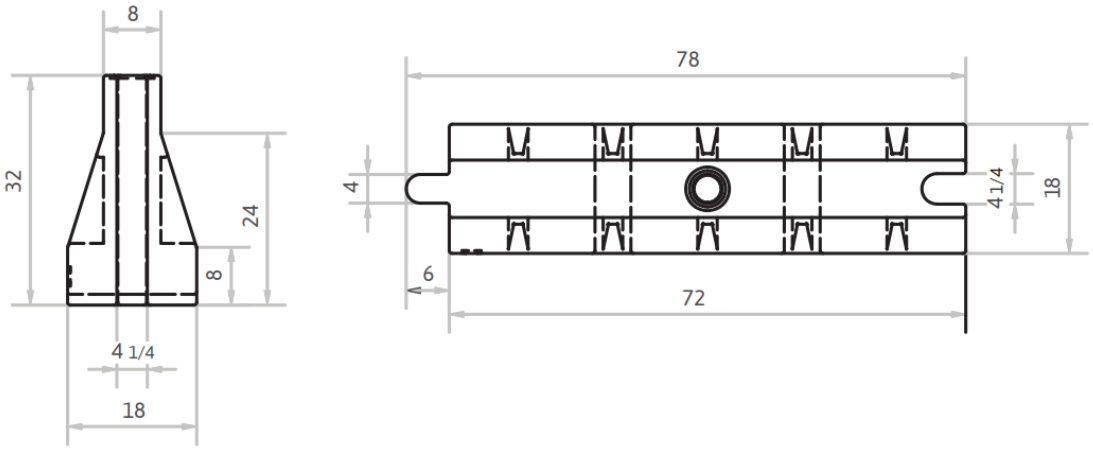

Figure 3- 3. Dimension of the Full-Scale JB-32 Barrier Specimen, inches

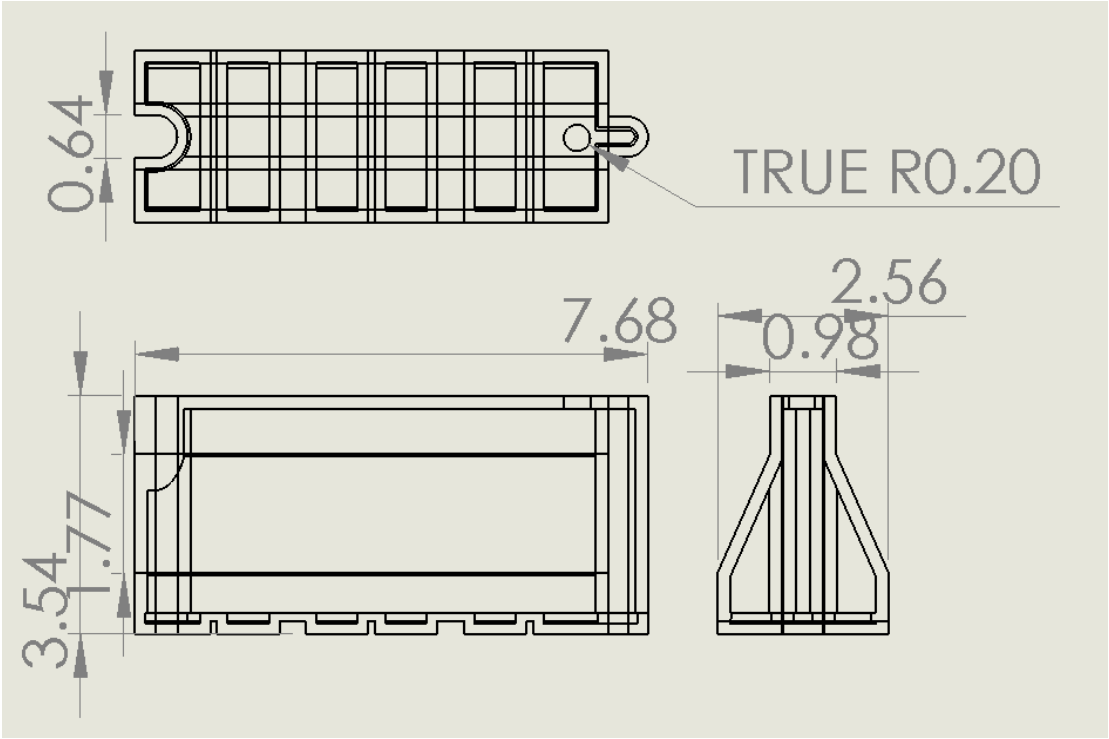

Figure 3- 4. Dimension of the Developed Small-Scale Barrier Specimen, inches

3.3 Test Parameters

3.3.1 Length Ratio

The length ratio is the ratio of the total interior cell length over the longitudinal length of barriers. In the design process, varied length ratios were considered in order to reach the most effective one in terms of energy absorption. A longer length of internal cells results in a higher total weight of barrier segments which reduce the portability. The printed specimens have four different length ratios as shown above. They are 0, ¼. ½ and ¾. The most effective length ratio will be determined during testing.

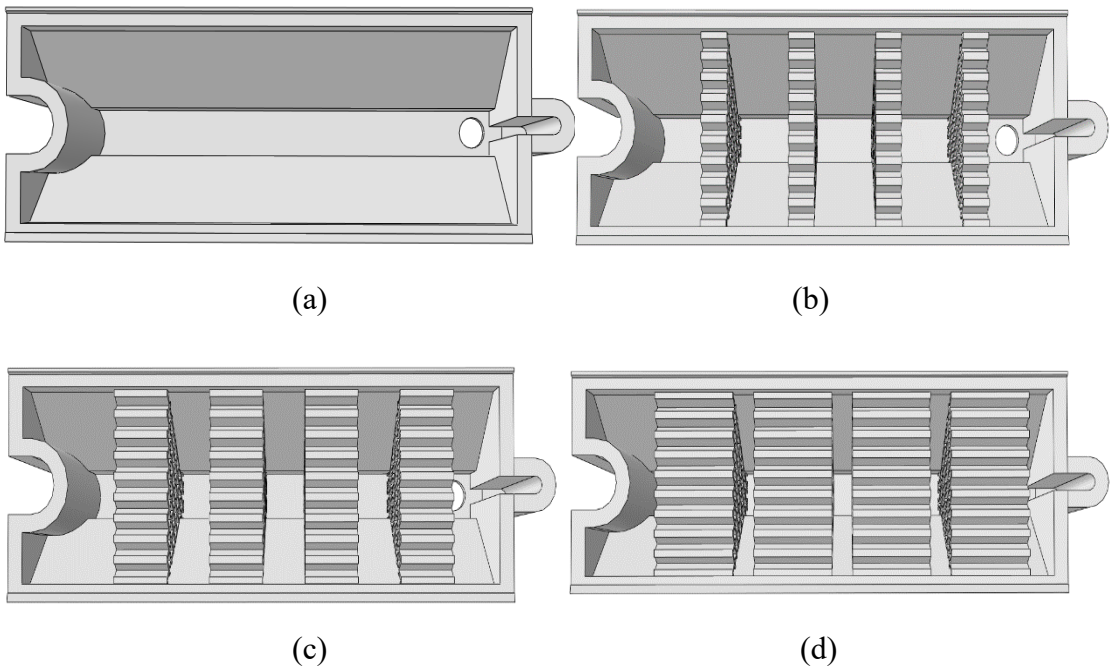

Figure 3- 5. Configuration of the Different Length Ratio of Internal Cells, (a) Ratio 0, (b) Ratio 0.25, (c) Ratio 0.5 and (d) Ratio 0.75

3.3.2 Water Level

Water as a cheap material and environmentally friendly, is commonly used for plastic traffic barrier as blast weight. Take consideration of the energy absorption provided by filled water. One consideration is that water increases the system's mass inertia and frictional dissipation. Another consideration is the sloshing effect of water, in which the excited water absorbs a portion of impact energy during impact loading. Both of these characteristics contribute to a higher energy absorption effect and make PWFBs a cost-effective road safety feature. However, the developed internal cells barriers potentially limit the motion of filled water which may reduce the total energy absorption of barrier systems. In order to properly evaluate these characteristics, four water levels were developed, classified as ¼, ½, ¾ and 1. Each of water level will be tested with each length ratio to assess the performance of each combination during testing.

3.3.3 Barrier Bottom Boundary Condition

In this testing, both friction boundary condition and fixed boundary condition were considered. In the friction BC, the bottom of barrier specimens is controlled by friction between the ground surface and the bottom surface of barrier. The friction BC investigates the energy dissipation under friction which is close to the real condition in-field. In the fixed BC, the base of barrier specimens is fixed on testing board to against translational and rotational displacement. The fixed BC is the worst scenario to address the impact resistance of barrier segments. In this case, the testing maximizes the impact effects to evaluate the structural adequacy. Unlike the friction case, the mass inertial and bottom frictional dissipation effects are eliminated in a

fixed BC. The fixed BC was designed to address the energy absorption behavior only caused by increasing the length ratio. Besides, the energy absorption equals to the sum of strain and contact frictional dissipation in fixed BC.

3.3.4 Critical Impact Angle

For longitudinal barriers, the impact angle is defined as the angle between normal direction of traffic and approach path of test vehicle into the test article (MASH). Safety hardware is generally placed along and parallels to the roadside; the impact angle may vary depending on the vehicle's collision path. Corresponding to the description of test, the prescribed test matrices for longitudinal barriers suggest impact angle is 25 degrees, and the maximum roll and pitch angles are not to exceed 75 degrees. Taking into consideration of the complex traffic model in temporary working zone; the impact angles were settled as 25 degrees, 45 degrees and 75 degrees for the small-scale test.

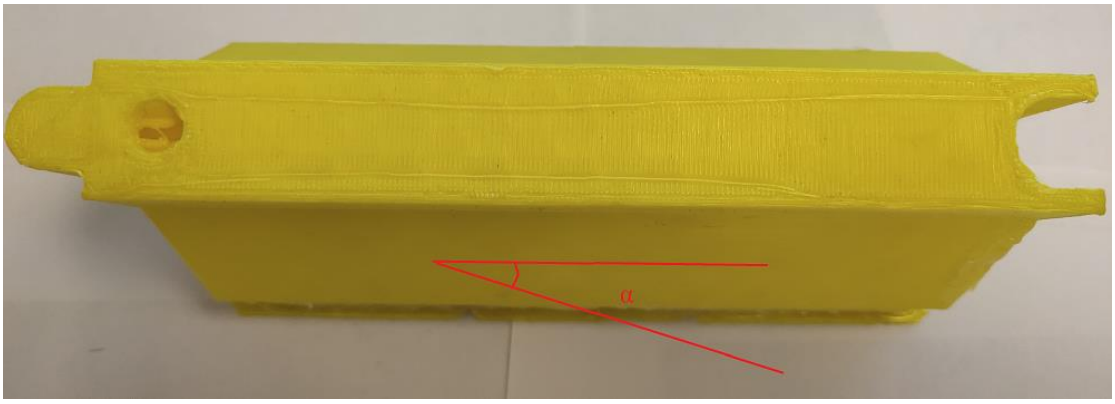

Figure 3- 6. Impact Angle for the Longitudinal Channelizing Devices

3.3.5 Critical Impact Location

For collision vehicles, there are two potential critical impact points. One potentially occurs at a hard point of wheel snagging. Another one may arise in the critical railing component of a collision vehicle such as a splice. The impact locations are determined based on the worst scenario of these two points, which maximize the risk of the failure. The significant variation of the impact location may dramatically affect the performance of the barrier. The bumper height of vehicles was considered in order to find the height of impact location of barrier specimens. Since the impact location can be determined from the ratio of bumper height to the height of the full-scale obstacles. Based on the recommendation from MASH, a mid-size test vehicle 1500A (Passenger Car) was selected, having 1500 kilograms. For most common vehicles, the bumper height is the 1/4 of vehicle height which generally around 370 mm (14.6 inches) based on 2012 Ford Focus Dimension. The height of full-scale barriers is 34 inches. Therefore, the ratio of bumper height to barrier height can be determined as 0.43. The impact location during this test is 1.42 inches from the bottom.

Table 3- 1. Vehicle Test Inertial Mass (MASH-2016)

Test Vehicle Designation and Type	Target Vehicle Weight, lb (kg)	Acceptable Variation, lb (kg)
1100C (Passenger Car)	2,420 (1,100)	±55 (25)
1500A (Passenger Car)	3,300 (1,500)	±220 (100)
2270P (Pickup Truck)	5,000 (2,270)	±110 (50)
10000S (Single-Unit Truck)	22,000 (10,000)	±660 (300)
36000V (Tractor-Van Trailer)	79,300 (36,000)	±1,100 (500)
36000T (Tractor-Tank Trailer)	79,300 (36,000)	±1,100 (500)

PWFBs are connected continuously along temporary work zone, and impact location may occur at any position of jointed barrier segments. Joints represent a discontinuity in the PWFB system, which the failure location has a higher chance happens around joint mechanisms. Failure of the joints due to complete tearing or fracturing of the barrier region surrounding the joint will render the barrier ineffective for vehicle re-direction (Thiyahuddin, etc. 2014). Current small-scale barriers have not developed the joint mechanisms to connect barriers segments. Additionally, behavior of joint mechanism is difficult to predict. Therefore, experimental impact testing is performed in the condition of single barrier and the critical impact point is selected at the middle point in longitudinal direction. The mid-point should obtain a more substantial deformation, compared to any other location which barriers have a higher potential to reach yield limit or fracture.

3.3.6 Scaled Impact Severity

The severity of an impact is typically measured in terms of impact severity (IS) for crash tests involving vehicle redirection, and kinetic energy (KE) for crash tests involving end-on impacts or breakaway devices (NCHRP Report 350). IS formulation shown below has been proved a good measurement to address the magnitude of loading on a longitudinal barrier. KE serve as an indicator of the severity of all head-on or end-on impacts, including test of breakaway devices, crash cushions, terminals, and truck-mounted attenuators (MASH). The IS and KE formulations are shown below.

$$KE = \tfrac{1}{2} M V^2 \quad (2)$$

Where:

KE = kinetic energy, kip-ft (kJ)

$$IS = \tfrac{1}{2} M \left(V \sin\theta\right)^2 \quad (3)$$

Where:

IS = impact severity, kip-ft (kJ)
M = vehicle mass, lb (kg)
V = impact speed, ft/s (m/s)
θ = impact angle, degrees

According to the test matrices description in MASH, Test 10 is selected; it is the most primary test conducted for all longitudinal barrier devices. Test 10 is designed to investigate a barrier's ability to successfully contain and redirect small passenger vehicles impacted within the length-of-need (MASH). However, the occupant risk associated with the collision vehicle and safety feature is difficult to measure and quantify especially in this small-scale testing. A more practical experimental study is supposed to emphasize evaluating the structural adequacy of honeycomb cell barriers. However, the evaluation criteria of this test are based on the energy-absorption of the system. The energy absorption can be seen by measuring the total energy reduction before and after the impact, in order to evaluate the effectiveness of honeycomb cells barriers.

The experiment performs at a small-scale condition by using 3D printed barrier specimens. Since impact energy in the motion process is expected to scale from a full-scale collision test. According to MASH, it recommends the practical range of IS value corresponding characteristics of testing. In the previous evaluation

criteria section, TEST 10 is selected as a template. The acceptable IS Range and Critical Value can be determined. Table 3-2 presents the Recommended Test Matrices for Longitudinal Barriers In the third column of the table, the first digit is used to identify the test level followed by the second digit that identifies the specific test in the series for each type of feature. The evaluation criteria of Test 10 in MASH is determined and suitable for this experiment. For this test, the full-scale IS value is determined as 17.4 KJ, as shown in column eight.

Table 3- 2. Recommended Test Matrices of Longitudinal Barriers for TL-1 (MASH-2016)

Test Level	Barrier Section[c]	Test No.	Vehic.	Impact Speed,[a] mph (km/h)	Impact Angle,[a] θ, deg.	Im-pact Point	Acceptable IS Range,[a] kip-ft (kJ)	Evaluation Criteria[b]
1	Length-of-Need	1-10 1-11	1100C 2270P	31 (50.0) 31 (50.0)	25 25	(c) (c)	≥13 (17.4) ≥27 (36.0)	A,D,F,H,I A,D,F,H,I
	Transition	1-20[d] 1-21	1100C 2270P	31 (50.0) 31 (50.0)	25 25	(c) (c)	≥13 (17.4) ≥27 (36.0)	A,D,F,H,I A,D,F,H,I

For purposed small-scale testing, the practical small-scale IS value is expected to scale from full-scale IS value. For three-dimensional small-scale energy, the energy density is constant during the scaling process (Hampton et al., 2013). Therefore, the scaled energy is linearly proportional to the volume of objects. A small-scale IS value can be determined based on volume ratio. Additionally, materials of full-scale and small-scale specimens are not identical. The small-scale barrier specimens made of Acrylonitrile Butadiene Styrene (ABS) plastic, and the large-scale barriers use Polyvinyl Chloride (PVC) plastic. Because of this, in order to properly scale the IS value, the difference in material density is considered. However, it is not practical to calculate the total volume of added interior cells; the current size of barrier specimens

is determined based on non-cells barrier specimens. Finally, the scaled IS value is determined as 0.88 KJ.

3.3.7 Mass and Velocity of the Impact Object

The small-scale mass of impact was obtained from a similar scaling process. The mass of steel ball is determined by the same density index of a sample Ford Focus. In impact testing, to simulate the vehicle crashes, a steel ball is used instead of a test vehicle, because the contact area of the steel ball and bumpers are sphere. In order to have a steel ball with 1.067 kg, the diameter needed for the ball was calculated approximately 2.5 inches. However, in comparing the contact area of the steel ball to vehicle bumper, the contact area is quite large which cannot adequately demonstrate the energy reduction due to dissimilar contact meaning. Because of this, the test utilized a smaller steel ball with a mass exactly 400 grams to reach the small-scale IS.

3.4 Methodology

The test used an idealized pendulum system to generate the collision energy and locate the impact location on barrier specimens. For impact testing, the idea of using a pendulum system to produce a desired impact energy is widely used in impact testing. The advantage of the pendulum is that it is easy to adjust the impact energy through changing the length of the swing arm and impactor release location. Besides, for other similar impact energy absorption test, the acquired impact resistance (absorbed energy) is more accurate based on kinetic energy difference (P.P. Li and Q.L. Yu, 2019). Similar pendulum impact tests have used a high-speed video camera

to record the post-response, and then the kinetic energy difference can be determined precisely. In this testing, the energy reduction is measured through calculation of the height difference from the initial release height and highest post-impact height. Based on the scale ratio and density index ratio, the scaled IS value can be determined. The mass of the impact object also holds a square relationship to impact velocity. A customized steel ball with 400 grams is released from a specified height then starts the circular motion under the influence of gravity. During the motion, gravitational potential energy transfers to kinetic energy and reaches the IS at the lowest point (collision location). After the collision, the remaining energy is transferred to gravitational potential energy, and the ball reaches a certain height. The energy absorption can be determined by the height difference between initial height and post height of the mass.

With respect to potential result errors, this developed test facility is idealized. The steel ball has a small surface area and smooth sphere solid shape; the air friction loss is minor and can be ignored. One could argue that, the system uses a cotton wire as swing arm, and therefore the tension in the wire could cause elongation, changing the intended impact location. In order to reduce the elongation of the wire, the wire is tension treated that has little strain under tensile stress in this test. Besides, the measurement of total energy reduction is completed through determining the height difference, recorded by a video camera. Comparing to the kinematic energy difference, the height recording may contain human errors. In order to minimize these errors, each test is performed three times, and results take an average of them.

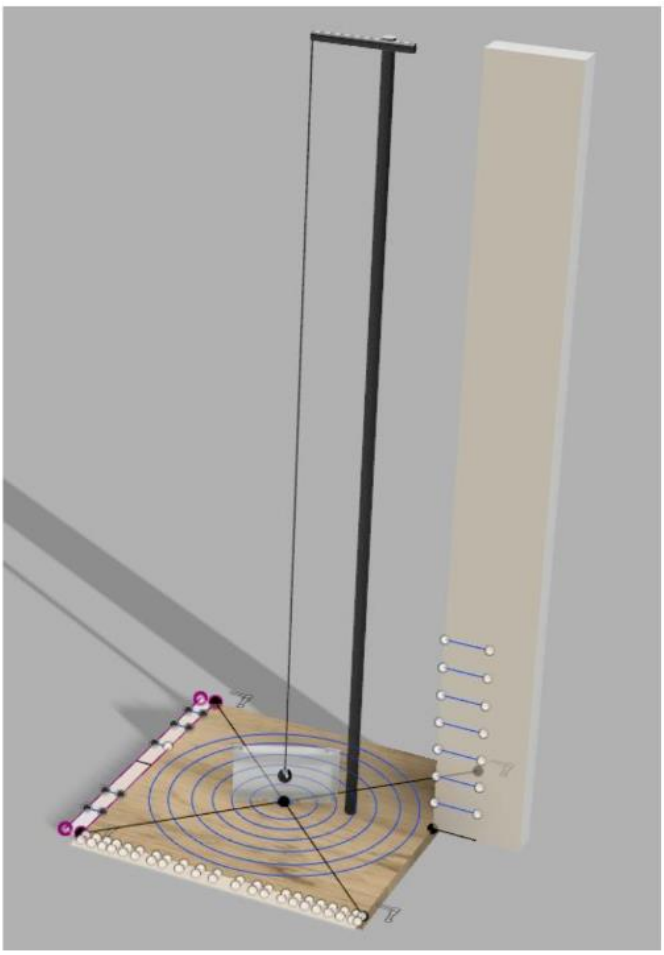

Figure 3- 7. Configuration of the Proposed Pendulum System (Li and Chen)

3.5 Test Conditions

Based on the developed critical test parameters, each test to be completed was composed of a different combination of each test parameters. With proper evaluation of each condition, the contribution of energy absorption due to various test parameters can be clearly addressed in the test result. The following flow chart helps to visualize the combinations of varied test parameters.

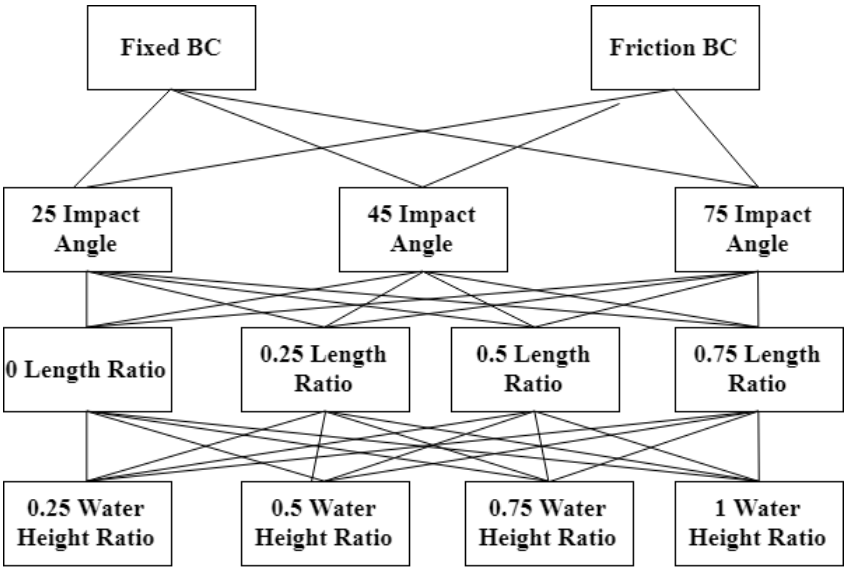

Figure 3- 8. Flow Chart of the Small-Scale Test Conditions

3.6 Testing Device

The small-scale pendulum testing facility is similar to a gravity pendulum, consisting of a frictionless pivot, massless rod, and massive bob. A steel rod acts as a frictionless pivot which anchors into different height onto a bolted steel column as shown in Figure 3-8. The bolted steel column allows easy adjustment to the length of the flexible swing arm flexible, which changes with increasing impact angle in the testing. A steel ball was selected as the impactor in this testing which the sphere contact surface is similar to the contact surface of the vehicle front bumper. In order to meet the mass demand of 400 grams, an ordered steel ball with approximately 520 grams has a section cut out of it. Additionally, the top surface of the steel ball is drilled into to create a hole which is used to place a plastic hook to connect the steel ball and cotton wire. Both operations reduce the mass of the original steel ball; finally, a 400-gram mass is obtained. The customized steel ball and plastic hook are shown below.

Figure 3- 9. Configuration of the Created Steel Ball and Plastic Hook Connection

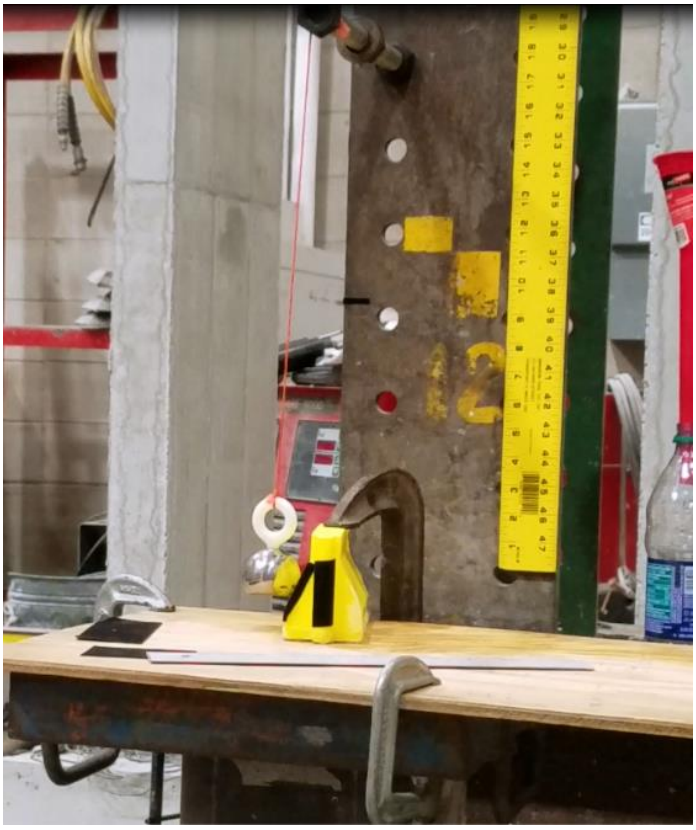

Figure 3- 10. Configuration of the Developed Pendulum Testing Device

The bottom timber board, on which the barrier rests, is fixed with a massive support base. For the friction boundary condition, the barrier specimens are simply placed on the bottom board. The bottom board has a rough surface that can provide a rational coefficient of friction simulating the bottom friction condition of full-scale barrier on the roadsides. With respect to the fixed condition, the barrier specimens are fixed on the board by using a steel clamp. In previous testing, the barrier specimens

were glued on the board; however, the glue connection was relatively weak, and did not provide full fixity to the board. A hard ruler is fixed on the steel column to measure the post-impact height. During the testing, a video camera is used to record the entire impact process and the final post-impact height is read from video analysis.

3.7 Test Result

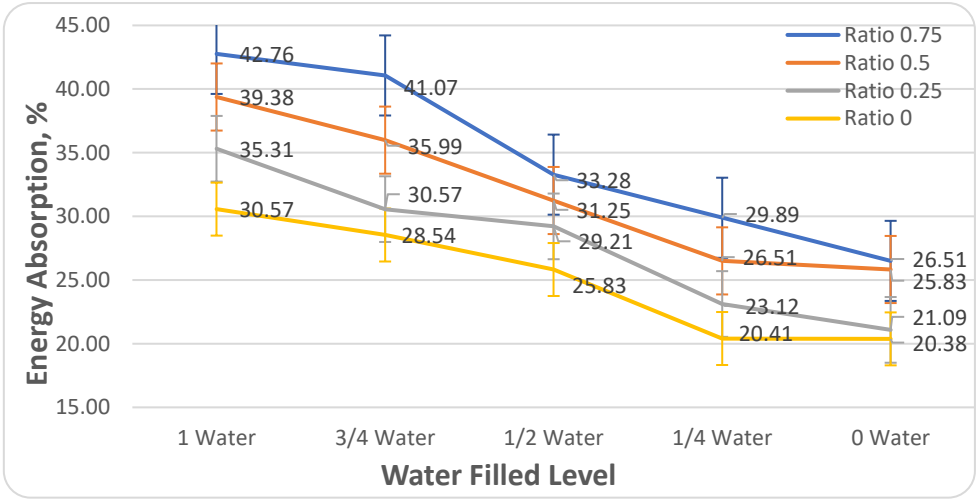

Figure 3- 11. Energy Absorption Results of 25 Impact Angle Fixed BC

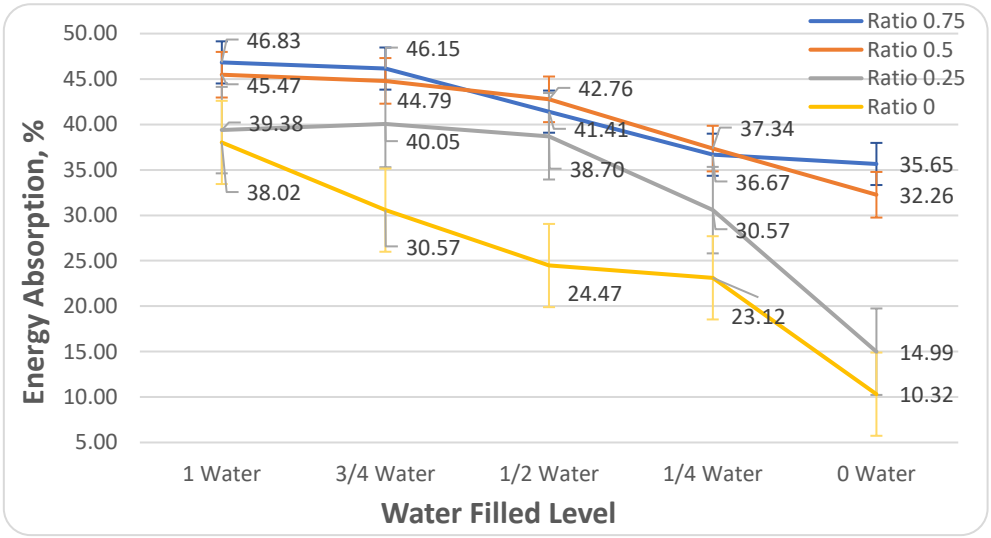

Figure 3- 12. Energy Absorption Results of 25 Impact Angle Friction BC

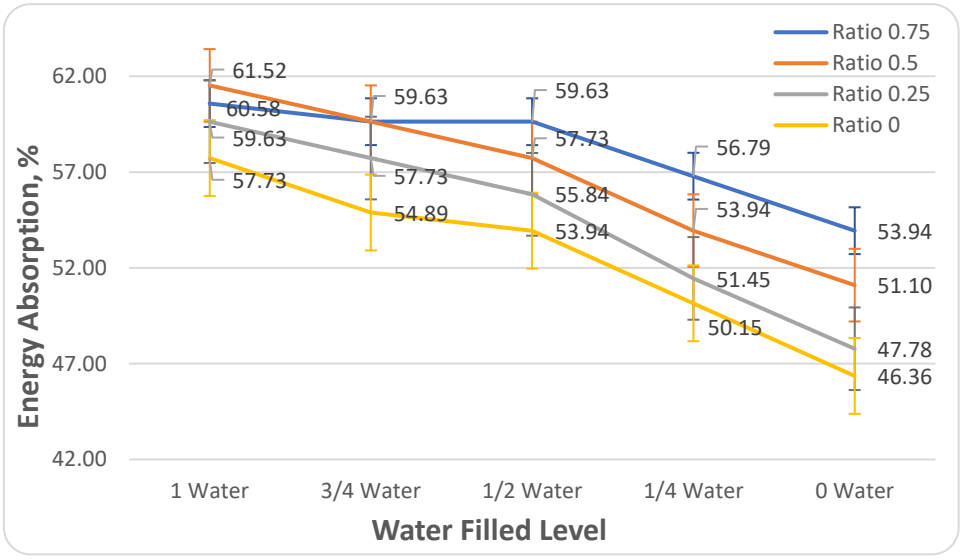

Figure 3- 13. Energy Absorption Results of 45 Impact Angle Fixed BC

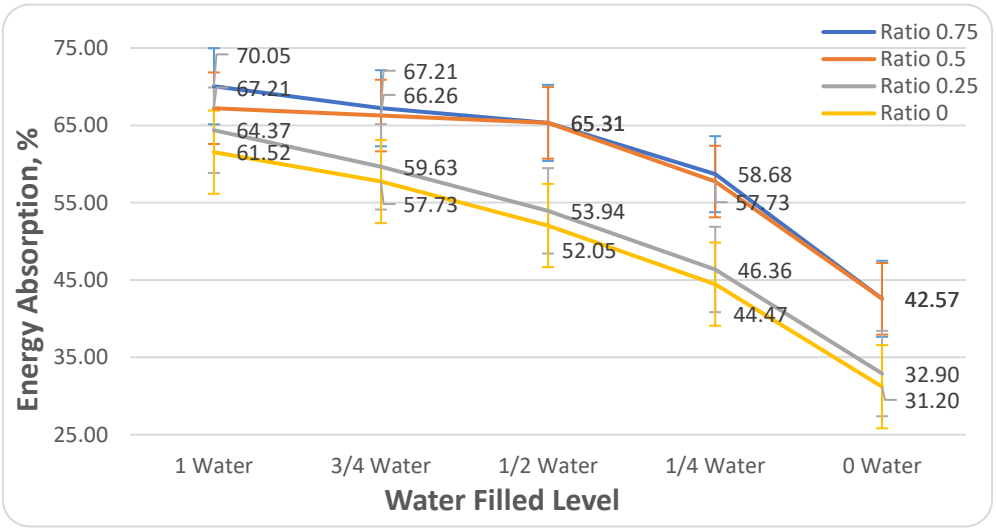

Figure 3- 14. Energy Absorption Results of 45 Impact Angle Friction BC

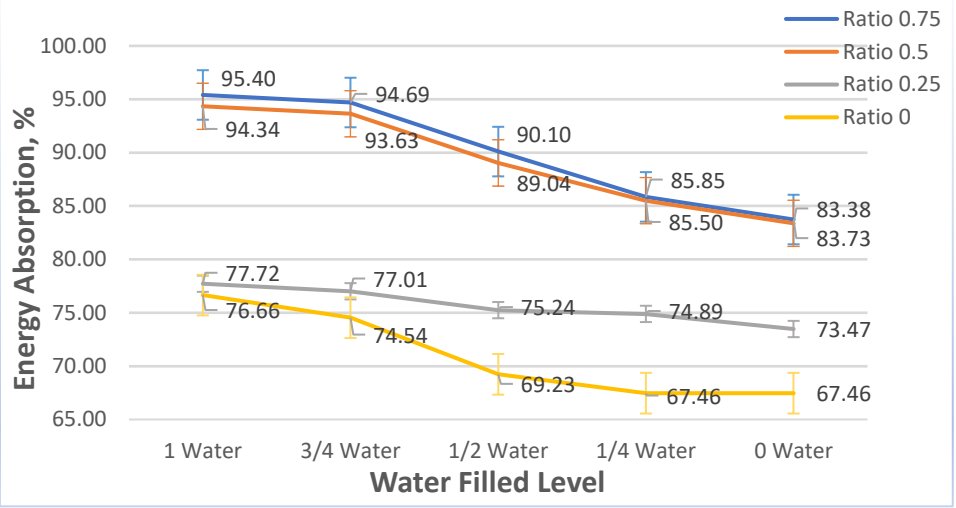

Figure 3- 15. Energy Absorption Results of 75 Impact Angle Fixed BC

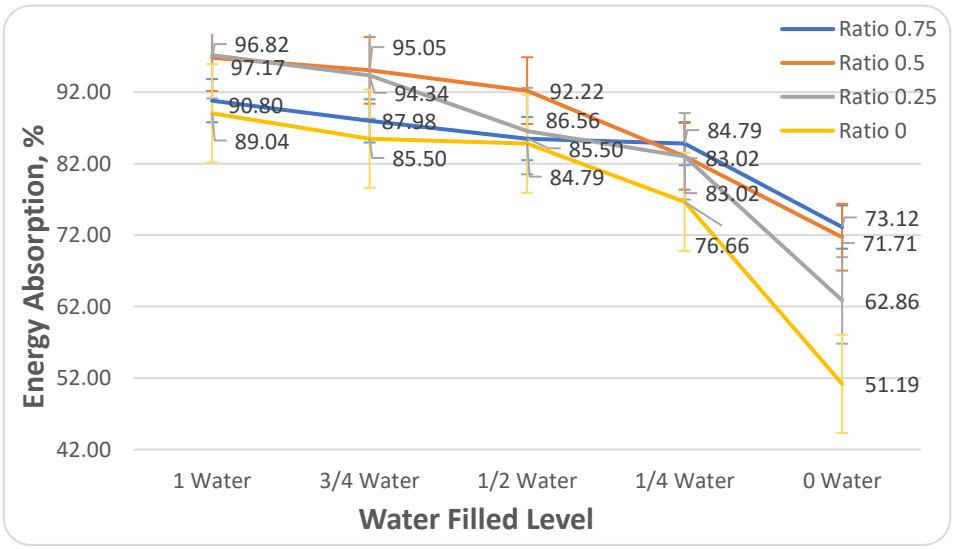

Figure 3- 16. Energy Absorption Results of 75 Impact Angle Friction BC

Table 3- 3. Test Data from Small-Scale Pendulum Test

Case	1 Water	3/4 Water	1/2 Water	1/4 Water	0 Water
Ratio 0.75 Percentage of Energy Absorption					
25 fixed	42.76	41.07	33.28	29.89	26.18
25 friction	46.83	46.15	41.41	36.67	35.76
45 fixed	60.58	59.63	59.63	56.79	53.94
45 friction	70.05	67.21	65.31	58.68	42.57
75 fixed	95.40	94.69	90.10	85.85	83.73
75 friction	90.80	87.98	85.50	84.79	73.12
Ratio 0.5 Percentage of Energy Absorption					
25 fixed	39.38	35.99	31.25	26.51	25.83
25 friction	45.47	44.79	42.76	37.34	32.12
45 fixed	61.52	59.63	57.73	53.94	51.10
45 friction	67.21	66.26	65.31	57.73	42.57
75 fixed	94.34	93.63	89.04	85.50	83.38
75 friction	96.82	95.05	92.22	83.02	71.71
Ratio 0.25 Percentage of Energy Absorption					
25 fixed	35.31	30.57	29.21	23.12	21.09
25 friction	39.38	40.05	38.70	30.57	14.99
45 fixed	59.63	57.73	55.84	50.15	46.36
45 friction	64.37	59.63	53.94	46.36	32.90
75 fixed	77.72	77.01	75.24	74.89	73.47
75 friction	97.17	94.34	86.56	83.02	62.86
Ratio 0 Percentage of Energy Absorption					
25 fixed	30.57	28.54	25.83	20.41	20.38
25 friction	38.02	30.57	24.54	23.12	10.32
45 fixed	57.73	54.89	53.94	50.15	46.36
45 friction	61.52	57.73	52.05	44.47	31.20
75 fixed	76.66	74.54	69.23	67.46	67.46
75 friction	89.04	85.50	84.79	76.66	51.19

3.8 Discussion

Each test was performed three times to minimize recording errors. In addition, average values were calculated, and percentage error bars are presented to address the credibility of test results. In both the friction and fixed BC, the motion of the steel ball is fluent, and the surface of barrier specimens is not penetrable. The kinetic response of the steel ball recorded by video camera indicates that the motion of steel ball is smoothly redirected, and barrier specimens absorb proportional impact energy.

Figure 3- 17. Configuration of Impact Response of Small-Scale Pendulum Testing

Since this observation illustrates the barrier specimens can contain and redirect the impact, the primary evaluation criteria in MASH is satisfied. After several impact tests, the barrier specimen without cells is relatively vulnerable, and a small number of horizontal cracks formed at the surface of specimen. This did not occur among the barrier specimens with cells. Overall, the four barrier specimens do not experience structural failures such as significant plastic deformation. In addition, the ABS plastic used in the 3D printing, consisted of high strength and relatively high elasticity, as

compared to other 3D printing materials. An assumption is made that the deformation pattern of barrier specimens remains in the elastic stage.

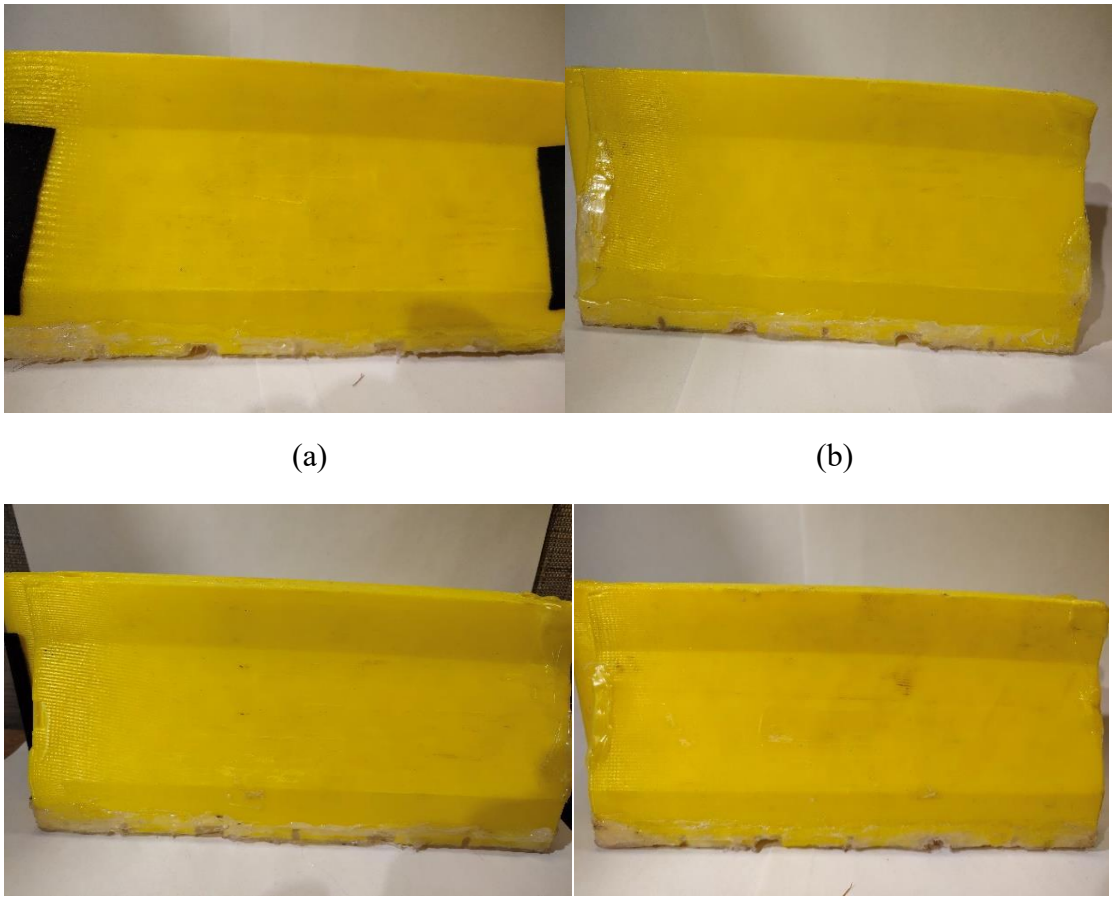

(a) (b)

(c) (d)

Figure 3- 18. Barrier Specimens after Testing (a) Ratio 0, (b) Ratio 0.25, (c) Ratio 0.5, and (d) Ratio 0.75

From the energy absorption bar charts, one observation can be found that increasing the length ratio of barriers results in higher energy absorption corresponding to varied bottom BC and impact angle. The elastic wave dissipation and contact frictional dissipation account for the absorbed energy in fixed BC case (Harb and Radwan, 2008). With respect to the friction BC, aside from elastic wave dissipation and frictional dissipation, a portion of the impact energy transfers to the kinematic energy of barrier shell. Comparing the non-water filled and water-filled

cases, the test results demonstrate that those barriers filled with water have a higher energy absorption in both fixed and friction BC. This is mainly because water has viscosity and helps to absorb the energy while movement occurs inside of barrier specimens. Additionally, filled water also increases the weight of barrier specimens which is another possible reason that filled water has higher energy absorption in friction boundary condition cases. Another observation found during the testing is that those full water filled barrier specimens tended to roll over after impact rather than remain standing upright. Comparing two cases, a standing up barrier has relatively more energy absorption compared to barrier that has rolled over. According to evaluation criteria, barrier specimens are expected to remain standing upright to minimize the risk of vehicle occupants.

The test results demonstrate that barrier specimens obtain more substantial energy absorption for an impact angle larger than 25 degrees. The reason is the expression of energy absorption is calculated based on energy reduction comparing to total impact energy. However, the overall impact energy is determined by IS value which decreases as the impact angle increases. More specifically, in looking at velocity vector, one can be decomposed the vector into perpendicular and parallel components to the barrier surface. While increasing the impact angle, the perpendicular vector remains constant while the parallel vector decreases. Therefore, the test results show a higher energy absorption while increasing the impact angle.

CHAPTER 4. FINITE ELEMENT MODELING

4.1 Introduction

Finite Element Analysis (FEA) is a numerical solution analysis and is commonly used to find approximate solutions to assess or investigate complex engineering problems. Once the testing is completed, the FEA can be carried out to validate the test result. In this study, the FEA is simulated by ABAQUS under Dynamics Explicit module. Each model was created two time-steps. The first is the linear acceleration of the impactor to reach purposed impact energy, and second involves the process of the impactor striking on the barrier surface and bouncing off. There are two main purposes of this FEM. The first is to validate the experimental data, and the second is to complete a further strength analysis. From the field output of Abaqus, the velocity vectors and system kinetic energy are plotted to obtain the energy reduction before and after the impact. The current small-scale testing missing deformation data is insufficient to evaluate the performance of the internal honeycomb structure barrier. However, additional FEMs are conducted to predict the deformation behavior for different length ratio. During the impact, filled water transfers from a state of rest to state of motion. The water movement inside of the barrier interacts with the interior surface of barrier, leading to an energy absorption effect. In order to consider this effect, the Computational Fluid Dynamic (CFD) models are developed to investigate the energy absorption by water sloshing effect.

4.2 Geometry and Modeling Definition

For the parametric study, several modeling cases are developed in terms of different boundary conditions. In this FEM, there is no significant change to modeling geometry, but just variation of the boundary conditions (BCs) such as fix, friction, impact angle, quantity of filled water. A parametric study was conducted regarding the combination of these BCs. Several primary parametric studies were conducted between fix and friction boundary condition. The fixed condition case consists of an impactor and barrier specimens. For the impactor, a solid steel ball was drawn with same dimension as used in experimental testing, which is determined based on the mass and density of steel in the testing. With respect to barrier specimens, the same geometry was used as used in testing. The geometries of the small-scale barrier specimens are imported from Solid Work files.

In the fixed case, the bottom of barrier is fixed to against rotational and translational displacement. The barrier shells resist all of impact energy and redirect the impactor. In friction boundary condition, an additional rigid plane shell is used to represent a friction board. The shell is defined as having a minimal thickness value and a coefficient of frictional factor between the surface and contact face of barrier specimens. The rigid shell has infinite stiffness, preventing it from deforming while resisting loads, and only exists to provide friction between two surfaces. For friction BC cases, the impact process is closed to reality which barrier shells are in state of motion after interacting with the impactor. Under normal gravity loading, the barrier specimens are free to rotate and move against friction. For both the fixed and friction

conditions, the contact method for interaction was defined by Isotropic Penalty Hard Contact method. In this method, the contact surfaces are defined separately such, steel ball-barrier surface and bottom barrier Surface-bottom shell surface. For Hard Contact Method, when surfaces are in contact, any contact pressure can be transmitted between them, and the surfaces separate if the contact pressure reduces to zero (Abaqus User's Manual). Considering the material of contact surface, the polythene-steel ball, and polythene-wood friction board coefficients are determined as 0.2 and 0.35, respectively. In Abaqus CAE, the velocity is assigned in vectors in the X, Y and Z direction and impact angle is defined through adjusting the velocity vectors. Purposed impact velocity is obtained through a linear tabular amplitude acceleration from static stage in modeling step 1. Then, in step 2, the steel ball is released from its constraint until impact is made with barrier surface. The following figures present the two primary assembly geometries in FE models.

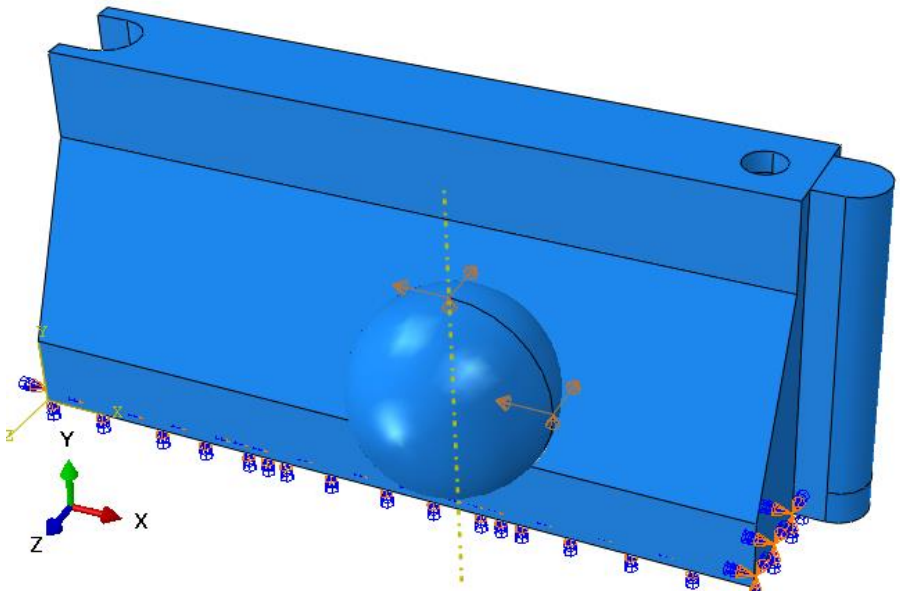

Figure 4- 1. Configuration of the Model Geometry in Fixed BC

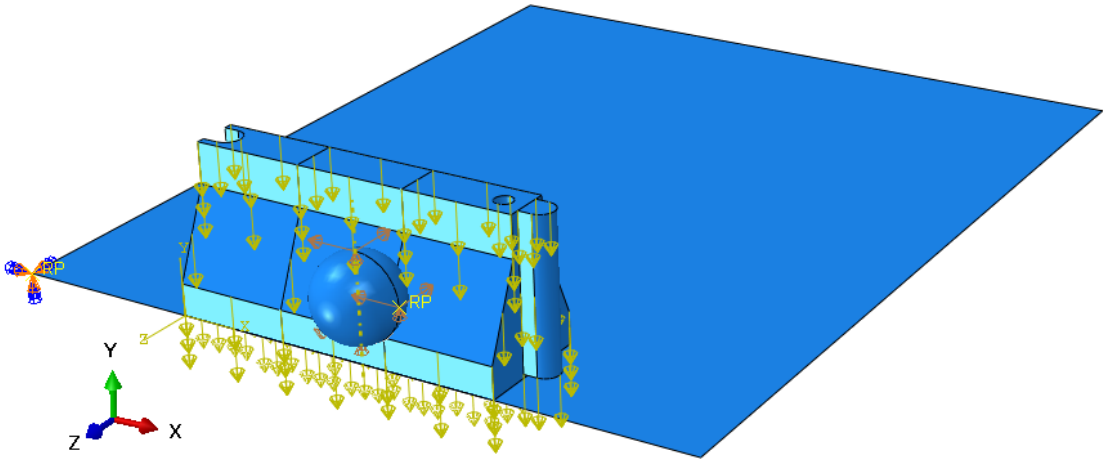

Figure 4- 2. Configuration of the Model Geometry in Friction BC

There are two methods for CFD problems in ABAQUS, which are Smoothed Particle Hydrodynamics (SPH) and Coupled Eulerian-Lagrangian method (CEL). According to the application description from Abaqus User's Manual, CEL is often used to simulate a hard face impacting and investigate the object's response (Abaqus User's Manual). The CEL is a contact formulation to simulate a highly dynamic event involving a fluid material (modeled using Eulerian elements) interacting with structural boundaries (modeled using Lagrangian elements) (Abaqus User's Manual). The definition of CEL can also be treated as boundary conditions. In the coupling process, deformation occurs on solid elements (Lagrangian elements) and interact with fluid elements when an external force is applied. Simultaneously, the movement of fluid elements generates hydrodynamic pressure acting on internal surfaces. CFD models consist of three element components, Lagrangian elements, Eulerian elements, and fluid domain elements. The fluid domain elements are generated by cutting geometry under merge option, creating the void that water can be filled in. In

addition, discrete filed requires assigning volume fraction between Lagrangian elements and fluid domain elements. Since that, for interior cells models, the fluid domain geometry also cut by internal honeycomb cells. With respect to Eulerian elements, if a material completely fills an element, its volume fraction is one; if no material is present in a component, its volume fraction is zero. Eulerian implementation in ABAQUS/Explicit is based on the volume-of-fluid method. In this method, the material is tracked as it flows through the mesh by computing its Eulerian fraction within each element (Abaqus User's Manual). The representative geometries are shown below, in which the outside geometry is the Eulerian element and the inside geometry is the fluid domain cut by internal cells

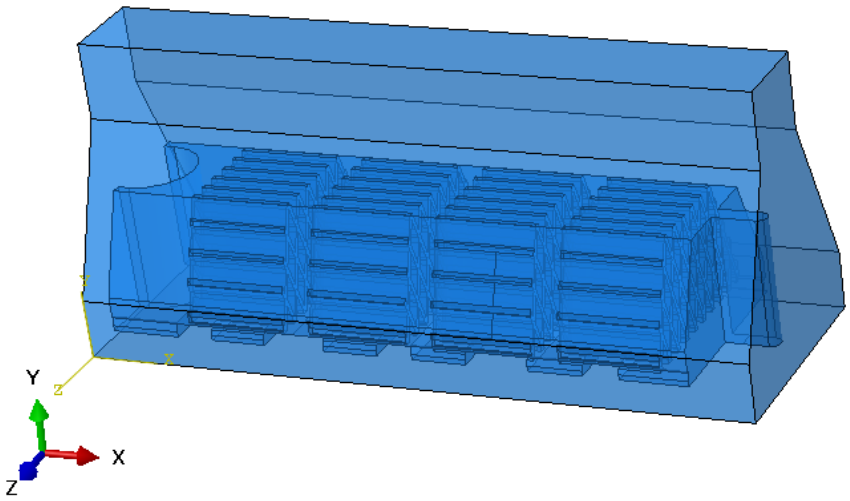

Figure 4- 3. Configuration of Eulerian and Fluid Domain Geometry with Internal Cells

4.3 Modeling Properties

4.3.1 Acrylonitrile Butadiene Styrene Plastic

The small-scale barrier specimens are made of Acrylonitrile Butadiene Styrene (ABS) which is a common 3D printing material. ABS is a terpolymer made through polymerizing styrene and acrylonitrile. The proportions normally vary from 15 % to 35 % acrylonitrile, 5% to 30% butadiene, and 40% to 60% styrene. Polymerizing styrene and acrylonitrile in the presence of polybutadiene makes ABS plastic highly impact resistant and increase the structural strength and stiffness compared to other plastic polymers. However, the mix of acrylonitrile, butadiene, and styrene is unknown from printing material properties. Additionally, the 3D printing process potentially affects the mechanical properties of the original material properties of ABS plastic due to the laminar printing process. These two uncertainties may affect the mechanical properties of ABS plastic. Therefore, tensile testing was completed on the material to determine the material properties, such as Young's modulus, passion's ratio, ultimate strength, and strain ratio while elongation. These mechanical properties are crucial to modeling the contact of an elastic material in FEA models. The tensile specimens used for the tensile test were produced from the same 3D printer and the dimension of specimens are followed the dimension of American Society for Testing and Materials (ASTM) D638 Type 1, which is a standard for plastic materials.

Table 4- 1. ASTM D638 Specimen Dimensions

Size	Type 1
Full Length, L3 (mm)	165
Parallel Length, L2 (mm)	57
Gauge Width (mm)	13
Gauge Length, L1 (mm)	50
Thickness, h (mm)	4
Distance between Grips (mm)	115

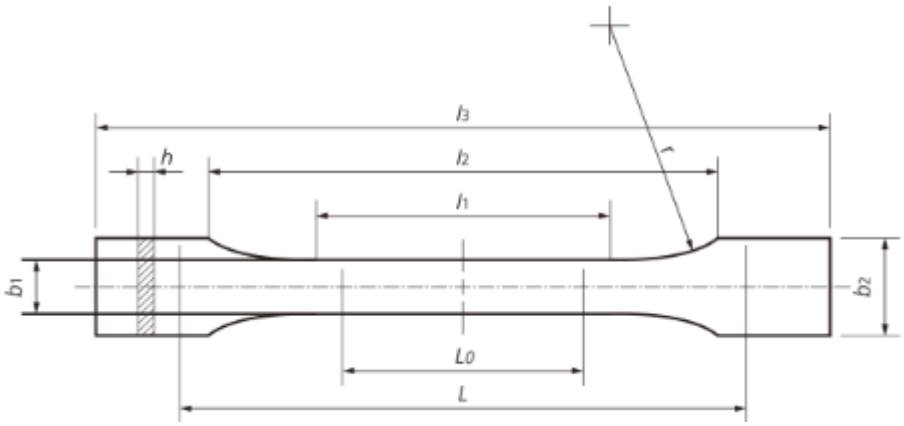

Figure 4- 4. Configuration of D638 Tensions Specimen (Plate Type 1)

Figure 4- 5. Configuration of Instron ASTM A379 Load Frame

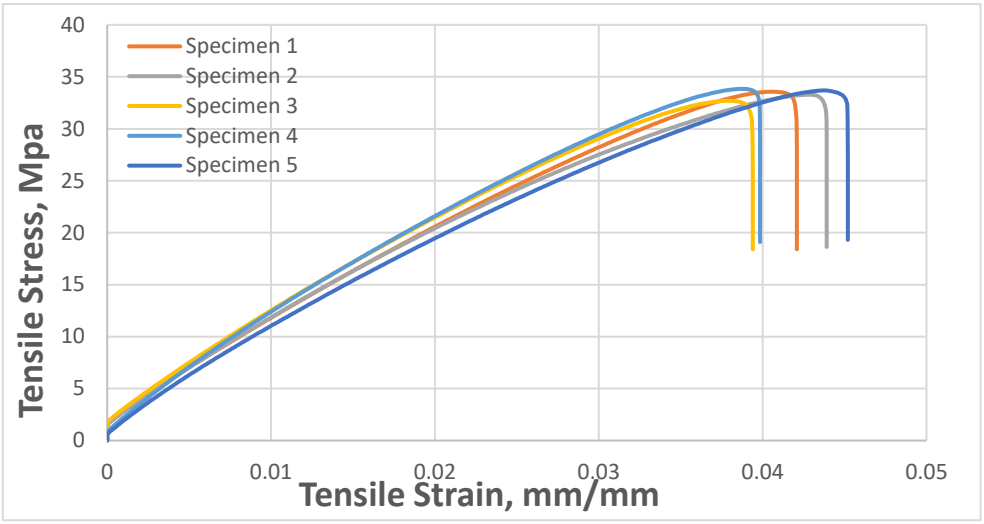

Figure 4- 6. Stress versus Strain Plot of Five Tensile Specimens

Table 4- 2. Stress and Strain Data for Test Specimens and Average

Tensile Specimens	1	2	3	4	5	Average
Young's Modulus, Mpa	1,478.37	1,379.27	1,626.2	1,329.4	1,336.65	1,429.98
Ultimate Strength, N	1,745.72	1,730.47	1,700.3	17,60.01	1,752.2	1,737.74
Ultimate Stress, Mpa	33.57	33.28	32.70	33.85	33.70	33.42
Ultimate Strain, mm/mm	0.042	0.044	0.039	0.04	0.045	0.042

ABS plastic is similar to other major polymers which presents a linear elastic behavior and fracture at the ultimate tensile strain. Based on the testing, Young's modulus, ultimate stress, and ultimate strain are 1.429 Gpa, 33.42Mpa, and 0.042, respectively. Density is 1.09g/cm^3 calculated based on mass and volume of tensile specimens. Poisson's ratio is obtained from the reference value as 0.4. Beyond the general properties of ABS polymer, although the failure of structure is not observed from testing, the damage properties is assigned. According to the stress vs s.train curve, it indicates the specimens breaks without significant plastic deformation. From the observation of the fractured specimen, they have a very flat cut plane which means less ductile characteristic of printed ABS polymer. Therefore, the brittle crack

damage properties are considered in this modeling to represent structural failure. In many brittle crack modeling cases, it is essential to know if the cracks will propagate. However, current modeling data is limited to address the propagated cracks. The ultimate tensile strain from testing governs the brittle crack.

Table 4- 3. Brittle Damage Properties

Direct Stress After Cracking	Direct Cracking Strain	Shear Retention Factor	Crack Opening Strain	Direct Cracking Failure Strain
33.42 Mpa	0	0	0	0.042
30 Mpa	0.001	1	0.001	
25 Mpa	0.003	1	0.003	
20 Mpa	0.005	1	0.005	
15 Mpa	0.007	1	0.007	
10 Mpa	0.009	1	0.009	

4.3.2 Water

The principal object of the CFD model is to simulate water movement and the interaction between the fluid and interior surface of barrier shells. Hence, the material properties of water such as density, viscosity and several input data related to Equation of State (EOS) are considered. With respect to viscosity, it is divided into two categories which are the kinematic and dynamic viscosity. Kinematic viscosity is a measurement of inherent resistance of flow in gravity. Dynamic viscosity, it measures the resistance of fluid when an external force applied. Therefore, the dynamic viscosity of water is preferred for this modeling. In general, fluid material properties vary with the temperature. Both density and dynamic viscosity vary with the environmental temperature. The variation in density and dynamic viscosity of

water with a change in temperature showed below (Viscosity Table-Measurement Data, Anton Parr). Based on the data table, the density and dynamic viscosity are taken at 25 degree Celsius which are 0.997 grams/cm^3 and 0.89 mPa·s.

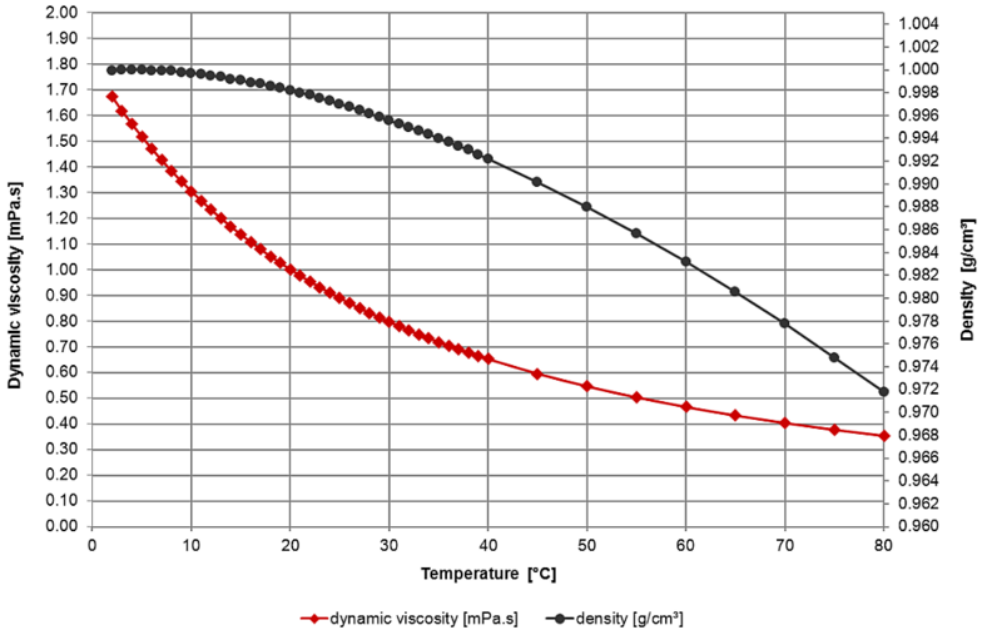

Figure 4- 7. Water- Dynamic Viscosity and Density over Temperature (Viscosity Table-Measurement Data, Anton Parr)

Some additional parameters were used to describe the properties of fluid through EOS. EOS is a thermodynamic equation describing the state of matter under a given set of physical conditions, such as pressure, volume, temperature, or internal energy (Perrot Pierre, 1998). The characteristics of fluid are divided into those that are compressible and those that are incompressible. The compressibility of fluid refers to a volume change of fluid when increasing the outside pressure. Filled water in this FEM is liquid and typical incompressible fluid, and EOSs for the incompressible fluid are also applicable. Abaqus User's Manual recommends that a linear U_s-U_p EOS can be used to model incompressible viscous and inviscid laminar flow governed by the

Navier-Stokes Equation of Motion (Abaqus User's Manual). A governing equation is given in Hugoniot form as followed.

$$p = \frac{\rho_0 c_0^2 \eta}{(1 - s\eta)^2}\left(1 - \frac{\Gamma_0 \eta}{2}\right) + \Gamma_0 \rho_0 E_m, \quad (4)$$

$\rho_0 c_0^2$: is equivalent to the elastic bulk modulus at small nominal strains

c_0 : reference speed of sound

s : a linear Hugoniot slope coefficient, dUs/dUp

Γ_0 : Grüneisen's gamma at the reference state

U_s : the shock wave velocity

U_p : particle velocity

With respect to input parameters in ABAQUS, it requires to specify the variables c_0, s, and Γ_0. Similarly, the reference of speed of sound is also a function of temperature. The reference speed of sound in water is determined as 1494 m/s at 25 degree Celsius (Engineering ToolBox, 2004). Concerning the Hugoniot slope coefficient (s) and Grüneisen's gamma (Γ_0), the values are taken as 0 from recommended material parameters for water (Abaqus Example Problems Guide).

4.4 Convergence Study and Modeling Precision

In finite element model, the accuracy of the modeling depends on the element shape function (element type) and discretization (element mesh size). The numerical software solves the problems using a series of discrete points and each of the system's point increases the degree of freedom (DOF) of the system. A finer mesh size results in more elements participating in calculation result in a more accurate calculation

result. In order to balance both modeling accuracy and computational cost, a mesh convergence study is needed. This FEM conducts a convergence study under the Dynamics Explicit modulus because the impact problems are associated with inertia of mass. The Dynamic Explicit solver correctly accounts for the propagating speed of dynamic effects. Furthermore, the Dynamic Explicit solver has higher mesh requirement compared to the static direct solver, as the mesh size in Dynamics Explicit solver must be fine enough to represent the spatial effects rather than just satisfying the geometric requirement.

The convergence study covers both non-water filled and water-filled cases (non-CFD models and CFD models). The geometries in non-CFD models only consist of the impactor, the barrier shell, and the additional friction board in friction BC. For CFD models, the Eulerian element and fluid domain have a higher requirement regarding the mesh size due to the highly deformable characteristics of water. For the most geometry non-linear model, there is a large quantity of fluid and cell surfaces coupling calculation. A friction board is used for friction boundary condition, which is defined as a rigid shell in the modeling. The element mesh of friction is assigned relatively coarser than other elements due to the linear geometry shape of the rigid shell.

The shape of the mesh element is typically a collection of polygons and geometric objects. The Tet (quadratic) mesh elements were used during the modeling due to the quadratic geometry order and geometry type-C3D10M (A 10-node modified quadratic tetrahedron). In order to save computational time, the mesh size

can be increased in unloading areas or geometry or if material properties and responses are linear. However, the barrier specimens contain a large portion of asymmetric geometry, coupled with fact that it is challenging to predict the load transferring inside of barrier. Hence, the study model uses uniformed mesh instead of local meshing. For this research, the convergence study conducts in two models regarding if the model is water filled.

4.4.1 Non-Computational Fluid Dynamic Models

In the first study model, the convergence study was conducted in the most simplified model which contained a ratio of 0, a 25 impact degree and no infilled water with fixed bottom boundary condition. For all non-water filled models, the assembly parts only consisted of an impact steel ball and barrier. Similar to all of models, the steel ball undergoes a linear acceleration phase to reach its impact velocity and the bottom of the barrier is fixed during the process. Taking into consideration the purpose of research, the energy absorption is the basis for measuring the accuracy of modeling. By re-running the model multiple times, the total element number versus energy absorption was plotted and shown below. From the plot, the energy absorption converges to around 20% while the total number of elements reached 150,000. When the total element numbers reached the interval of 75,000 to 250,000, there was a small energy absorption deviation. Overall, considering the balance of accuracy and computational cost, 0.3 mesh size was recommended in non-CFD models. Followings represent the modeling geometry and modeling result for non-CFD models.

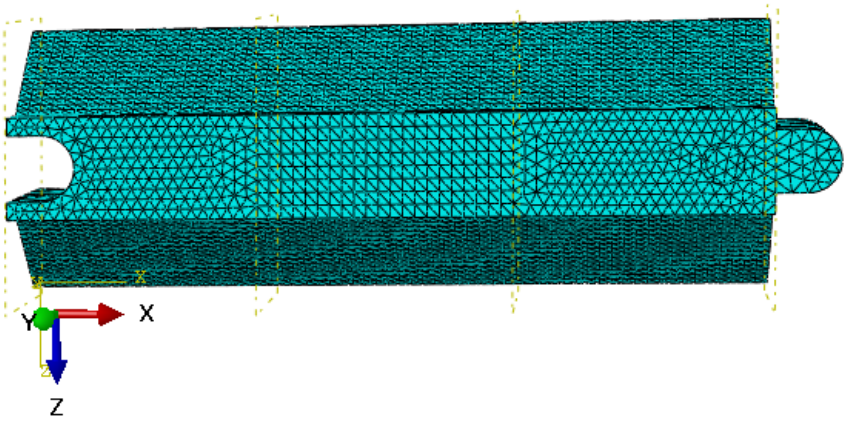

Figure 4- 8. 0.3 Mesh Size Configuration of Top Surface of Barrier

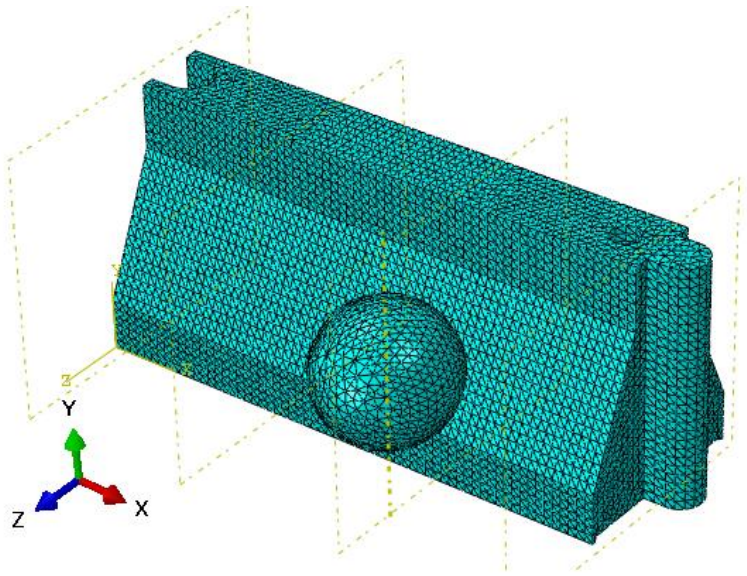

Figure 4- 9. 0.3 Mesh Size Configuration of Non-CFD Model

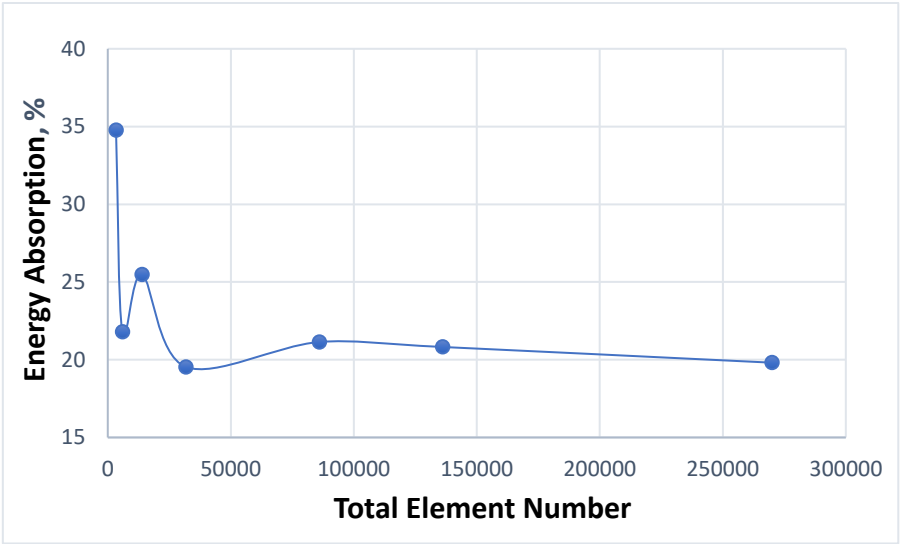

Figure 4- 10. Element Number versus Energy Dissipation Plot of Non-CFD Model

Table 4- 4. Mesh Convergence Study of Non-CFD Models

Case	Mesh Size	Element Number	Number of elements on top face of barrier	Energy Absorption, %	Solve time, hr
1	1.5	3,348	1	34.77	0.7
2	1	5,930	2	21.79	1.2
3	0.6	13,927	4	25.48	3.7
4	0.45	31,739	12	19.54	6.4
5	0.3	85,939	16	21.14	15
6	0.25	136,033	20	20.82	31
7	0.2	269,957	24	19.81	69

4.4.2 Computational Fluid Dynamic Models

The convergence study was conducted in terms of locating the optimal mesh size of CFD elements in the CFD model. In ABAQUS, the CFD simulation consists of two additional parts, which consist of Eulerian domain and fluid domain. These elements participate in the CEL calculation. According to the Abaqus User's Manual, the specification of Eulerian domain is the geometry shape of existing fluid. The 0.5 filled water level is selected for CFD convergence study models. Similar to the previous convergence study, this study was conducted by changing both the mesh size of the fluid domain and Eulerian domain simultaneously and comparing the result accuracy regarding total energy absorption. The mesh size obtained from the previous convergence study was used for the steel ball and barrier geometry in CFD models. After several running, the whole element number versus energy dissipation is plot as shown below. As shown in the plot, when the total element number reached 200,000, the energy absorption results converged to about 26%. There is a small fluctuation of modeling result when the element number reaches to 250147 (0.25 Mesh Size), associated with an approximate forty hour solve time. The convergence model is

relatively simplified, in that the interaction only happens between fluid and interior surface of barriers. With respect to the barriers having interior cells, there is a huge quantity of interaction calculation between contact boundaries. Overall consideration, the mesh size of 0.25 is recommended for the Eulerian and fluid domain elements in CFD models.

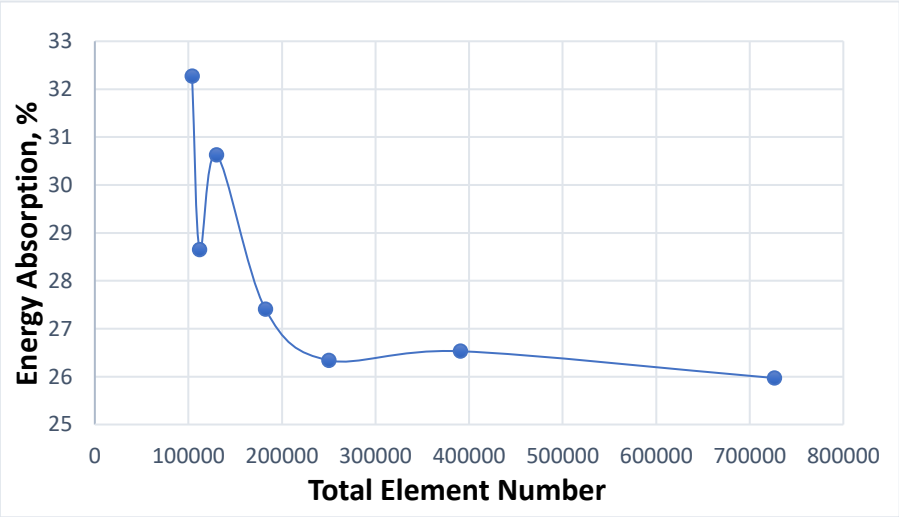

Figure 4- 11. Element Number versus Energy Dissipation Plot of CFD Model

Table 4- 5. Mesh Convergence Study of CFD Models

Case	1	2	3	4	5	6	7
Eulerian Size	0.6	0.5	0.4	0.3	0.25	0.2	0.15
Eulerian Number of Element	4,092	6,435	12,103	30,680	56,628	113,190	258,180
Fluid Domain Number of Element	11,045	16,792	29,143	62,767	104,724	188,763	379,422
Total Number of Element	103,932	112,022	130,041	182,242	250,147	390,748	726,397
Surface Element Number, Eulerian	4	5	6	8	10	13	17
Surface Element Number, Fluid	11	13	15	20	25	31	39
Energy Absorption, %	32.27	28.65	30.63	27.41	26.34	26.53	25.97
Solve Time, Hr	4	7	14	22	40	67	106

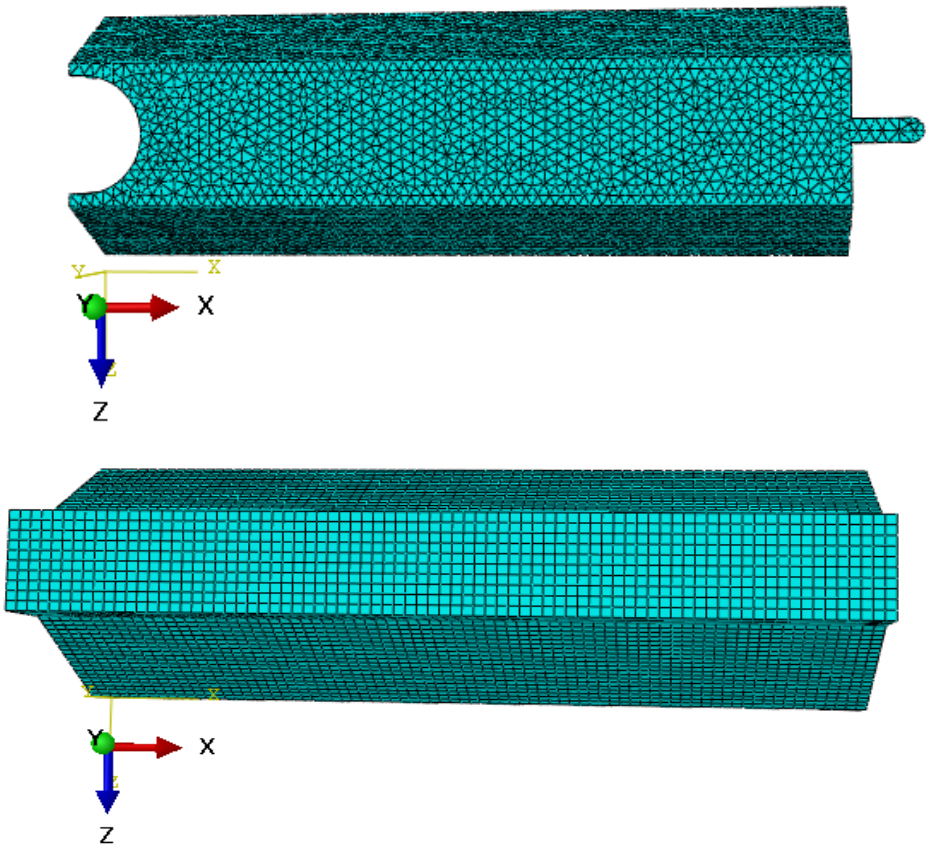

Figure 4- 12. Mesh Configuration of Eulerian and Fluid Domain Element in CFD Model

4.4.3 Double Precision

Double precision is the option of analysis assignment which a computational method in FE analysis. Double precision also known as a double-floating-point format is a computer number format which occupies 64 bits in computer memory. Compared to single precision, the floating-point format occupies 32 bits. From a computer standpoint, the double precision increases the maximum bit value can be stored and leads to a more accurate result than single precision. In the most solid mechanics modeling, single precision is adequate to meet the accuracy requirement. Based on the Abaqus/CAE User's Manual, the manual recommends using the double precision when solving following model type, explicit analysis where a number of cycles are

substantially large, implicit analysis using linear element formulation and any model where single precision results are suspect (Abaqus User's Manual). The application in Finite Element Analysis, the double precision subdivides the analysis step interval to sufficiently small increment, which significantly increases the stability of solution (LS-DYNA Support). In some cases, the stability is governed which higher stability of running process leading to a more accurate result. In CFD modes, the modeled water is highly deformable when resisting an impact loading. Single precision cannot subdivide an analysis interval to small enough, which has a high potential to result in an error due to excessive distorted elements. When using ABAQUS to compute CFD models, from an accuracy perspective, the application of double precision is needed. There are several options in terms of double precision, analysis only, constraints only, and a combination of two. For this research, only double precision-analysis is applied.

4.5 Modeling Results and Parametric Study

A parametric study was completed to describe, analyze and examine the different relations amongst various parameters. In other words, the goal of study was to investigate the impact behavior of developed barriers through comparing the experiment data and FEM results. FE models grossly are classified as non-CFD models and CFD models. For non-CFD models, the primary study is the impact resistance and energy absorption behavior of the internal cells. However, added interior cells might affect the water sloshing inside barrier specimens which lead to an unpredictable energy absorption effect. Therefore, water-filled FE models (CFD models) are developed to evaluate the energy absorption effect of water. For each

criterion, it is unpractical to run all of cases of varied length ratio. In order to reduce the number of models, in CFD models, ratio 0 and ratio 0.75 are selected for the fixed BC, and each length ratios are evaluated in friction BC. Only the 25-degree impact angle modes are conducted in CFD models. A control group addressed the energy absorption behavior of added honeycomb cells, with ratio of 0, representative of current commercial PWFBs in market. After validating the rationality of both experimental data and FEM results, the FE models are also used to predict the deformable pattern of barrier specimens. In fixed BC models, displacement versus time plots are developed in terms of most critical nodal sets. With respect to friction BC, the barrier shells changed from state of static to state of motion. A flow chart of entire parametric study has been prepared as follows:

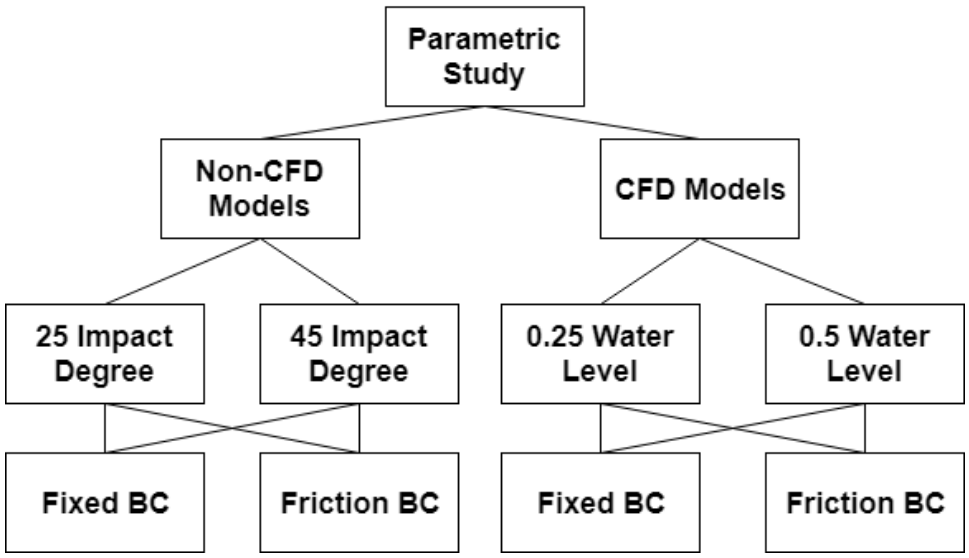

Figure 4- 13. Developed Flow Chart of Parametric Studies

4.5.1 Non-Computational Fluid Dynamic Models

In terms of energy absorption of barrier shells, the total absorption is composed of three parts: strain dissipation of barriers, frictional dissipation, and the absorbed kinetic energy. Based on the observation from impact testing, the barrier specimens are undamaged and there is no apparent permanent deformation. Since the FE investigation primarily considers barrier specimens in the elastic deformation stage, elastic strain and frictional dissipation account for total dissipation. Hunter (1957) proved the theory that there is a small amount of energy dissipation when an object presents an elastic deformation upon resisting impact loading. This is because the longitudinal, transverse and surface wave deformation transfers a small portion of impact energy irrecoverably (Hunter, 1957). Several models have been developed in this case which changed length ratio, boundary condition, and impact degrees, all consistent with the experimental investigation.

4.5.1.1 25 Impact Degree Fixed Boundary Condition Models

The first parametric study models are considered in the condition of 25 impact degree fixed BC. The energy reduction is obtained by calculating the reduction of impact velocity and post-impact velocity (PIV). The magnitude and vector components are generated from ABAQUS field output. The velocity history plot directly presents the energy absorption effects in terms of varied length ratio. For detail analysis, the velocity components respectively are X-direction, Y-direction, and Z-direction.

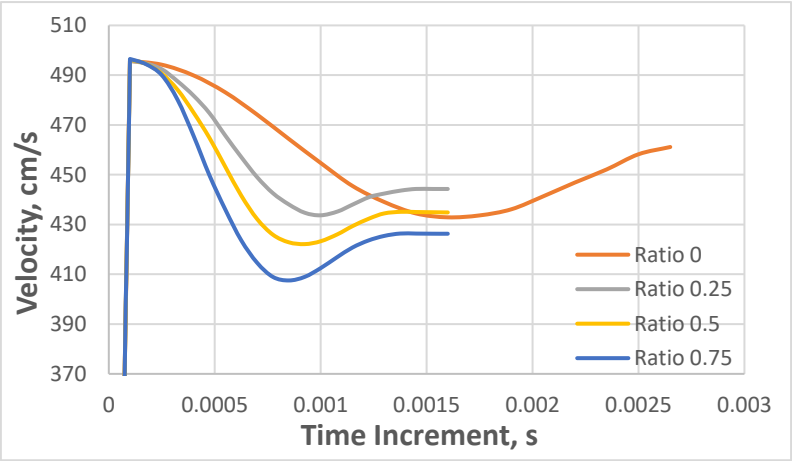

Figure 4- 14. 25 Impact Degree Fixed BC Velocity History Plot

Table 4- 6. Post-Impact Modeling Result of 25 Degree Fixed BC

Cases	Ratio 0	Ratio 0.25	Ratio 0.5	Ratio 0.75
X-Vector, cm/s	-417.14	-409.81	-395.78	-380.06
Y-Vector, cm/s	141.55	143.39	145.51	147.48
Z-Vector, cm/s	123.89	127.15	134.04	138.96
Sum of Vectors, cm/s	461.58	447.13	442.47	429.19
FEM Result, %	14.62	17.91	23.57	28.78
Testing Result, %	20.38	21.09	25.83	27.18
Deviation, %	5.76	3.18	3.74	1.6

Both from modeling and testing results, it can be observed that there is an acceptable deviation between the testing result and modeling result which validate the results and FE modeling. Generally, from the velocity magnitude plot, the PIVs decrease with increasing the length of interior honeycomb cell when contact method is constant for all models, which means higher strain energy dissipation is presented. The result is positively addressed that adding 0.25 length ratio of internal cells contribute to 6% more energy absorption, and there is around 3% of absorption increment from ratio 0.25 to 0.75. Furthermore, in fixed BC, the energy dissipation accounts for all absorbed energy. This observation verifies the assumption in the

design process that increasing the length ratio of interior honeycomb cell contributes to more energy absorption.

In looking at the PIV vectors, it shows a decreasing trend in negative X-direction from ratio 0 to ratio 0.75; this decreasing trend shows that the denser the cells, the greater ability to retain the collision vehicle. Similar, in Y-direction, the magnitude of PIV vector also decreases with increasing the cell length. Smaller PIV in Y-direction may help in preventing the overturning of collision vehicles. The Z-direction is perpendicular to the longitudinal direction. In the Z-direction, the PIV increases with longer interior cell length, which means honeycomb cell barriers present higher capability to redirect the impactor. Although higher PIV in Z-direction is desirable, the evaluation criteria from MASH limits Z-direction, as an excessive PIV in the Z-direction may potentially increase the risk of vehicle occupants. Hence, full-scale impact test is required to evaluate the potential risk of occupants in terms of Z-direction PIV.

4.5.1.2 25 Impact Degree Friction Boundary Condition Models

The friction BC is the most critical evaluation criteria, showing the performance of barriers in the closest fashion to a real vehicle collision. In these models, the modeling parameters from previous models remain the same, besides the boundary condition change to friction BC. In the friction BC model, a large portion of the impact energy transfers to the kinetic energy of barrier specimens. Similarly, the velocity magnitude and vectors plots are generated as showed below.

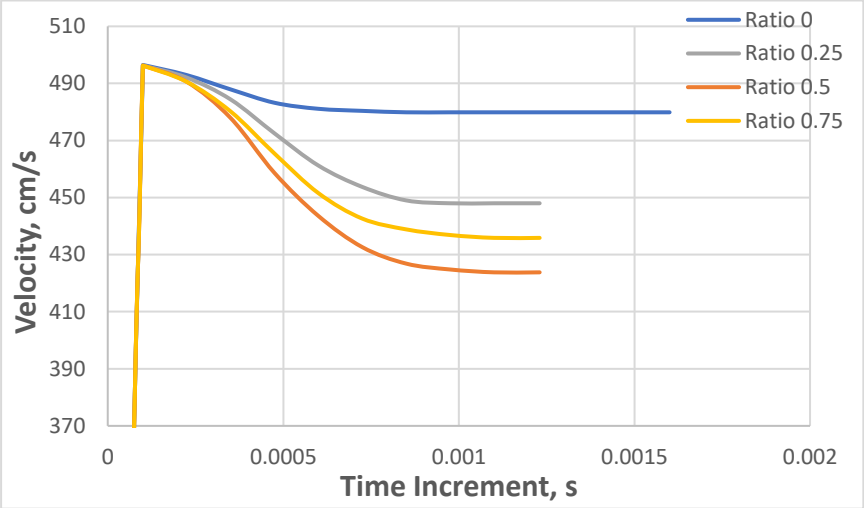

Figure 4- 15. 25 Impact Degree Friction BC Velocity History Plot

Table 4- 7. Post-Impact Modeling Result of 25 Degree Friction BC

Cases	Ratio 0	Ratio 0.25	Ratio 0.5	Ratio 0.75
X-Vector, cm/s	-442.5	-427.81	-419.99	-413.5
Y-Vector, cm/s	11.58	74.84	81.32	85.06
Z-Vector, cm/s	-183.4	-103.48	-87.65	-67.02
Sum of Vectors, cm/s	479.09	450.88	435.88	428.798
FEM Result, %	8.22	18.45	22.85	24.89
Testing Result, %	10.32	14.99	32.12	35.76
Deviation, %	2.1	3.46	9.27	10.87

From time increment versus velocity plots, the energy absorption is calculated, and the results demonstrate that the 0.75 ratio model has more energy absorption. In this case, the energy absorption effect of internal cell barriers is significant where there is 10% reduction between ratio 0 and ratio 0.25 barrier shells. The absorption increment is relatively small while increasing the length ratio. In the friction BC, there are two possible reasons that lead to the internal cell barriers having higher energy absorption. One aspect is that the added internal cells contribute a high in-plane stiffness leading to higher energy dissipation. Another aspect is that the added cells also increase the system mass of the barrier specimens which lead to higher mass

inertia causing the kinetic response of barrier shell to absorb more energy. More importantly, PIV in Z-direction has a significant reduction which means the impactor is effectively contained the collision vehicles. However, the internal cell barrier shows a higher PIV in Y-direction, meaning that the collision may have a higher up-ward PIV and potentially lead to overturning of collision vehicles. These two findings only address the potential post-impact behavior of crash; however, full-scale impact tests are required to be conducted for further analysis.

4.5.1.3 45 Impact Degree Models

Based on the recommended impact angle from MASH, a 25-degree impact angle is developed primarily in this research. Additional 45-degree impact models are developed to consider the complex traffic model in temporary construction working zone. Impact velocities in the Z-direction are constant while increasing and decreasing the impact angle. For the 45-degree impact models, the PIV in the Y direction is kept constant, while the PIV in the X direction is decreased.

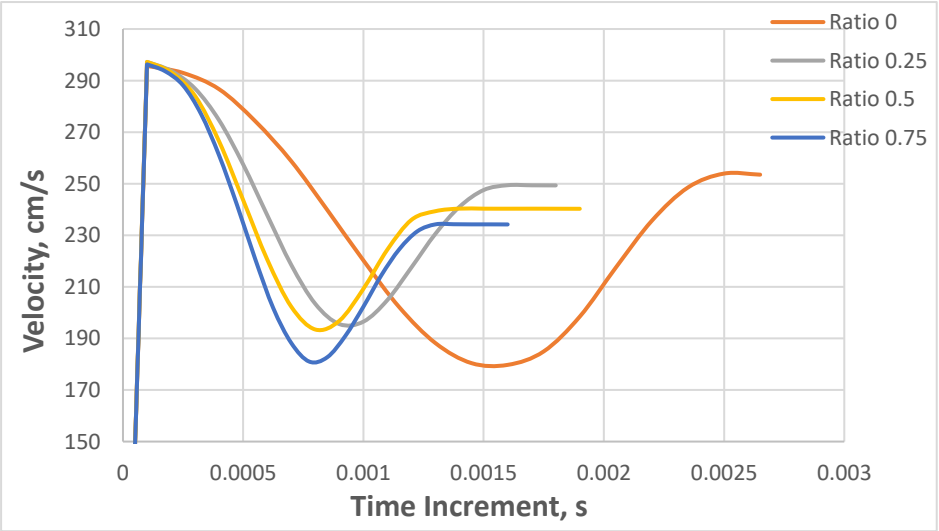

Figure 4- 16. 45 Impact Degree Fixed BC Velocity History Plot

Table 4- 8. Post-Impact Modeling Result of 45 Degree Fixed BC

Cases	Ratio 0	Ratio 0.25	Ratio 0.5	Ratio 0.75
X-Vector, cm/s	-161.17	-158.98	-153.29	-140.40
Y-Vector, cm/s	138.08	130.30	123.78	119.47
Z-Vector, cm/s	136.99	138.86	140.71	144.46
Sum of Vectors, cm/s	253.51	249.34	240.28	234.21
FEM Result, %	26.65	29.04	34.20	37.45
Testing Result, %	46.36	46.36	51.10	53.94
Deviation, %	19.71	17.32	16.90	16.40

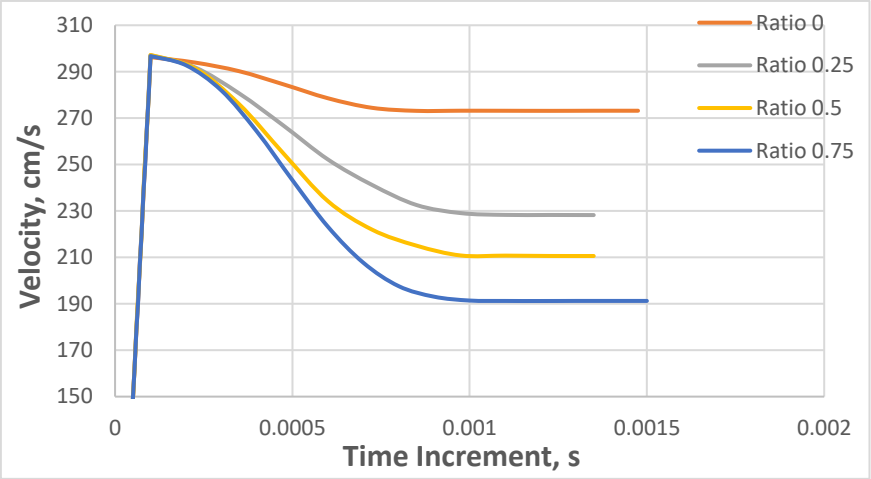

Figure 4- 17. 45 Impact Degree Friction BC Velocity History Plot

Table 4- 9. Post-Impact Modeling Result of 45 Degree Friction BC

Case	Ratio 0	Ratio 0.25	Ratio 0.5	Ratio 0.75
X-Vector, cm/s	202.83	-171.53	-165.66	-168.36
Y-Vector, cm/s	11.79	72.60	76.25	83.37
Z-Vector, cm/s	183.31	-34.47	-21.12	-21.64
Sum of Velocity	273.17	230.42	210.58	190.184
FEM Result, %	15.35	41.71	45.39	50.35
Testing Result, %	31.2	32.9	42.57	42.57
Deviation, %	15.85	8.81	2.82	7.78

Comparing PIVs from both lab and FE modeling result, there is a relatively large deviation in fixed BC. For the 45-degree impact case, the recorded post-impact response is relatively difficult to read the data precisely especially in fixed BC. With

the increase in the impact angle, the release height reduced based on the formulation IS. The larger deviation may due to the systematic errors of testing. Overall, the energy reduction behavior in 45-degree impact models presents a similar outcome to the 25-degree impact models. Based on the expression of impact severity, IS = $\frac{1}{2}M(v\sin\theta)^2$. In both testing and FEM, the IS value is constant which means the impact energy decreases with increased impact angle. While decomposing the velocity into vectors, the velocity vector in Z-direction is constant when the impact angle increases from 25 degrees to 45 degree. Since the velocity vectors in the X-direction is relatively small in the 45 degree impact angle models, and equals to velocity vector in Z-direction. This effect also explains the larger energy absorption from both testing and FE modeling with the same impact IS value.

In both the fixed and friction cases, the presence of internal cells effectively increases the energy absorption of barrier shell. More specifically, with an increasing length of internal cells, there is approximately 5% of energy absorption variation in fixed BC. In friction BC, the difference is energy absorption from a ratio of 0 to a ratio of 0.75 is about 25%. Additionally, PIV vectors present a small decrease trend in the fixed condition when comparing two barrier specimens. In friction BC, the model with a ratio of 0.75 model demonstrated a higher energy absorption quality.

4.5.2 Impact Strength of Internal Cell Barrier

While both testing and FE result matched, FE models are qualified to analyze the deformation pattern of barrier specimens. Based on the testing and modeling results, the barrier shells do not reach the damage stage in terms of impact severity of

TL 1 from MASH. Based on the material properties, the printed ABS material is an elastic material which the impact displacement is linearly proportional to impact equivalent load. The purpose of developing the deformation pattern through FEA is to evaluate the increased strength against impact loading. Based on the evaluation criteria from MASH, PWFB systems are expected to retain their structural integrity. Therefore, impact penetration and discontinuous redirection are prohibited. Displacement controlled models are developed to find the failure stage of developed internal cell PWFBs.

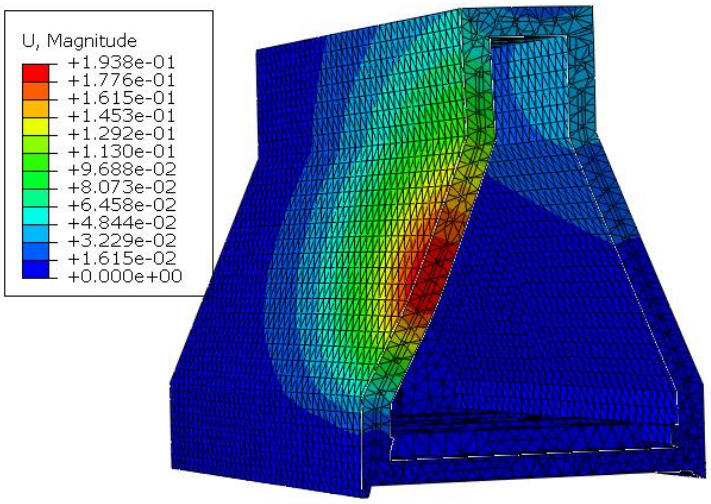

Figure 4- 18. Configuration of Deformation Pattern in Ratio of 0 Model

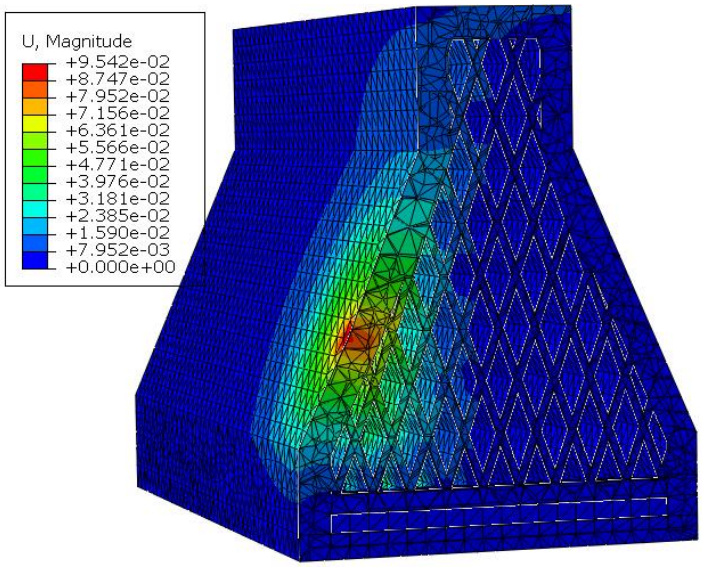

Figure 4- 19. Configuration of Deformation Pattern in Ratio of 0.75 Model

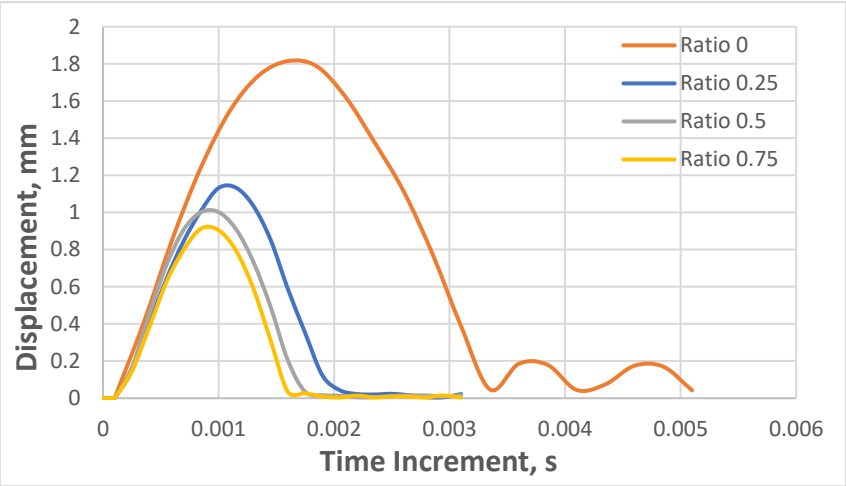

Figure 4- 20. 25 Impact Degree Fixed BC Displacement History Plot

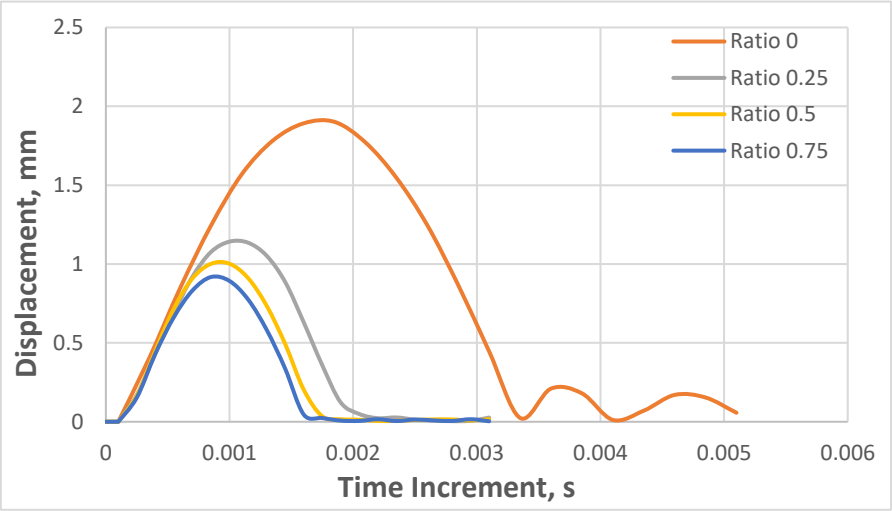

Figure 4- 21. 45 Impact Degree Fixed BC Displacement History Plot

From the deformation configuration of barrier specimens, it presents a radial deformation pattern. Based on the magnitude of deformation, dense interior cells result in a smaller contact displacement. Closer adjacent cells have a more significant effect for resisting impact loading. Comparing the 25 and 45-degree impact cases, the contact displacement history plots present almost the same trend because the impact velocity vector in Z-direction is the same. Moreover, it is clear to observe that the interior cell modes have a smaller magnitude of deformation. Internal cells barriers

have a significantly smaller spatial displacement, but they have a little displacement reduction increment with a longer internal cell length. There is no irreversible deformation which only elastic deformation is presented.

To evaluate the impact resistance of interior cells, the displacement-controlled models are developed, in which the brittle damage properties are applied. Based on the stress vs. strain curve, ABS polymer exhibits general mechanical behavior associated with brittle materials, breaking without significant plastic deformation. The failures of barrier shells and internal cells are governed by direct cracking failure strain when the brittle cracks will form while the strain components reach to direct crack strain. A general configuration of fracture shown as below.

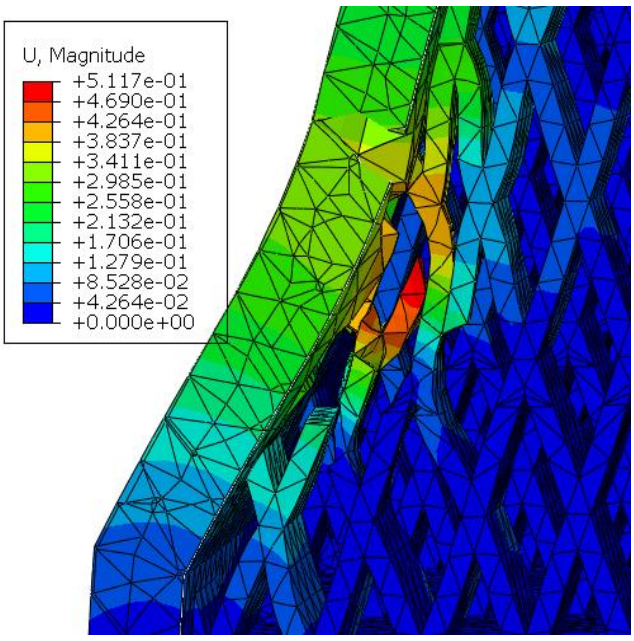

Figure 4- 22. Configuration of Fracture of Internal Cells in Displacement Controlled Model

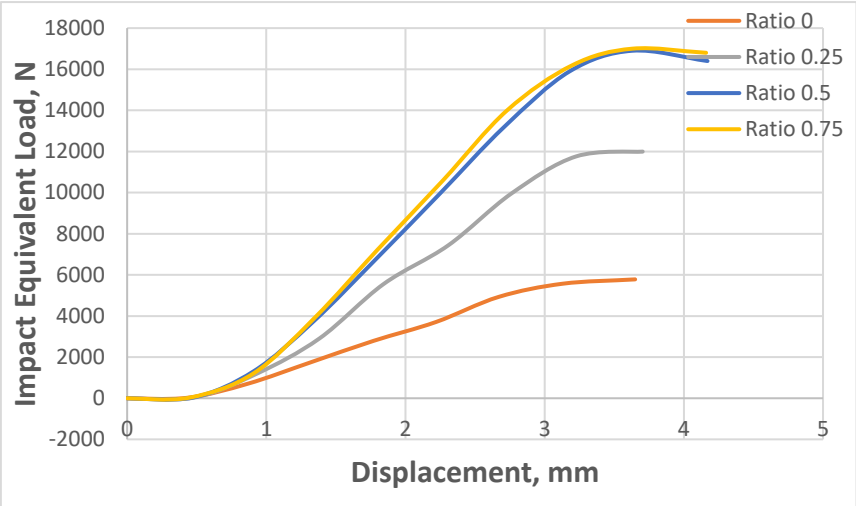

Figure 4- 23. Contact Displacement versus Impact Equivalent Load

Table 4- 10. Modeling Results of Ultimate Impact Equivalent Load

Case	Ultimate Strength, N	Displacement, mm
Ratio 0	5932.76	3.67
Ratio 0.25	11896.49	3.27
Ratio 0.5	14763.56	3.64
Ratio 0.75	14770.93	3.68

In these models, displacement control is used on the steel ball until reaching the stage of internal cells being fractured. During the process, the fracture of barrier shell is first observed, then the internal cells fractured in the next. According to the plot, the barrier is still able to resist impacting even as fracturing occurs on the barrier surface. However, the fracture of internal cells results in a heavy reduction of impact resisting strength. Hence, the ultimate strength is selected at the stage of internal cells fractured. From Figure 4-23, the peak load gives the failure load at which fracture of internal cells occurred in the mode. Increasing the length of internal length has a positive effect of increasing the strength of barriers. Between ratio 0 and ratio 0.25, there is around 6 KN increment in terms of failure strength. Ratio of 0.5 and 0.75 show a very similar failure strength and displacement. This is mainly because both

ratios have relatively longer cell segments and the failure strengths are dependents on initial stiffness and effective contact area. General speaking, higher length ratios will have an overall initial stiffness, but which is not same in terms of point impact loading.

4.5.3 Computational Fluid Dynamic Models

It is required that PWFBs are filled with ballast weight in the field due to the heaviness that the ballast weight adds to the light weight of the PWFB shell. The filled blast weight significantly increases the crashworthiness of PWFB systems. Additionally, filled water is a typically incompressible fluid which has viscous median contributing to impact energy absorption while external excitation is activated. In CFD models, the objective is to investigate the energy absorption behavior of barriers with filled water, along with the effect of internal cells. Some advanced features are introduced to eliminate the increased mass inertia by filled water.

With filled water, the system's mass is increased, making a larger proportion of impact energy converts to the kinetic energy of barrier segments in the friction BC. Therefore, precise evaluation of the energy absorption behavior of water should take into count the increased mass inertial effects. In the CFD models, 0.25 and 0.5 filled water levels are considered based on the practical, filled water level from Thiyahuddin and Thambiratnam's recommendation in their testing. Higher level of filled water increases self-weight and increases the crashworthiness of PWFBs. However, higher water levels may also lead to the overturning of PWFBs, which significantly reduces the energy absorption ability.

4.5.3.1 Fixed Boundary Condition Models

Fixed BC parametric models combine a ratio of 0 and 0.75 barrier specimens with 0.25 water filled, 0.5 water filled, and no water filled cases. The fixed BC investigates the case when the barrier shell does not have translation displacement. In this case, a filled ballast weight does not affect the total energy absorption, only the filled water, strain energy dissipation, and frictional energy dissipation have positive effects on energy absorption. The velocity history plot is shown below.

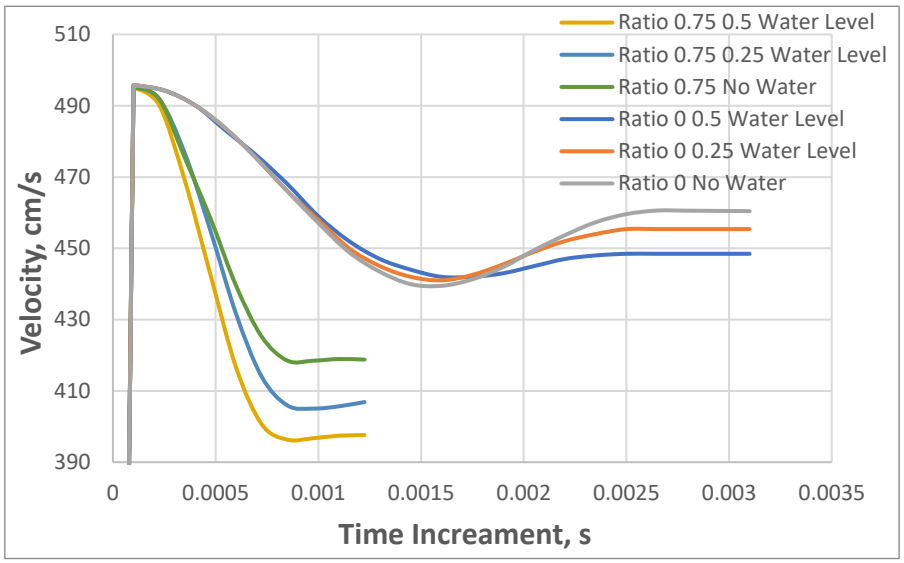

Figure 4- 24. CFD Parametric Study of the Ratio of 0 and 0.75 in Fixed BC

Table 4- 11. Parametric Study Velocity History Plot of Ratio of 0 and 0.75 Models in Fixed BC

Case	Impact Velocity, cm/s	Post-Impact Velocity, cm/s	FE Result, %	Test Result, %	Deviation, %
Ratio 0-No Water	495.726	460.428	13.74	18.38	4.64
Ratio 0-0.25 Movable Water	495.837	455.385	15.75	21.41	5.66
Ratio 0-0.5 Movable Water	496.014	448.463	18.15	25.82	7.67
Ratio 0.75-No Water	495.485	418.174	28.69	27.19	1.5
Ratio 0.75-0.25 Movable Water	495.948	407.038	32.45	29.89	2.56
Ratio 0.75-0.5 Movable Water	495.483	397.602	35.74	33.28	2.46

Based on the velocity plot, it can be observed that systems obtain a positive energy reduction as the water level increases. More specifically, from testing and modeling results, there is approximately a 3% energy reduction with increased water levels in both ratios of 0 and 0.75 specimens. However, both of two barrier specimens show only a small energy absorption effects due to water sloshing. Overall, the energy absorption caused by the internal cells is more significant compared to the energy absorption by the filled water in fixed BC. The main reason for this is the translation of barriers is limited, and relative displacement only occurs at the impact location. By knowing the nature of CEL, the excitation of water depends on the displacement of the barrier shell which larger translational displacement of barrier shell leads to a more dramatic sloshing effect or higher energy absorption by water. The configuration of water movement in Figure 4-25 demonstrates this effect.

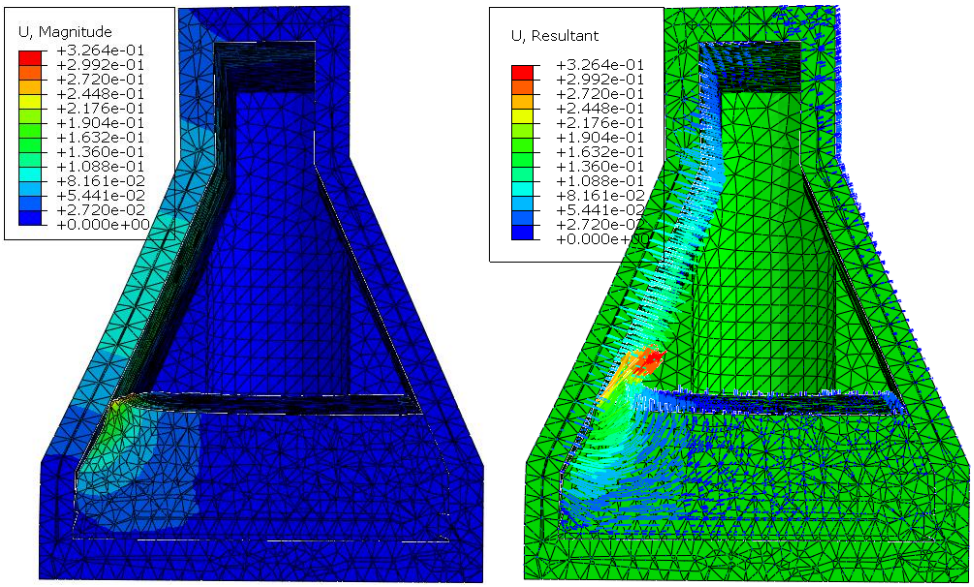

Figure 4- 25. Deformation and Deformation Symbol Configuration of Ratio 0 with 0.25 Water Level Fixed BC Model

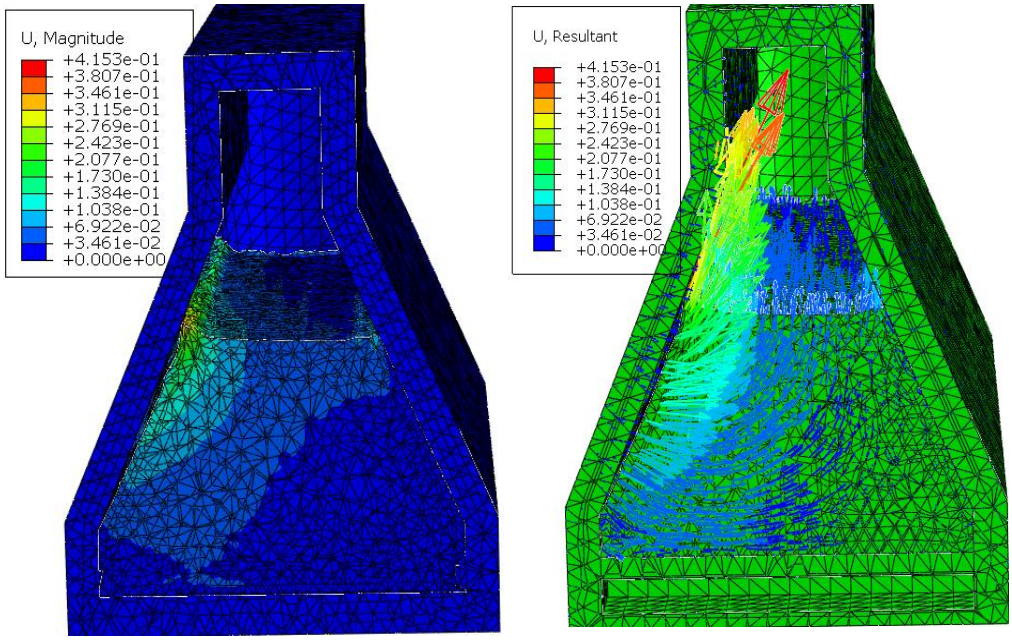

Figure 4- 26. Deformation and Deformation Symbol Configuration of Ratio 0 with 0.5 Water Level Fixed BC Model

In order to clearly visualize the movement of filled water, critical cross-section deformation configurations are shown above. The deformation of the water demonstrates that the excitation of water depends on the interaction of barrier shell

and fluid domain. Water movement occurring at the interior contact surface follows the deformation pattern of the barrier shell. The deformation symbol is shown in the figures to address the tendency of water movement. In this case, the deformation symbol is more representative to describe the tendency than streamlines. From the configuration, the movement of filled water follows an arc path upwards due to the viscosity of water. Overall, the filled water has little contribution to energy absorption in fixed BC.

4.5.3.2 Friction BC Models

In friction BC models, a portion of energy is converted to the kinetic energy of barrier shell due to the movement. In order to precisely study the energy absorption behavior of the water sloshing effect, no water movable (solid water) FE models have been developed which treat fluid domain is solid and highly deformable. These FE models were created same density of water, so the element type used does not affect the energy absorption behavior of barrier specimens. The purpose of these developed solid water models is to eliminate the increased mass inertia effect in terms of energy absorption. The control groups add the ability to address only the energy absorption of filled water due to the characteristic of sloshing (viscous). The energy absorption due to sloshing is showed in the expression of velocity. The combined velocity history vector plots are shown below.

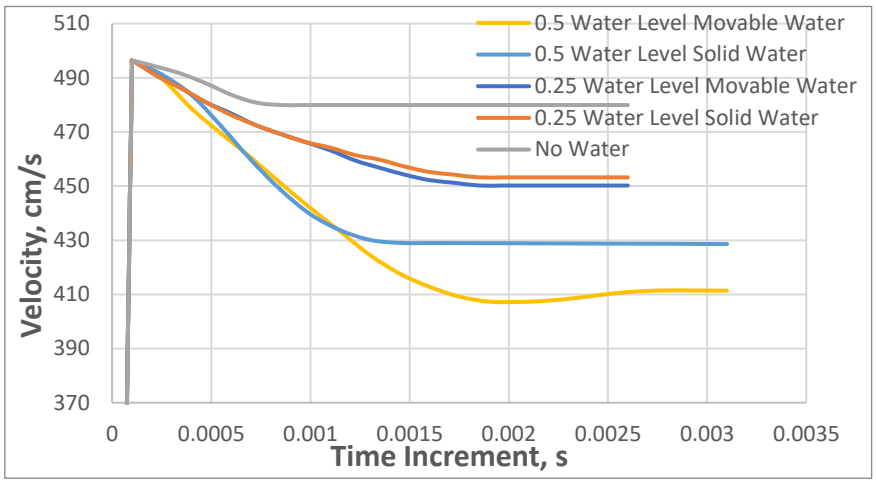

Figure 4- 27. CFD Impact Velocity History Plot of Ratio 0 Models in Friction BC

Table 4- 12. Parametric Study Modeling Results of Ratio 0 Models in Friction BC

Case	Impact Velocity, cm/s	Post-Impact Velocity, cm/s	FE Result, %	Test Result, %	Deviation, %
Ratio 0-No Water	495.302	479.952	7.46	10.32	2.86
Ratio 0-0.25 Solid Water	495.473	456.174	15.14	N/A	N/A
Ratio 0-0.25 Water	495.348	450.215	17.69	23.12	5.43
Ratio 0-0.5 Solid Water	495.307	427.413	25.59	N/A	N/A
Ratio 0-0.5 Water	495.449	413.39	30.05	24.54	5.51

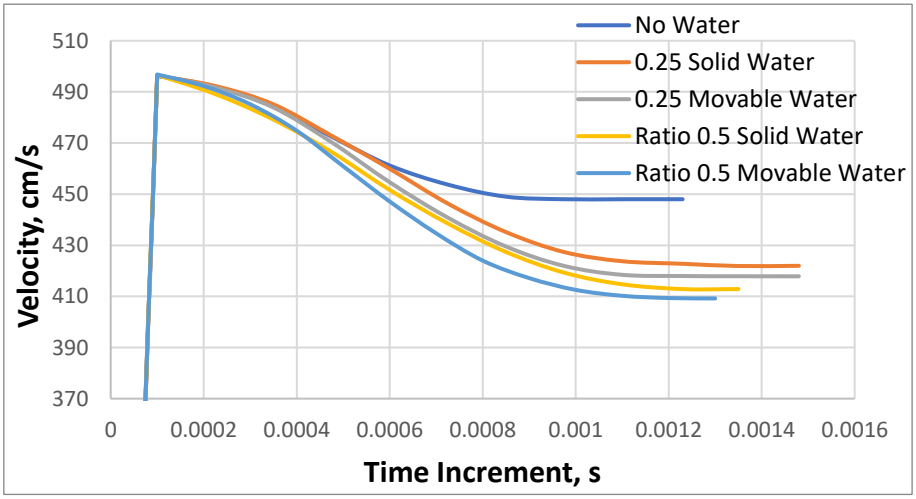

Figure 4- 28. CFD Impact Velocity History Plot of Ratio 0.25 Models in Friction BC

Table 4- 13. Parametric Study Modeling Results of Ratio 0.25 Models in Friction BC

Case	Impact Velocity, cm/s	Post-Impact Velocity, cm/s	FE Result, %	Test Result, %	Deviation, %
Ratio 0.25-No Water	495.235	448.13	18.47	21.09	2.62
Ratio 0.25-0.25 Solid Water	495.054	427.96	25.72	N/A	N/A
Ratio 0.25-0.25 Water	495.164	420.842	27.66	30.57	2.91
Ratio0.25-0.5 Solid Water	495.254	415.847	29.12	N/A	N/A
Ratio 0.25-0.5 Water	495.021	409.199	32.63	38.7	6.07

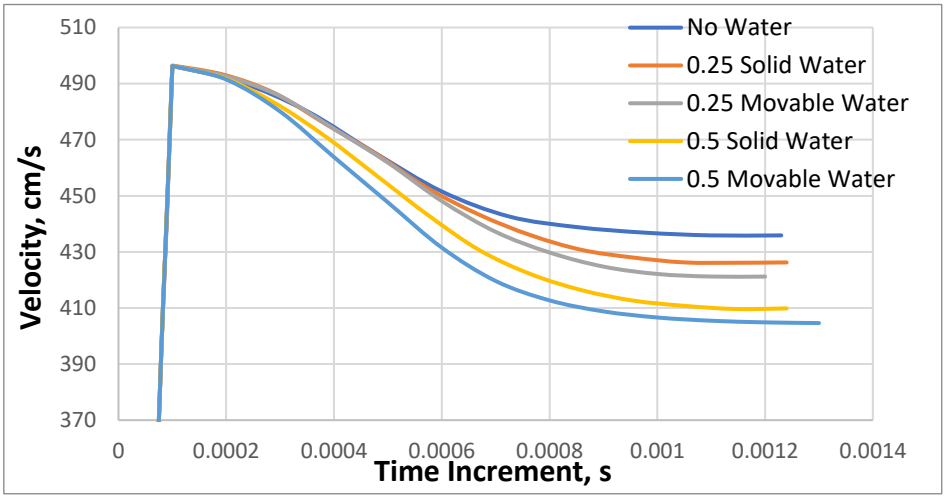

Figure 4- 29. CFD Impact Velocity History Plot of Ratio 0.5 Models in Friction BC

Table 4- 14. Parametric Study Modeling Results of Ratio 0.5 Models in Friction BC

Case	Impact Velocity, cm/s	Post-Impact Velocity, cm/s	FE Result, %	Test Result, %	Deviation, %
Ratio 0.5-No Water	495.755	435.88	22.85	32.12	9.27
Ratio 0.5-0.25 Solid Water	495.254	426.24	26.36	N/A	N/A
Ratio 0.5-0.25 Water	495.953	422.1	27.87	37.34	9.47
Ratio0.5-0.5 Solid Water	495.124	407.83	32.33	N/A	N/A
Ratio 0.5-0.5 Water	495.234	404.61	34.01	42.76	8.75

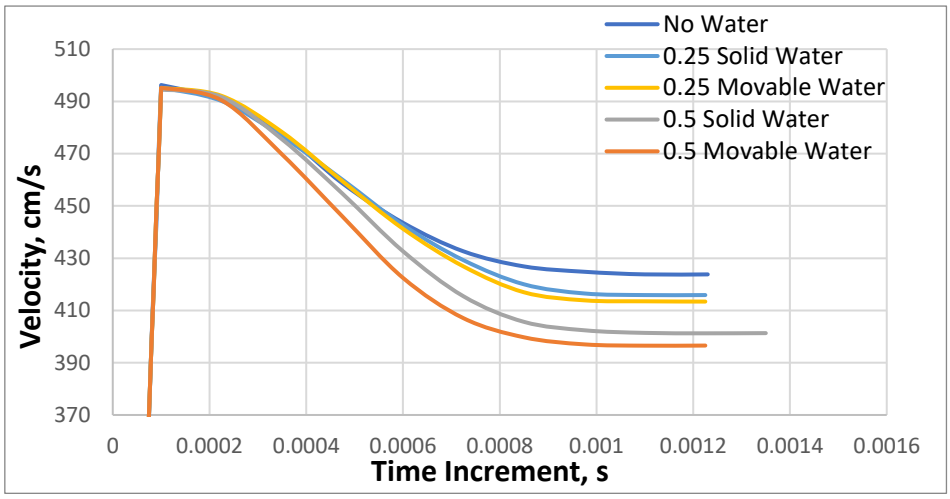

Figure 4- 30. CFD Impact Velocity History Plot of Ratio 0.75 Models in Friction BC

Table 4- 15. Parametric Study Modeling Results of Ratio 0.75 Models in Friction BC

Case	Impact Velocity , cm/s	Post-Impact Velocity, cm/s	FE Result, %	Test Result, %	Deviation, %
Ratio 0.75-No Water	495.082	423.798	26.7	29.89	3.19
Ratio 0.75-0.25 Solid Water	495.537	415.885	29.77	N/A	N/A
Ratio 0.75-0.25 Movable Water	495.452	413.397	30.06	36.67	6.61
Ratio0.75-0.5 Solid Water	495.127	401.034	34.63	N/A	N/A
Ratio 0.75-0.5 Movable Water	495.221	396.562	36.08	41.41	5.53

Based on the velocity history plot, the variation of total energy absorption between movable water, solid water, and no water filled cases are presented. Comparing the PIV difference from models with ratio of 0 to 0.75 for water-filled cases, it can be observed that barrier filled with water result in an obviously higher total energy absorption due to the effects of higher system mass and higher absorbed energy by water. The parametric study is conducted to investigate the energy absorption associated with the increased mass with filled water.

In a 0.25 water level cases, barrier specimens address a small amount of energy reduction between movable water and solid water which means the absorbed energy by water sloshing is minor comparing to the effect of increased system weight. The calculated energy differences between movable water and solid water are between 2.5% and 0.5% for ratio 0 to ratio 0.75. The differences between no water and solid water cases are approximately 8% and 3%. In 0.5 water level cases, the velocity history plots address a higher energy absorption by water sloshing effect, especially in the non-internal cell model. The variation of total energy absorption between ratio 0 and ratio 0.75 in terms of movable and solid water for the case 0.5 water level respectively are around 6% and 3%. Additionally, the influence of energy absorption caused by increased system weight is 18% and 9 %. Overall, the barrier with filled water and increased water levels lead to higher total energy absorption, because the increase in weight and sloshing effect contributing to more energy absorption. Comparing these two effects, a higher system weight is more significant to energy reduction than water sloshing. The water sloshing absorption is related to the filled water level and internal cell structure. A higher water level obtains more energy absorption by sloshing and internal cell decrease the energy absorption ability of water. The configuration of water movement and movement symbols are shown below to analysis sloshing energy absorption by water.

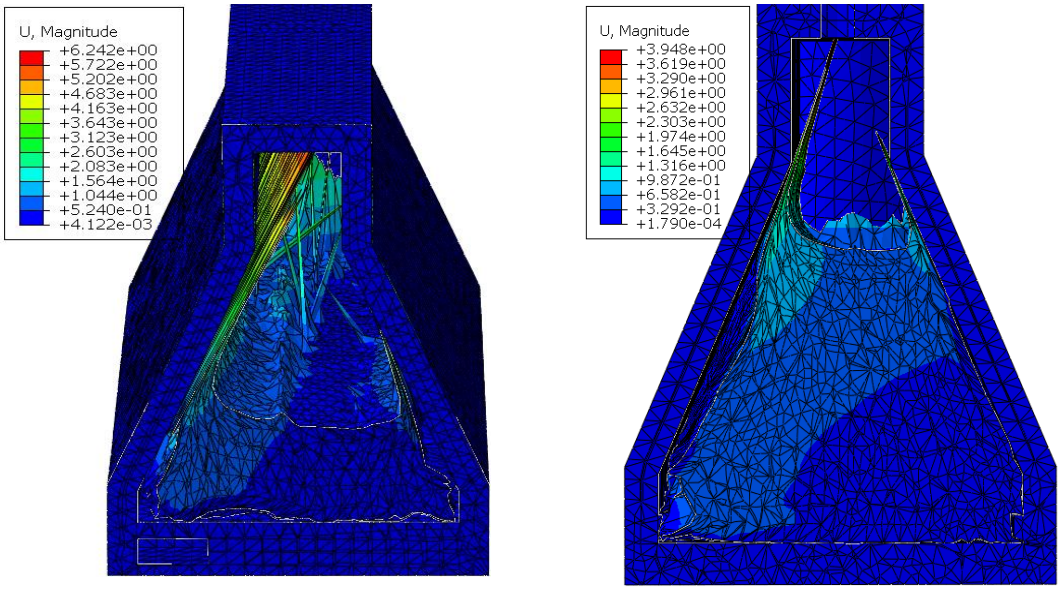

Figure 4- 31. Configuration of 0.25 and 0.5 Filled Water Movement in Non-Internal Cells Barrier

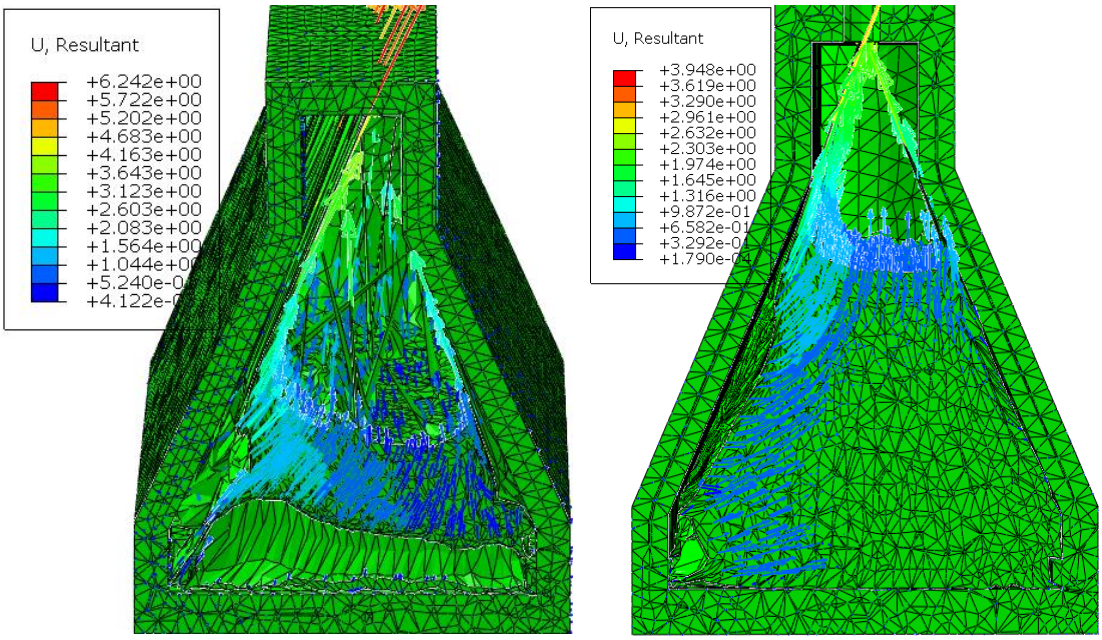

Figure 4- 32. Configuration of 0.25 and 0.5 Filled Water Movement Symbol in Non-Internal Cells Barrier

Figure 4-31 and Figure 4-32 present the configuration of water movement.

Overall, the movement of filled water is similar to fixed BC. The sloshing effect is more dramatic compared to the fixed BC case, due mainly to relatively more

translation movement. Based on the modeling result, the intensive sloshing effect results in a higher energy absorption by water, increasing as the water-level increases. Therefore, the conclusion can be made that intense sloshing effect and higher filled water level lead to higher energy absorption by water. However, the internal cells may potentially limit the movement of filled water. Therefore, the water movement among the internal cells are shown as followed.

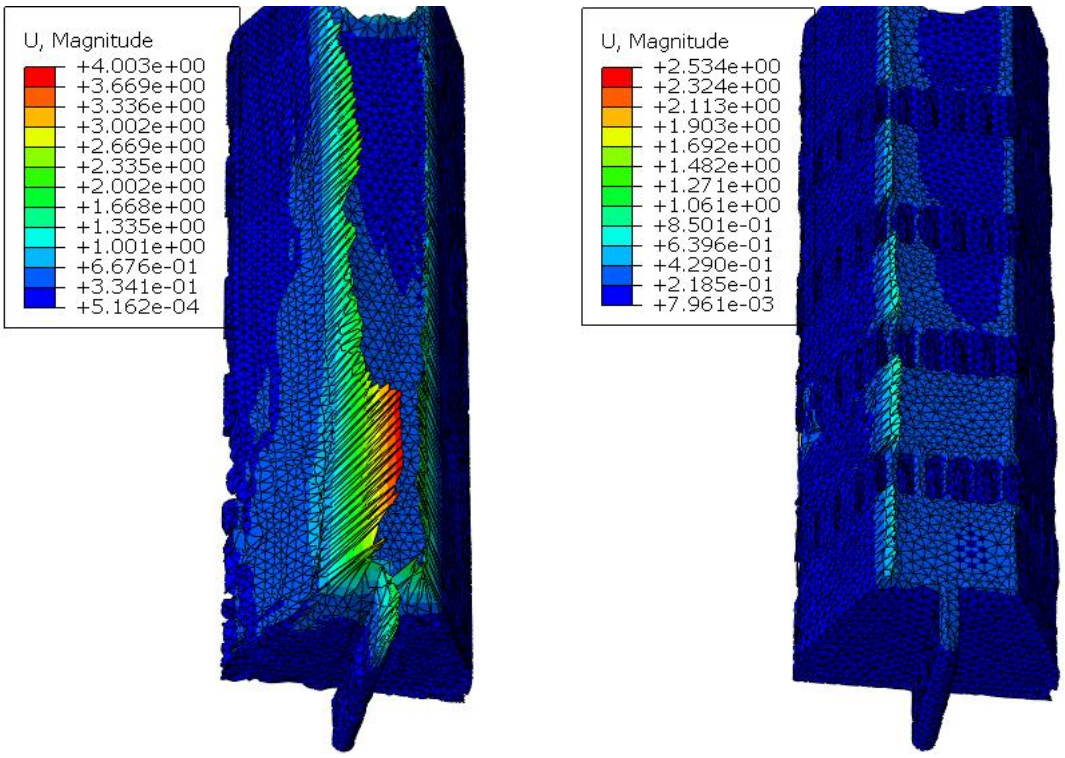

Figure 4- 33. Configuration of Fluid Domain Movement in Ratio of 0 and 0.25 Models

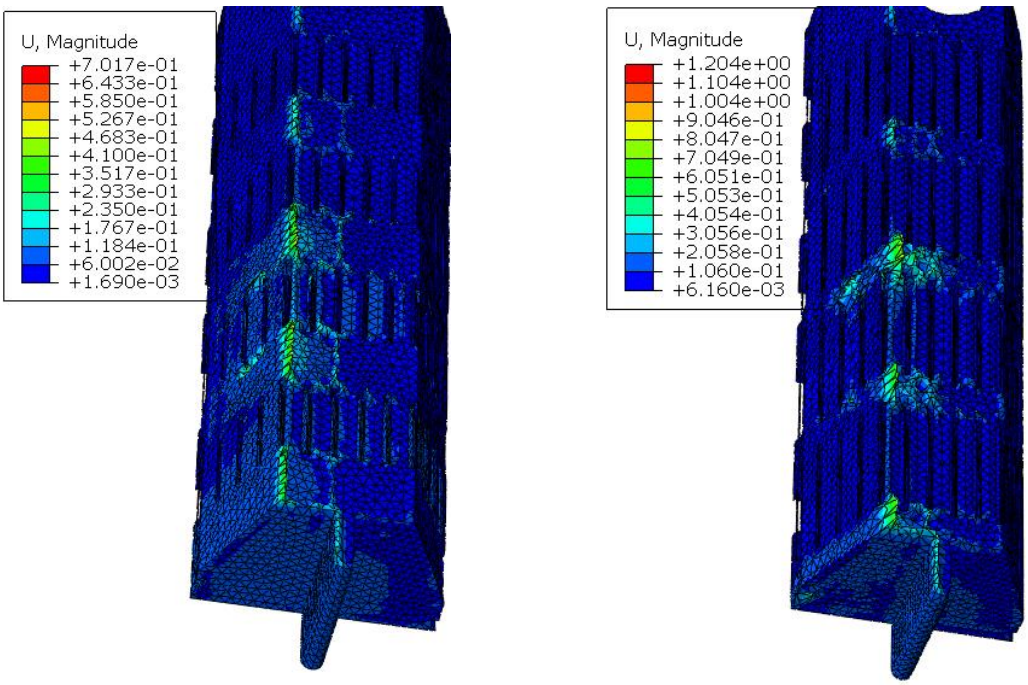

Figure 4- 34. Configuration of Fluid Domain Movement in Ratio of 0.5 and 0.75 Models

According to Figure 4-33 and Figure 4-34, the geometries only present 0.5 level fluid domain to help visualize the movement of filled water. All fluid domains are cut by internal cells regarding different length ratio. From ratio 0 to ratio 0.75, it can be observed the water movement is limited by internal cells; the movement constrained at the area between the adjacent cells. This observation accounts for the energy absorption by sloshing effect presents a decreasing trend while the length of internal cells increasing. Moreover, considering energy dissipation behavior absorbed by filled water. For a viscous fluid, there is a large velocity gradient giving rise to high fluid shearing in the radial direction, thereby making the viscous dissipation effect significant (Siddhartha et al., 2017). A large gradient movement of filled water will also positively dissipate the absorbed energy. Overall, a more dramatic sloshing effect is desirable for reducing impact energy in terms of filled water.

4.6 Discussion of Parametric Study

With validating of the FE results, detailed analysis has been conducted in terms of the energy absorption combined with different parameters. A few plots are presented based on the modeling results from conducted parametric studies.

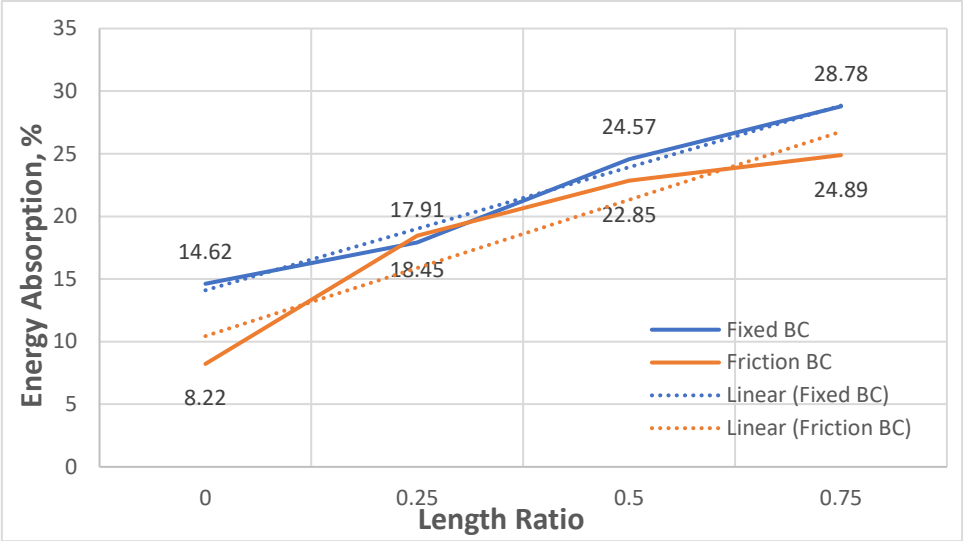

Figure 4- 35. Total Energy Absorption in Non-Water Filled Models

Figure 4-35 presents the total energy absorption combined with different length ratios in no water filled case. Approximately by plotted trend lines, the total energy absorption will increase with increasing of internal length ratio for both fixed and friction BCs. In fixed BC, the total energy absorption equals to the sum of contact frictional dissipation and strain energy dissipation. The increment of strain energy dissipation by internal cells can be calculated by the increment of total energy absorption. Concerning friction BC, the kinetic response of system weight is an additional energy absorption term due to barrier movement. However, current study is not able to address the quantity of this effect. The total energy absorption in friction BC increased with longer length ratios, which might due to increased weight.

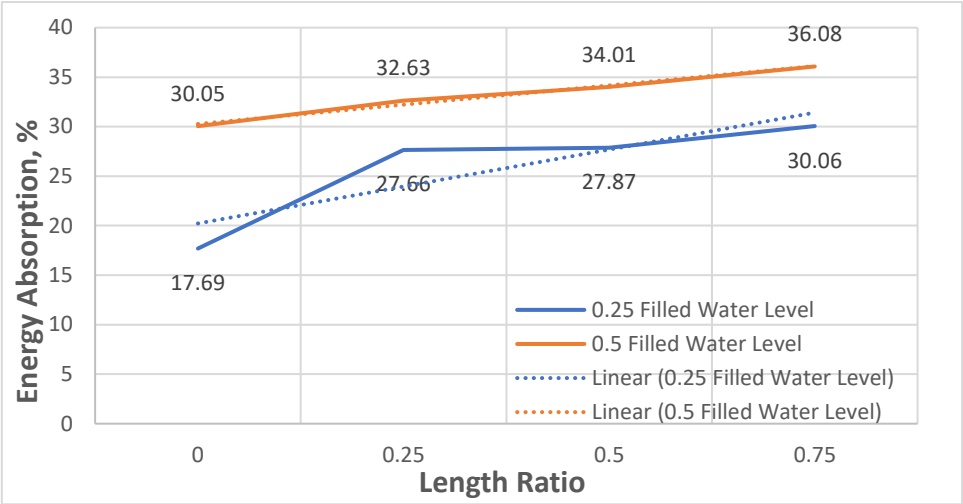

Figure 4- 36. Total Energy Absorption in Water-Filled Models

The figure addresses the total energy absorption in friction BC with 0.25 and 0.5 water filled level. The conducted parametric studies with water-filled cases enable to represent the typical application of PWFBs at roadway network. With higher water-filled level, PWFBs present higher energy absorption. There are two consequences resulting in higher energy absorption in friction BC. First one is the energy absorption due to the viscosity of water. Another one is filled water also increase the weight of PWFB systems, which the kinetic response of filled ballast weight leads to higher energy absorption.

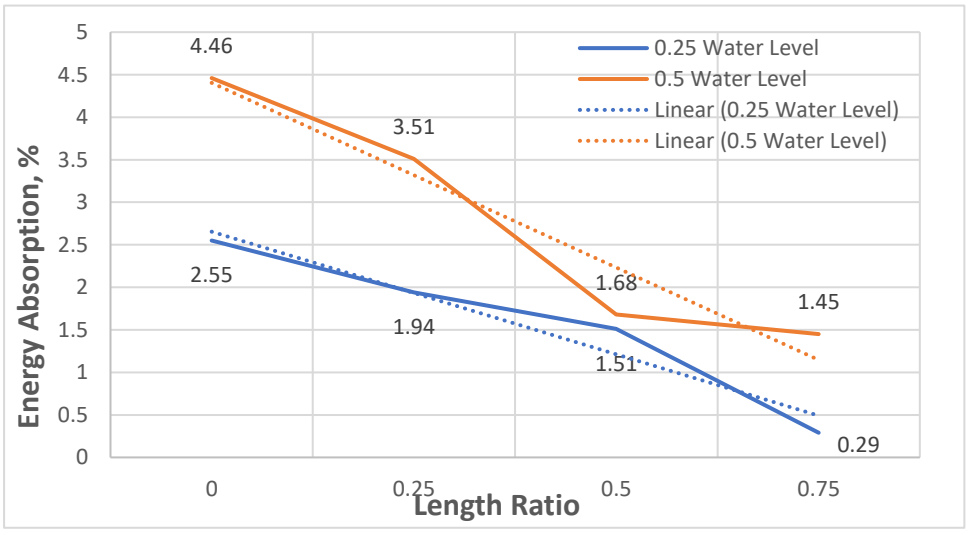

Figure 4- 37. Viscosity Energy Absorption in Water-Filled Models

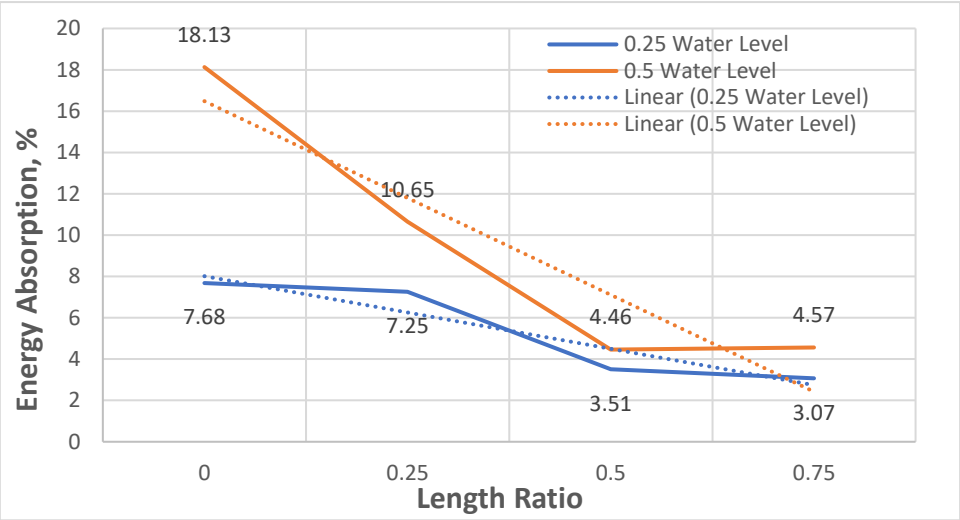

Figure 4- 38. Kinetic Response Energy Absorption of Filled Ballast Weight

Concerning these effects, the energy absorption due to the viscosity and kinetic response of filled ballast weigh can be addressed by introducing the solid water models. Figure 4-37 addresses the energy absorption due to the sloshing effect which is calculated by using total energy absorption in water-filled case subtracts the energy absorption in solid water case. Figure 4-37 and configuration of water movement indicate that internal cells potentially limited the sloshing effect of filled water. Besides, the kinetic response energy absorption is presented in Figure 4-38. The energy absorption is obtained from using total energy absorption of solid water subtracts no-water filled cases. Similarly, less energy absorption due to kinetic response is contained with longer internal cells. In the real application, high energy absorption of these two terms are preferred due to the portability.

CHAPTER 5. DESIGN RECOMMENDATIONS

The primary objective of this thesis was the energy absorption of developed PWFB with internal cells. In this preliminary research, developed small-scale testing and FE modeling only considered the singular barrier segment. Design recommendations were developed, based on the energy absorption behavior of barrier segments associated with the energy absorption by water sloshing effect, and kinetic response. Based on the conducted parametric study, the ultimate impact strength of varied internal cell length is evaluated based on the FE modeling. Furthermore, considering that the PWFB systems are intended to be used as temporary channelizing devices, portability is also an important evaluation criterion for PWFB systems. The design recommendation gives global design consideration combining the total energy absorption, energy absorption by water sloshing effect, impact strength, and portability.

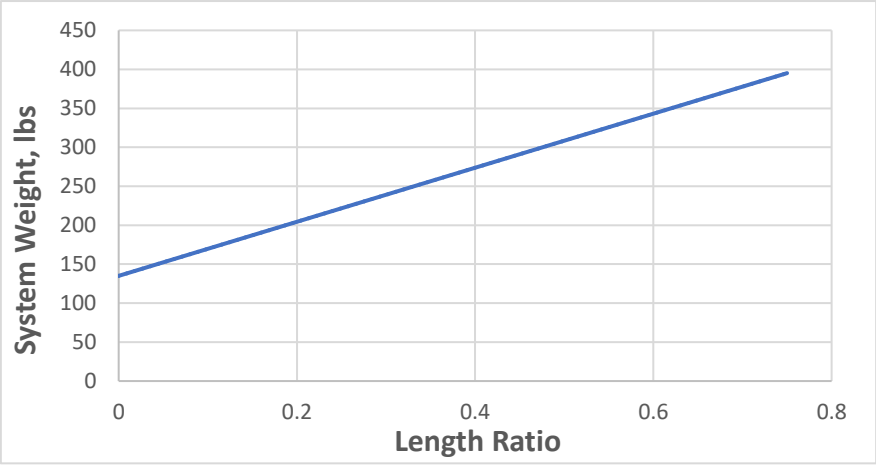

Figure 5- 1. Length Ratio versus System Weight Plot of Full-Scale Barrier Segment

The typical application of PWFB is that the PWFB segments are transported to the job site, then connected and filled blast weight manually by labors. Since the light weight of barrier shell is desirable for the application, the effect of the internal cells on the weight of the barrier was considered. Current developed PWFB with internal cells are based on the JB-32 PWFB. Although this barrier resembles currently marketed PWFBs, the portability is lower than average due to thicker barrier shells. The JB-32 PWFB does not have internal reinforcement, which is used thick barrier shell to increase the impact resistance. Besides, as a fact of increasing the length of internal cells, the system weight also increases as well. Smaller length ratios are recommended for practicality in terms of portability. Based on the FE modeling, the developed PWFB still can resist impact loading while the shell is fractured and internal cells keep their structural integrity. Therefore, it is appropriate to reduce the thickness of barrier shells to increase the portability, which also remains a high overall strength of barrier segments.

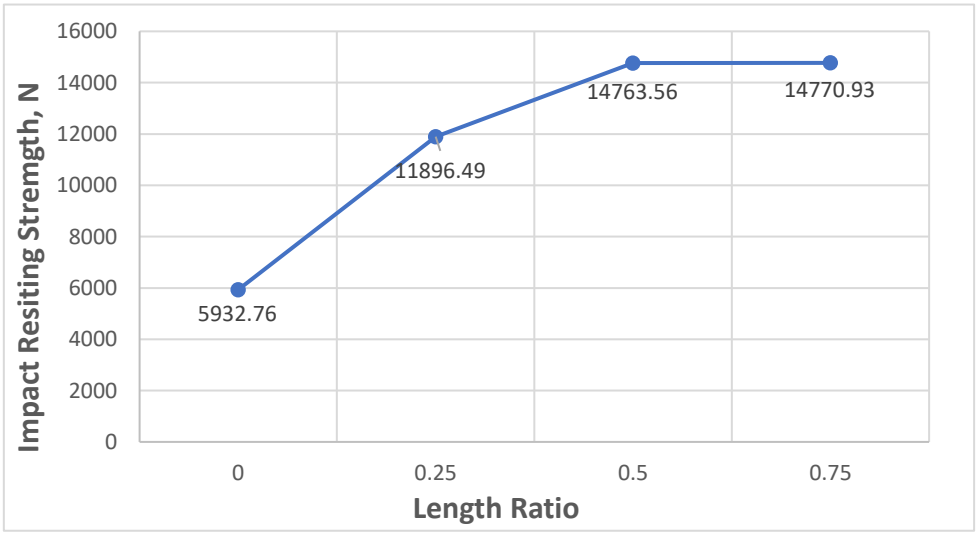

Figure 5- 2. Trend Line Plot of Length Ratio versus Impact Resisting Strength

Aside from the aspect of portability and energy absorption, internal cells also increase the overall structural strength. Figure 5-2, the trend line is plotted based on the ultimate strength point of ratio 0, ratio 0.25, ratio 0.5, and ratio 0.75. From the plot, a large length ratio of internal cells does not increase the resisting strength as expected. There is a significant strength increment between ratio 0 and ratio 0.25. During an impact, the impact equivalent load depends on both the mass inertia of the impactor and the barrier segments instead of only the mass inertia of impactor. Overall, 0.25 small-scale barrier is adequate for a 12 kN equivalent impact which would be 133 kN for a full-size barrier.

Based on the conducted parametric study, in terms of energy absorption, a higher length ratio, higher water-filled water level, and higher system mass will result in higher energy absorption. However, higher length ratio limits the sloshing effects of filled water leading to less energy absorption by water.

Figure 5-3 presents the reduction trend line of energy absorption by water is from FE results. It roughly addresses the decreasing tendencies of energy absorption as the length ratio increases. However, the energy absorption caused by the sloshing effect is minor compared to the total system energy absorption. This is because the energy absorption caused by both the elastic strain dissipation and kinetic response of the barrier segment are more significant as compared to the effect of water sloshing. However, higher energy absorption by increasing system weight may not be achievable due to portability. For this case, two typical parameters affect the total system energy absorption, the internal length ratio and the filled water level.

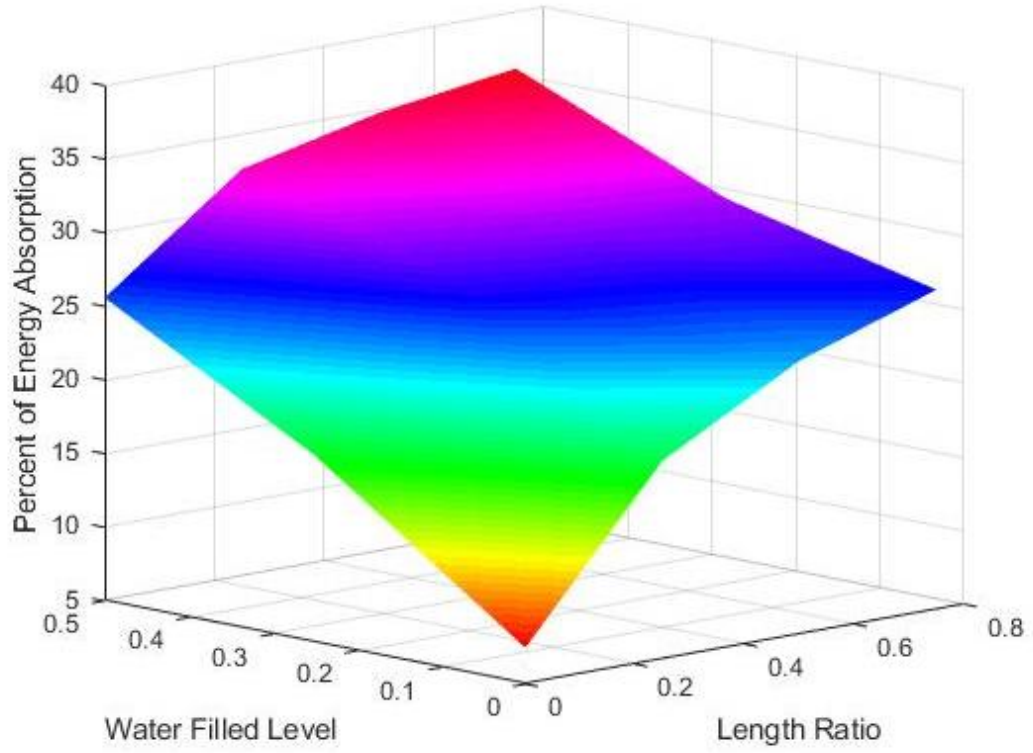

Figure 5- 3. Surface Plot of Percentage of Energy Absorption Combined with Water Filled Level and Length Ratio

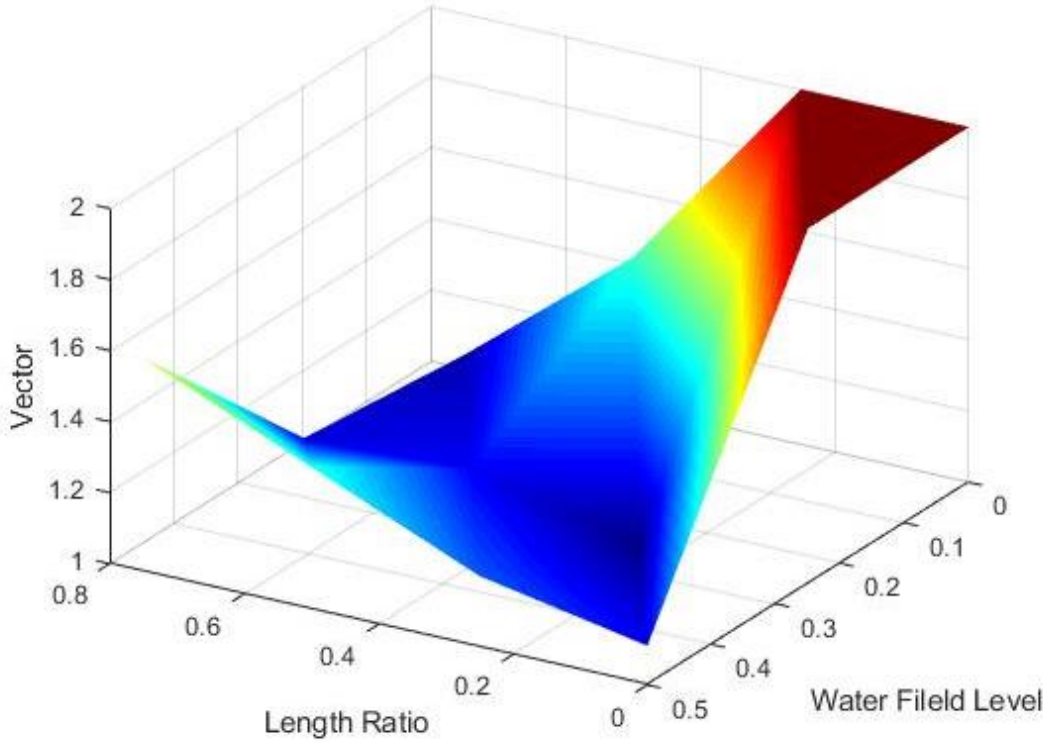

Figure 5- 4. Surface Plot of Vector Minimum Value Associated with Length Ratio and Water Filled Level

Figure 5-3 gives a global configuration of energy absorption variation in terms of length ratio and water-filled level in friction BC. The total energy absorption is a function of two variables, length ratio and water-filled level. Overall, the optimal solution is found by optimizing the two variables in terms of total energy absorption. The global criterion method effectively solves the multiple-objective problems, which locates the minimization of objective functions (Davalos and Qiao, 1996). In this method, the optimal solution can be obtained from locating the minimal value of the objective function.

$$\sum_i^K \left(\frac{\mathrm{f}\,(x\mathrm{i}\,)-\mathrm{f}\,(x*)}{\mathrm{f}\,(x*)}\right)^2 \tag{5}$$

Where K and i respectively represent the different objective functions and the number of objective functions. f (x_i) and f $(x*)$ are the value of total energy absorption and optimal total energy absorption. In this formulation, the minimum vector value indicates the optimal solution in terms of length ratio and filled water level. In this study, the optimal process is based on the numerical solution from previous parametric study, and the restrain of two variables also follows the parametric study. From the result of optimization, ratio 0.25 with 0.25 water filled water and 0.75 with no water filled give similar global minimum vector value which means these two cases address the optimal total energy absorption. Considering the energy absorption effect and the portability of system, these factors are governed by system weight. Current popular PWFBs have a system weight ranging from 90 lbs from 170 lbs adequate up to TL-3. The developed barriers are over the average empty weight of the barrier segment. Although ratio 0.75 has a higher energy absorption

capacity, ratio 0.25 is preferred due to the minimized self-weight. Besides, 0.5 filled water level is more practical in terms of total energy absorption.

Polymeric Foam filled with Low-Density Polyethylene can be installed on the impact side to increase the energy absorption ability of PWFBs (Gover and Oloyede, 2014). The Polymeric Foam presents a good option of absorbing more impact energy before the lateral deflection begins. Additionally, Extruded Polystyrene Foam presents a higher impact resistant capacity comparing to other type of Polymeric Foam. Therefore, in the later design and application, the Extruded Polystyrene Foam can be installed to increase the impact energy absorption and minimize the occupant risks.

CHAPTER 6. CONCLUSIONS AND FUTURE WORK

Because of an increased crash frequency in the temporary work zone, the hazardous natures of vehicle collisions draw public's concerns. Recently published research work demonstrates that honeycomb cells contributing higher in-plane stiffness and impact energy absorption. This research applied the idea of honeycomb cells to PWFBs to increase both impact strength and energy absorption. Developed PWFB with honeycomb type internal cells aims at improving the impact of energy absorption to reduce vehicle occupant risks and provide safety guarantee for pedestrian and workers. This research studies the total energy absorption, the energy absorption behavior of water sloshing effect, and impact resistance strength in terms of the developed Quadrangle shaped internal cells. Based on small-scale impact testing and FE modeling, a parametric study is conducted concerning several possible evaluation criteria which regard different impact conditions. By considering the energy absorption effect due to the barrier segment and water sloshing effect, and portability of PWFBs, the design recommendation is given and the optimal case is determined in the previous chapter. Overall, the application of internal cells to PWFBs is successful in terms of energy absorption. However, current developed PWFBs have a large weight issue which is required to increase the portability by reducing the thickness of designed PWFBs.

Full-scaled vehicular impact tests are expected to further investigate both vehicle occupant risk and post-impact vehicular response recommended by MASH. The additional testing may include as followed; Test 13 is designed to assess a

barrier's ability to contain and redirected lightweight trucks and SUVs for preventing barrier override within the length-of-need; Test 11 and Test 21evaluate the maximum impact strength up to TL-3. The current investigation is followed using MASH guidelines regarding the 1100C passenger car and impact TL-1. The impact behavior associated with 2270P pickup truck and higher TL should be addressed in the future work.

One of the reasons that PWFB systems are vulnerable to high impact speed is inability of joints connections to provide appropriate stiffness (Thiyahuddin and Thambiratnan, 2014). For the majority of assembled segments, the connections present vulnerable behavior comparing to the continuous section. The weak joint mechanism reduces the overall impact resistance capacity and fails to meet the evaluation criteria. The joint mechanism connection also should be well considered in future work.

REFERENCES

Abaqus/CAE User's Manual (6.12) – Abaqus Version 6.12. (2012).

Corben, B., Logan, D., Fanciulli, L., Farley, R. and Cameron, I. (2010). Strengthening road safety strategy development 'Towards Zero' 2008–2020 – Western Australia's experience scientific research on road safety management SWOV workshop 16 and 17 November 2009. *Safety Science*, 48(9), pp.1085-1097.

Davalos, J. F., Qiao, P., & Barbero, E. J. (1996). Multiobjective material architecture optimization of pultruded FRP I-beams. Composite Structures, 35(3), 271–281. https://doi.org/10.1016/0263-8223(96)00035-9

Double precision. (n.d.). *LS-DYNA Support*. https://www.dynasupport.com/howtos/general/double-precision

Friction and Friction Coefficients. (n.d.). Retrieved from https://www.engineeringtoolbox.com/friction-coefficients-d_778.html

Gaitanaros, S., & Kyriakides, S. (2015). On the effect of relative density on the crushing and energy absorption of open-cell foams under impact. International Journal of Impact Engineering, 82, 3-13. doi:10.1016/j.ijimpeng.2015.03.011

G.f.s. (1925). The heat developed during plastic extension of metals. Journal of the Franklin Institute,199(5), 696. doi:10.1016/s0016-0032(25)91211-2

Gover, R., Oloyede, A., Thambiratnam, D., Thiyahuddin, M., & Morris, A. (2015). Experimental and numerical study of polymeric foam efficacy in portable water filled barriers. *International Journal of Impact Engineering,76*, 83-97. doi:10.1016/j.ijimpeng.2014.09.005

Grzebieta RH, Zou R, Jiang T, Carey A. (2005). Roadside Hazard and Barrier Crashworthiness Issues Confronting Vehicle and Barrier Manufacturers and Government Regulators. *National Highway Traffic Safety Administration.*

Hampton, C. E., & Gabler, H. C. (2013). Development of a Missing Post Repair Guideline for Longitudinal Barrier Crash Safety. *Journal of Transportation Engineering, 139*(6), 549-555. doi:10.1061/(asce)te.1943-5436.0000524

Harb, R., Radwan, E., Yan, X., Pande, A., & Abdel-Aty, M. (2008). Freeway Work-Zone Crash Analysis and Risk Identification Using Multiple and Conditional Logistic Regression. *Journal of Transportation Engineering,134*(5), 203-214. doi:10.1061/(asce)0733-947x(2008)134:5(203)

Li, P., & Yu, Q. (2019). Responses and post-impact properties of ultra-high performance fibre reinforced concrete under pendulum impact. *Composite Structures, 208*, 806-815. doi:10.1016/j.compstruct.2018.10.071

Manual for assessing safety hardware. (2016). Washington, DC: American Association of State Highway and Transportation Officials.

Material Parameters for Water." (n.d.). Abaqus Example Problems Guide. https://www.sharcnet.ca/Software/Abaqus/6.14.2/v6.14/books/exa/default.htm?startat=ch02s03aex87.html

Mohammed, H. and Zain, M. (2016). Experimental application of EPS concrete in the new prototype design of the concrete barrier. *Construction and Building Materials*, 124, pp.312-342.

NCHRP Report 350: Recommended Procedures for the Safety Performance Evaluation of Highway Features. (1993). Transportation Research Board, National Research Council, Washington, DC.

Perrot, P. (2008). *A to Z of thermodynamics*. Oxford: Oxford University Press.

Roadside design guide. (2012). Place of publication not identified: American Association of State Highway and Transportation Officials.

Salgo, S. (2004). Crash barrier. *Catalyst, ABC Australia, Sydney.*

Siyuan C, Hongchuan, L. (2017). Water Filled Traffic Control Barrier. *CE 490 Final Report.*

Speed of Sound in Water. (n.d.). Retrieved from https://www.engineeringtoolbox.com/sound-speed-water-d_598.html

Thiyahuddin, M., Gu, Y., Thambiratnam, D., & Thilakarathna, H. (2014). Impact and energy absorption of portable water-filled road safety barrier system fitted with foam. *International Journal of Impact Engineering, 72*, 26-39. doi:10.1016/j.ijimpeng.2014.04.008

Thiyahuddin, M., Thambiratnam, D., & Gu, Y. (2014). Effect of joint mechanism on vehicle redirectional capability of water-filled road safety barrier systems. *Accident Analysis & Prevention, 71*, 60-71. doi:10.1016/j.aap.2014.05.010

Thomas, T., and G. Tiwari. (2018). Energy Absorption and in-Plane Crushing Behavior of Aluminium Reinforced Honeycomb. *Vacuum, 2018*, doi:10.1016/j.vacuum.2018.10.057.

Uang, C., & Bertero, V. V. (1990). Evaluation of seismic energy in structures. *Earthquake Engineering & Structural Dynamics, 19*(1), 77-90. doi:10.1002/eqe.4290190108

Viscosity of Water – viscosity table and viscosity chart :: Anton Paar Wiki. (n.d.). Retrieved from https://wiki.anton-paar.com/en/water/

Waleczek, H., Geistefeldt, J., Cindric-Middendorf, D., & Riegelhuth, G. (2016). Traffic Flow at a Freeway Work Zone with Reversible Median Lane. *Transportation Research Procedia*, 15, 257-266. doi:10.1016/j.trpro.2016.06.022

Wang, A., & Mcdowell, D. L. (2003). Effects of defects on in-plane properties of periodic metal honeycombs. International Journal of Mechanical Sciences, 45(11), 1799-1813. doi:10.1016/j.ijmecsci.2003.12.007

Wang, Y., Chen, K., Ci, Y., & Hu, L. (2011). Safety performance audit for roadside and median barriers using freeway crash records: Case study in Jiangxi, China. *Scientia Iranica, 18*(6), 1222-1230. doi:10.1016/j.scient.2011.11.020

Zhang, X., Hu, Y., Xie, K., Wang, S., Ngai, E., & Liu, M. (2014). A causal feature selection algorithm for stock prediction modeling. Neurocomputing, 142, 48-59. doi:10.1016/j.neucom.2014.01.057

APPENDIX. RAW DATA SHEET OF PENDULUM IMPACT TEST

Initial Released Height (in)

Impact Degree	Released Height
25 Impact Degree	49.21
45 Impact Degree	17.59
75 Impact Degree	9.43

Post-Impact Height Response of Ratio 0.75 Barrier Specimen (in)

Test Numbers	1 Water	3/4 Water	1/2 Water	1/4 Water	0 Water
25 Degree Fixed B.C.					
1	28.5	29.5	33.5	36.5	36.5
2	29.5	29	31.5	32.5	37
3	26.5	28.5	33.5	34.5	35
25 Degree Friction B.C.					
1	28.5	27.5	28.5	29.5	32
2	26.5	26.5	29.5	32.5	32.5
3	23.5	25.5	28.5	31.5	30.5
45 Degree Friction B.C.					
1	6.1	6.1	7.1	8.1	10.1
2	5.1	5.1	5.1	6.6	10.1
3	4.6	6.1	6.1	7.1	10.1
45 Degree Fixed B.C.					
1	7.1	7.1	7.1	8.1	8.1
2	6.6	7.1	7.1	8.1	8.1
3	7.1	7.1	7.1	6.6	8.1
75 Degree Friction B.C.					
1	0.4	1.8	1.3	1.5	2.3
2	1.2	0.7	1.5	1.5	2.3
3	1	0.9	1.3	1.3	3
75 Degree Fixed B.C.					
1	0.5	0.7	1.1	1.4	1.6
2	0.4	0.5	0.9	1.4	1.5
3	0.4	0.3	0.8	1.2	1.5

Post-Impact Height Response of Ratio 0.5 Barrier Specimen (in)

Test Numbers	1 Water	3/4 Water	1/2 Water	1/4 Water	0 Water
25 Degree Fixed B.C.					
1	31.5	31.5	35.5	36.5	36.5
2	29.5	29.5	32.5	36.5	35.5
3	28.5	33.5	33.5	35.5	37.5
25 Degree Friction B.C.					
1	27.5	26.5	24.5	30.5	39.5
2	26.5	29.5	27.5	29.5	30.5
3	26.5	25.5	32.5	32.5	30
45 Degree Friction B.C.					
1	6.1	7.1	6.1	7.1	10.1
2	5.6	5.6	5.1	7.1	11.1
3	5.6	5.1	7.1	8.1	9.1
45 Degree Fixed B.C.					
1	6.1	8.1	8.1	9.1	9.1
2	6.6	7.1	7.1	8.1	8.6
3	7.6	6.1	7.1	7.1	8.1
75 Degree Friction B.C.					
1	0.4	0.5	0.7	1.8	2.5
2	0.2	0.4	0.5	1.5	2.5
3	0.3	0.5	1	1.5	3
75 Degree Fixed B.C.					
1	0.7	0.8	1	1.5	1.7
2	0.5	0.5	1.2	1.4	1.5
3	0.4	0.5	0.9	1.2	1.5

Post-Impact Height Response of Ratio 0.5 Barrier Specimen (in)

Test Numbers	1 Water	3/4 Water	1/2 Water	1/4 Water	0 Water
25 Degree Fixed B.C.					
1	30.5	36.5	34.5	36.5	38.5
2	30.5	32.5	33.5	37.5	40.5
3	34.5	33.5	36.5	39.5	37.5
25 Degree Friction B.C.					
1	29.5	31.5	27.5	33.5	42.5
2	31.5	29.5	32.5	36.5	41.5
3	28.5	27.5	30.5	32.5	41.5
45 Degree Fixed B.C.					
1	7.1	7.1	8.1	9.1	10.1
2	6.1	8.1	7.1	9.1	10.1
3	8.1	7.1	8.1	8.1	8.1
45 Degree Friction B.C.					
1	7.1	6.1	8.1	12.1	12.2
2	6.1	7.1	9.1	9.1	11.1
3	5.6	8.1	7.1	7.1	12.1
75 Degree Friction B.C.					
1	0.2	0.7	1.3	1.8	3.5
2	0.2	0.5	1.3	1.5	3.5
3	0.4	0.4	1.2	1.5	3.5
75 Degree Fixed B.C.					
1	2	2.1	2.4	2.2	2.4
2	2.2	2.1	2.2	2.5	2.6
3	2.1	2.3	2.4	2.4	2.5

Post-Impact Height Response of Ratio 0.5 Barrier Specimen (in)

Test Numbers	1 Water	3/4 Water	1/2 Water	1/4 Water	0 Water
25 Degree Fixed B.C.					
1	32.5	33.5	36.5	39.5	41.5
2	33.5	34.5	35.5	36.5	37.5
3	36.5	37.5	37.5	41.5	38.5
25 Degree Friction B.C.					
1	27.5	36.5	34.5	37.5	40.4
2	32.5	33.5	36.5	38.5	44.5
3	31.5	32.5	40.5	37.5	47.5
45 Degree Friction B.C.					
1	7.1	7.1	9.1	10.1	12.1
2	7.1	8.1	8.1	10.1	13.1
3	6.1	7.1	8.1	9.1	11.1
45 Degree Fixed B.C.					
1	8.1	7.1	9.1	9.1	10.1
2	7.1	8.1	8.1	8.1	9.1
3	7.1	8.6	7.1	9.1	9.1
75 Degree Friction B.C.					
1	1.2	1.4	1.5	2.5	4.5
2	1	1.4	1.4	2.1	4.8
3	0.9	1.3	1.4	2	4.5
75 Degree Fixed B.C.					
1	2.2	2.5	3.1	2.9	2.8
2	2.1	2.3	2.9	3.2	3.3
3	2.3	2.4	2.7	3.1	3.1